AD-A095 554 OHIO STATE UNIV COLUMBUS ELECTROSCIENCE LAB F/G 20/14
ELECTROMAGNETIC SCATTERING BY OPEN CIRCULAR WAVEGUIDES.(U)
DEC 80 T W JOHNSON, D L MOFFATT N00014-78-C-0049
UNCLASSIFIED ESL-710816-9 NL

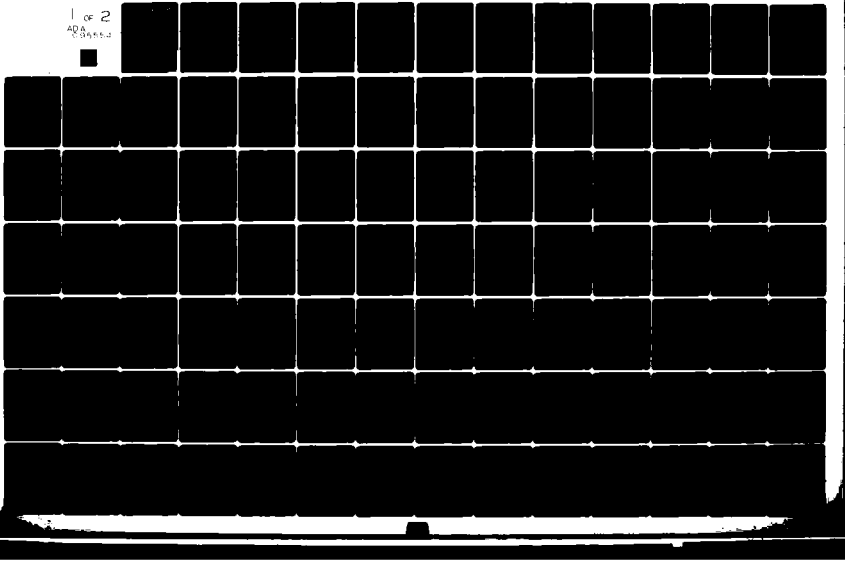

LEVEL II

12

ELECTROMAGNETIC SCATTERING BY OPEN CIRCULAR WAVEGUIDES

T. W. Johnson
D. L. Moffatt

The Ohio State University

AD A095554

The Ohio State University

ElectroScience Laboratory

Department of Electrical Engineering
Columbus, Ohio 43212

402251

TECHNICAL REPORT 710816-9

Contract N00014-78-C-0049

December 1980

Dept. of the Navy
Office of Naval Research
Arlington, Virginia 22217

81 1 27 047

NOTICES

When Government drawings, specifications, or other data are used for any purpose other than in connection with a definitely related Government procurement operation, the United States Government thereby incurs no responsibility nor any obligation whatsoever, and the fact that the Government may have formulated, furnished, or in any way supplied the said drawings, specifications, or other data, is not to be regarded by implication or otherwise as in any manner licensing the holder or any other person or corporation, or conveying any rights or permission to manufacture, use, or sell any patented invention that may in any way be related thereto.

SECURITY CLASSIFICATION OF THIS PAGE (When Data Entered)

REPORT DOCUMENTATION PAGE

READ INSTRUCTIONS BEFORE COMPLETING FORM

1. REPORT NUMBER	2. GOVT ACCESSION NO. AD-A095 554 / 3. RECIPIENT'S CATALOG NUMBER
4. TITLE (and Subtitle) ELECTROMAGNETIC SCATTERING BY OPEN CIRCULAR WAVEGUIDES	5. TYPE OF REPORT & PERIOD COVERED Technical Report
	6. PERFORMING ORG. REPORT NUMBER ESL-710816-9
7. AUTHOR(s) T. W. Johnson, D. L. Moffatt	8. CONTRACT OR GRANT NUMBER(s) Contract N00014-78-C-0049
9. PERFORMING ORGANIZATION NAME AND ADDRESS The Ohio State University ElectroScience Laboratory, Department of Electrical Engineering, Columbus, Ohio 43212	10. PROGRAM ELEMENT, PROJECT, TASK AREA & WORK UNIT NUMBERS
11. CONTROLLING OFFICE NAME AND ADDRESS Dept. of the Navy, Office of Naval Research, 800 Quincy Street Arlington, VA 22217	12. REPORT DATE December 1980 / 13. NUMBER OF PAGES 119
14. MONITORING AGENCY NAME & ADDRESS (if different from Controlling Office)	15. SECURITY CLASS. (of this report) Unclassified / 15a. DECLASSIFICATION DOWNGRADING SCHEDULE

16. DISTRIBUTION STATEMENT (of this Report)

ELECTE FEB 23 1981 C

17. DISTRIBUTION STATEMENT (of the abstract entered in Block 20, if different from Report)

18 SUPPLEMENTARY NOTES

The material contained in this report is also used as a dissertation submitted to the Department of Electrical Engineering, The Ohio State University as partial fulfillment for the degree Doctor of Philosophy.

19 KEY WORDS (Continue on reverse side if necessary and identify by block number)

Intake
Engine
Circular
Waveguide
Wiener-Hopf
Electromagnetic
Scattering

20 ABSTRACT (Continue on reverse side if necessary and identify by block number)

Open circular waveguides are used to model jet engine inlets. The exact Wiener-Hopf solution for scattering by a semi-infinite cylinder is studied in the resonance region, where the cylinder diameter is of the order of a wavelength. In particular, the Wiener-Hopf factorization functions are calculated by numerical integration and compared to various approximations, to define regions of validity. Scattering from the rim is studied as a function of frequency, incidence angle,

DD FORM 1 JAN 73 1473 EDITION OF 1 NOV 65 IS OBSOLETE

SECURITY CLASSIFICATION OF THIS PAGE (When Data Entered)

20.

and time. A ray-optic model for rim backscatter is discussed. The relative power absorption of the five lowest order waveguide modes is evaluated. Coupling of incident plane waves to waveguide modes, and radiation by these modes are shown to be related by reciprocity.

The waveguide termination model for a jet engine assumes an incident waveguide mode strikes an axially symmetric cone on a flat plate. The various techniques for evaluating scattering by this structure are discussed, and the problem is solved for a few cases.

FOREWORD

The radar cross sections of modern aircraft and aerospace vehicles are greatly influenced by the jet engine configurations. However, the prediction and interpretation of electromagnetic wave interactions with open cavities housing realistic jet engine configurations presents a perverse challenge to the electromagnetic theorist. No single study can possibly address all aspects of the problem. While some approximate low and high frequency results are also given, emphasis in this report is concentrated over a frequency span where the cavity aperture is of resonant dimensions, on a circular aperture and on an approach to reasonably realistic engine models.

T. W. Johnson is a Captain in the United States Air Force and attended the Ohio State University under the Air Force Institute of Technology's Civilian Institution Program. Some of the material in this report was also used as a dissertation submitted to the Department of Electrical Engineering, the Ohio State University as partial fulfillment of requirements for the degree Doctor of Philosophy. Computational funding was provided by the Department of Electrical Engineering. The results were felt to be of sufficient interest to warrant report publication and report preparation funding was provided by the Joint Services Electronics Program.

ACKNOWLEDGMENTS

The authors benefited from discussions with Professors Jack H. Richmond and Leon Peters, Jr. and were also aided by Professors Robert G. Kouyoumjian, Henry D. Colson and Dr. Prabhaker H. Pathak who offered their advice freely. A discussion with Dr. Arthur D. Yaghjian was also extremely helpful at a critical stage of the research. The manuscript was capably typed by Mrs. LaVerne Wemmer.

TABLE OF CONTENTS

LIST OF FIGURES

LIST OF TABLES

LIST OF SYMBOLS

α	Fourier transform variable for spatial transform with respect to z
$\alpha_{nm}, \alpha_{nm}'$	Waveguide mode wavenumber for axial propagation of TM and TE modes, respectively
$\gamma_{nm}, \gamma_{nm}'$	Waveguide mode decay constant for axial decay of evanescent TM and TE modes, respectively
ε_n	Neumann epsilon 1 n=0 2 n=1,2,3...
θ	Polar angle in spherical coordinates (see Figure 1-2)
$\hat{\theta}$	Unit vector for polar angle in spherical coordinates
θ_i, θ_s	Polar angle for incident and scattered fields, respectively
θ_n	Angle of asymptotic approximations of Bessel functions
λ	Free space wavelength
ρ	Radial distance in polar coordinates
$\hat{\rho}$	Unit vector in radial direction in polar coordinates
σ	Radar cross section
ϕ	Azimuthal angle in both spherical and polar coordinates
$\hat{\phi}$	Unit vector for azimuthal angle
ϕ_i, ϕ_s	Azimuthal angle for incident and scattered fields, respectively
ϕ_n	Phase angle of asymptotic approximation of derivatives of Bessel function

$\sqrt{\frac{\epsilon_o}{\mu_o}}$	Characteristic impedance of free space
$\sqrt{\frac{\mu_o}{\epsilon_o}}$	Characteristic admittance of free space
a	Radius of waveguide
$A^{\theta}_{nm}, A^{\phi}_{nm}$	Coupling coefficients for incident plane wave to TM waveguide modes
$B^{\theta}_{nm}, B^{\phi}_{nm}$	Coupling coefficients for incident plane wave to TE waveguide modes
c	Speed of light in vacuum, free-space
$C_{0E}, C_{\theta H}, C_{\phi E}, C_{\phi H}$	Radiation coefficients of waveguide modes; θ,ϕ denote orientation of radiated field; E, H denote TM or TE mode, respectively
D	Diameter of waveguide = 2a
E_{nm}	Magnitude of TM waveguide mode n,m
E^i, E^s	Incident and scattered electric field, respectively
$E_\rho, E_\phi, E_z, E_\theta$	Radial, azimuthal, axial (in polar coordinates), polar (in spherical coordinates) component of electric field
$f(x)$	Transition function defined by Kouyoumjian and Pathak (1974)
f_n	Ratio of two Wiener-Hopf factorization functions
H_ρ, H_ϕ, H_z	Radial, azimuthal, axial (in polar coordinates) components of magnetic field
$H_n^{(1)}(), H_n^{(1)'}()$	Cylindrical Hankel function of the first kind (cylindrical Bessel function of the third kind) or order n, and its derivative
i	Square root of minus one
$I_n()$	Modified Bessel function of order n
$\overline{J}$	Current density
$J_n(), J_n'()$	Cylindrical Bessel function of the first kind of order n, and its derivative

j_{nm}	m-th zero of $J_n(x)$, i.e., $J_n(j_{nm})=0$
j'_{nm}	m-th zero of $J'_n(x)$, i.e., $J'_n(j'_{nm})=0$
k	Free space wavenumber
$K_n()$	Modified Bessel function of order n
L+()	Wiener-Hopf factorization function
m	Index of radial variation for a given azimuthal variation, e.g. the zeroes of $J_1(x)$ are j_{1m},m=1,2,3 → j_{11},$j_{12}$$j_{13}$
M+()	Wiener-Hopf factorization function
n	Index of azimuthal variation
P	Power flow
r	Radial distance from the origin in spherical coordinates
$\bar{r}$,R	Generalized position vectors locating a point in 3-dimensional coordinate system
S_{00},$S_{0\phi}$,$S_{\phi 0}$,$S_{\phi\phi}$	Scattering coefficients for rim of semi-infinite cylinder
x,y,z	Rectangular coordinates
$\hat{x},\hat{y},\hat{z}$	Unit vectors appropriate to rectangular coordinates

CHAPTER I
INTRODUCTION

The radar cross section (RCS) of jet intakes has been extensively studied. There are several reasons that it is of interest. One is simply that it is a major element in the radar cross section of aircraft and must be accurately evaluated to estimate total aircraft RCS. Another reason for study is that potentially the RCS of the aircraft could possibly be reduced if the scattering mechanisms are well understood. A third (though certainly not final) reason is that many aircraft identification or classification techniques propose to use modulation of the radar return imposed by the aircraft engine as a significant identifiable feature. It would be a questionable approach to establish such a system on an effect which is not well understood, particularly in terms of establishing the system's susceptibility to intentional confusion or camouflage.

This study is somewhat limited to the region for which $D \sim \lambda$; the asymptotic forms developed for higher frequencies may fail in this region, and the very low frequency techniques (for which little or no energy penetrates the intake) are invalid.

This study develops two of the practical problems involved in calculating the RCS. The coupling coefficients at the mouth of the intake are known in principle, but difficult to compute in practice. The effect of the engine structure is known only generally, and has been very loosely approximated in past studies.

The jet intake can generally be modeled as an open ended waveguide with an obstacle (the engine) some distance down the waveguide. Figure 1-1 illustrates the geometry. The problem can then, in principle, be solved by the generalized scattering matrix technique. The scattering matrices of the significant scatterers, if known, can be self-consistently manipulated to produce the backscattered field. Let

u^i represent the incident field,

u^{bs} = the backscattered field,

$[S_{11}]$ = a matrix, representing (in some sense) the direct backscatter of the open waveguide

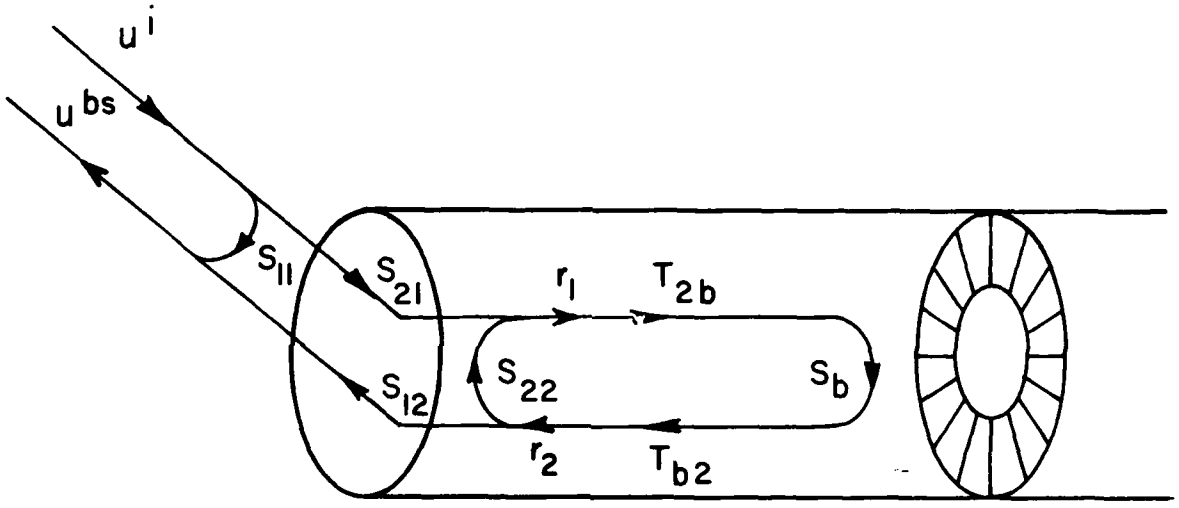

Figure 1-1. GSMT elements for modeling engine inlet.

$[S_{12}]$ = radiation characteristics of waveguide modes

$[S_{21}]$ = coupling matrix of incident field to waveguide modes

$[S_{22}]$ = reflection of waveguide modes from the open end

$[S_b]$ = reflection of waveguide modes from the obstacle

$[T_{2b}]$ = transmission down waveguide

$[T_{b2}]$ = transmission back from waveguide to aperture.

Note that off-diagonal terms in each transmission and reflection matrix will represent mode conversion from one mode to another.

From Figure 1-1 we can easily show that:

$$u^{bs} = S_{11}u^i + S_{12}r_2 \tag{1-1}$$

$$r_1 = S_{21}u^i + S_{22}r_2 \tag{1-2}$$

$$r_2 = T_{b2}\, S_b\, T_{2b}\, r_1 \tag{1-3}$$

$$r_2 = T_{b2}\, S_b\, T_{2b}\, (S_{21}u^i + S_{22}r_2) \tag{1-4}$$

$$\left[I - T_{b2}S_bT_{2b}S_{22}\right]r_2 = T_{b2}S_bT_{2b}S_{21}u^i \tag{1-5}$$

$$\left[(T_{b2}S_bT_{2b})^{-1} - S_{22}\right]r_2 = S_{21}u^i \tag{1-6}$$

$$r_2 = \left[(T_{b2}S_bT_{2b})^{-1} - S_{22}\right]^{-1} S_{21}u^i \tag{1-7}$$

$$u^{bs} = \left\{S_{11} + S_{12}\left[(T_{b2}S_bT_{2b})^{-1} - S_{22}\right]^{-1} S_{21}\right\}u^i \tag{1-8}$$

The matrices S_{11}, S_{12}, S_{21}, and S_{22} have been solved for by the Wiener-Hopf technique.[2] These results are quite complicated algebraically, The heart of the problem, however, is calculation of the Wiener-Hopf factorization functions. Considerable effort has been given to calculating these functions, which is presented in Appendix A. This study has emphasized circular waveguides, because much prior work has been done in the area, and the symmetry of the geometry simplifies the problem somewhat. Also, since engine geometries are circular, non-circular inlets require an additional model of the mode conversion as the energy travels down a waveguide of varying cross-section. Thus our matrices T_{b2} and T_{2b} are diagonal, having only the relevant phase delay for each mode. This study does not address further development of this effect for non-uniform waveguides.

Summary of Circular Waveguide Modes

Propagation in a circular waveguide is limited to a discrete set of modes, which can propagate only for waveguide diameters larger than a certain minimum (cutoff) diameter. The notation used in this study is consistent with Harrington: TE_{11} refers to a mode with electric field transverse to the axis of propagation. In the Russian literature (Weinstein) this is referred to as a magnetic mode, since it has a z-directed magnetic field, and all other field components can be simply derived from it.

The number of modes that can propagate in a circular waveguide goes roughly as the square of the diameter. Table 1-1 lists the first

TABLE 1-1

SUMMARY OF LOW-ORDER CIRCULAR WAVEGUIDE MODES AND CUTOFF FREQUENCIES

Mode	cutoff $\frac{D}{\lambda}$	cutoff ka
TE11	.5861	1.8412
TM01	.7655	2.4048
TE21	.9722	3.0542
TM11	1.2197	3.8317
TE01	1.2197	3.8317
TE31	1.3373	4.2012
TM21	1.6347	5.1356
TE41	1.6926	5.3176
TE12	1.6970	5.3314
TM02	1.7571	5.5201
TM31	2.0309	6.3802
TE51	2.0421	6.4156
TE22	2.1346	6.7061
TE02	2.2331	7.0156
TM12	2.2331	7.0156
TE61	2.3877	7.5013
TM41	2.4154	7.5883
TE32	2.5513	8.0152
TM22	2.6793	8.4172
TE13	2.7172	8.5363
TE71	2.7304	8.5778
TM03	2.7546	8.6537
TM51	2.7921	8.7715
TE42	2.9547	9.2824
TE81	3.0709	9.6474
TM32	3.1070	9.7610
TM61	3.1628	9.9361
TE23	3.1734	9.9695

28 modes in order of increasing cutoff diameter. The cutoff is calculated by noting the $J_n(j_{nm})=0$ or $J_n'(j_{nm}')=0$ and then $ka=j_{nm}$ or j_{nm}'. Since $ka = \frac{2\pi}{\lambda}\frac{D}{2} = \pi\frac{D}{\lambda}$ the cutoff in terms of ka can be simply derived. It seems more intuitive to discuss D/λ. Figure 1-3 presents electric field line pictures for the first few modes.

This study employs the $e^{-i\omega t}$ time convention; the choice is necessary for consistency with the vast majority of Weiner-Hopf literature (Einarsson et al). The coordinate system chosen will be standard spherical and/or cylindrical coordinates, with the origin at the center of the waveguide mouth. See Figure 1-2. The polar angle is θ, the azimuthal angle ϕ. The radius will be designated by r, in spherical coordinates, and ρ in cylindrical coordinates. The waveguide radius is a, and the waveguide extends from $z=0$ to $z=-\infty$ at $\rho=a$.

Since a large part of the literature is concerned with the Weiner-Hopf solution to scattering by a semi-infinite circular cylinder, an heuristic description will be presented here. Tutorial discussions of the Weiner-Hopf technique can be found in [Noble (1958)] and [Morse and Feshback (1953)].

The Weiner-Hopf technique is based on the fact that the Fourier transform of a causal function is entire in a half plane. For example, the function

$$x(t) = \begin{cases} e^{-\alpha t} & t > 0 \\ 0 & t < 0 \end{cases} \qquad (1\text{-}9)$$

has the Fourier transform

$$X(\omega) = \int_{-\infty}^{\infty} e^{i\omega t}\, e^{-\alpha t}\, u(t)\, dt = \int_{0}^{\infty} e^{(i\omega-\alpha)t}\, dt$$

$$= \frac{1}{(i\omega-\alpha)}\left[e^{-\alpha\infty} - e^{0}\right] = \frac{1}{\alpha - i\omega} \qquad (1\text{-}10)$$

[Recall that we are using $e^{-i\omega t}$ time dependence]. Hence $X(\omega)$ has a single pole at $\omega = -i\alpha$ and is entire (has no poles) for $Im(\omega)>0>-i\alpha$. In the Weiner-Hopf technique, the Fourier transform of the field component is taken with respect to the coordinate along one axis of the problem (the axis parallel to the semi-infinite object). The incident and scattered field are then related by means of the

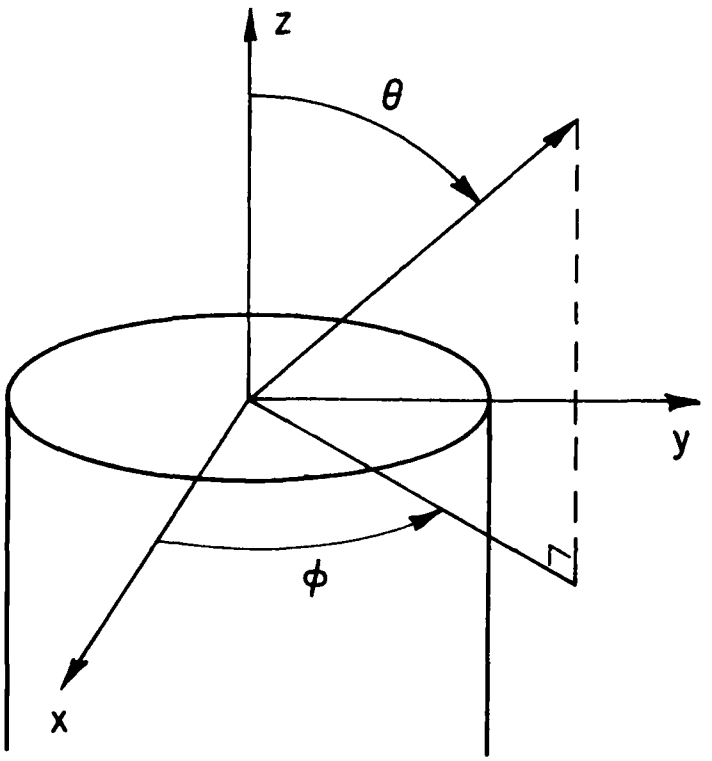

Figure 1-2. Coordinate system for modeling engine inlet.

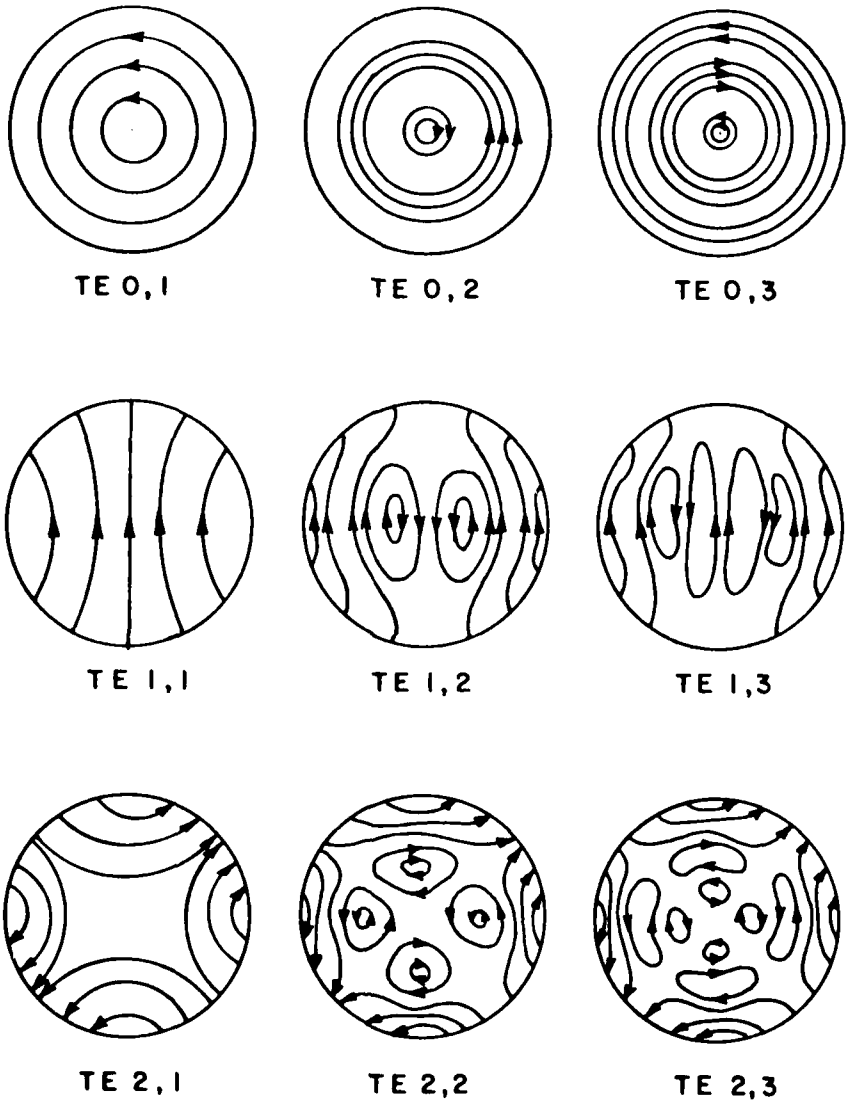

Figure 1-3. Electric field lines for TE modes in circular waveguide.

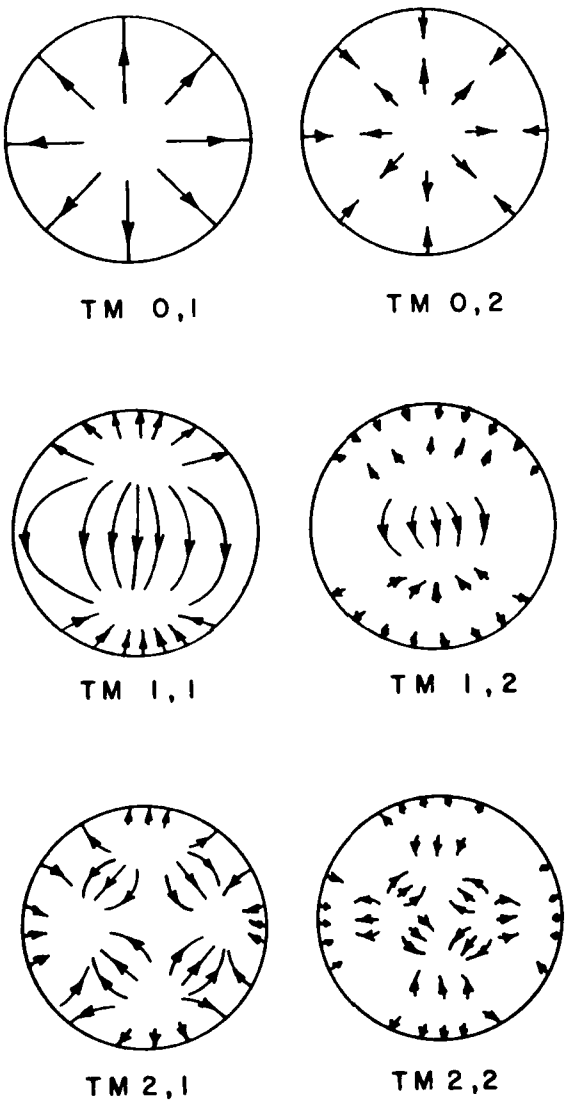

Figure 1-3 (continued). Electric field lines for TM modes in circular waveguide.

physics of the problem. Noble cites three different techniques for doing this: field matching, Green's function integral equation, and dual integral equations. The resultant equation is manipulated so that the left-hand side must be entire in one half-plane and the right-hand side in the other half-plane, with a region of overlap. These are then equated to a third function, which must be entire over the whole α-plane. Because of Liouville's Theorem, this new function ends up being a constant, equal to zero. This separately sets each side of the equation to zero, which leads to the solution (by taking the inverse Fourier transform).

For the cylinder scattering problem, the incident field is decomposed into cylinder waves by the Bessel function addition theorem. The transform is taken with respect to the z-axis:

$$\epsilon(\alpha,r,\phi) = \int_{-\infty}^{\infty} E(z,r,\phi)e^{-i\alpha z}\, dz \quad . \tag{1-11}$$

For each cylinder wave, the incident and scattered fields are related by imposing the boundary conditions that the tangential electric field must vanish at the cylinder walls, and the surface current must vanish in free space. These are used to manipulate the problem into a Weiner-Hopf form. This process is described by [Weinstein (1969) and Einarsson et al (1966)].

The analysis of interactions at the mouth of an open waveguide goes back to [Chu (1940)]. By using the Kirchoff approximation the radiation fields for the lowest order propagating modes for a circular, and a rectangular waveguide are calculated. In terms of the GSMT, this would enable us to compute elements of $[S_{12}]$.

[Levine and Schwinger (1948)] evaluate the acoustic radiation and reflection characteristics of a hollow circular pipe. An integral equation for the velocity potential is solved via the Weiner-Hopf technique. Their study is confined to symmetrical modes incident on the open end of the pipe. In a circular acoustic waveguide, the symmetrical modes are given by

$$\Phi(\rho,\phi) = J_0(j_{0,m}\rho/a) \quad \text{or} \quad J_0(j_{0m}'\rho/a) \tag{1-12}$$

where

j_{0m} are the zeroes of $J_0(x)$

j_{0m}' are the zeroes of $J_0'(x)$

[Pearson (1953)] was the first to apply the Weiner-Hopf technique to the electromagnetic problem. He considers a transverse magnetic plane wave incident on the open end, and obtains equations for the Laplace transforms of the axial and azimuthal currents on the waveguide walls. These equations are then solved by the Weiner-Hopf techniques, and the currents can be obtained by inverse Laplace transform. The fields far from the mouth down the pipe are then evaluated asymptotically and found to result from propagating modes, thus giving the coupling coefficients. The backscattered fields are not evaluated, nor is the behavior near the mouth studied.

[Jones (1955)] analyzes the scattering of sound waves by a solid semi-infinite cylinder. He considers both hard and soft boundary conditions although numerical results are evaluated for only the hard (du/dn=0) case. An approximation for high frequency (large diameter) is developed, and a low frequency expression is presented. A variational expression is developed to establish limits of error on the approximations used in evaluating the exact expressions. Both the pressure field on the cylinder, and the scattered far field are evaluated. The end cap pressure time response due to an incident unit step is evaluated by taking the inverse Laplace transform of the frequency domain response.

[Noble (1958)] treats the scalar problem for both radiation of the lowest order mode, and coupling of an incident plane wave to the lowest order mode in a circular waveguide. His discussion is tutorial in nature, drawing somewhat from Jones' work. There is a more complete treatment of the general technique used to solve Weiner-Hopf problems than is found in most other references.

[Jones (1964)] applies the Weiner-Hopf technique to radiation from a semi-infinite hollow pipe. This study is somewhat tutorial in nature, being part of a textbook, and considers only a few of the lowest order modes. Jones notes that TE modes radiate more efficiently than TM modes. TM modes have higher reflection coefficients at the open end of the pipe.

[Einarsson et al (1966)] give an exhaustive study of diffraction by both the infinite and semi-infinite circular cylinder. The backscatter for a plane electromagnetic wave incident on a solid, semi-infinite, perfectly conducting rod is given. The scalar (sound) scattering from a semi-infinite (both solid and thin walled) tube is evaluated. The radiation and reflection for a propagating scalar wave incident on an open end are evaluated (reproducing the results of Levine and Schuinger and also Weinstein). There is a brief discussion of finite cylindrical resonators with one end open, one end closed (rigid, Dirchlet boundary condition).

The general solution for scattering of a plane electromagnetic wave from a semi-infinite thin walled, perfectly conducting tube occupies about half the report. This includes both the backscatter far-field [S_{11}] and coupling coefficients, for the general plane wave (neither TE nor TM). The special case of axial incidence is considered. Radiation from a source inside the tube [S_{21}] and reflection from an open end [S_{22}], are evaluated, largely copied from Weinstein. Asymptotic radiation of the far-fields is compared to the Kirchoff approximation.

A substantial part of this study concerns evaulation of the Weiner-Hopf factorization functions. A number of forms of integral expressions which exactly define them are developed. Power series approximations to the low frequency are developed. Unfortunately these expressions are still quite complex.

In addition, only the magnitude of the functions is approximated; the phase is not. A large effort to develop high frequency approximation yields some useful simplifications, but the results are expressed in terms of another unknown function, albeit much simpler. Numerical data is given for varying values of ka with the α parameter fixed. This,is inconvenient since, generally, α=kcosθ, and we are primarily interested in fixing ka and varying α. Experimental data are presented for finite cylinders. No experimental data are presented for a semi-infinite cylinder.

[Witt and Price (1968)] analyze the problem of a finite tube without recourse to Weiner-Hopf techniques. Instead, the direct backscatter from the rim, and the coupling coefficients to waveguide modes are calculated by what amounts to the Kirchoff approximation. The incident field tangential to the aperture is expanded as a sum of waveguide modes, and a waveguide admittance for each mode is computed. The reradiation is also calculated via the Kirchoff method, using the Stratton-Chu integral. The termination is modeled as an impedance, which results in a simple (scalar) reflection coefficient. The reflection coefficient is then transformed to its equivalent impedance as seen at the mouth of the waveguide. The total waveguide admittance for that mode is then calculated, and the scattered field is expressed as a sum over the waveguide modes, times the incident field projection on that mode, times the generalized admittance.

For backscatter with vertical polarization (TE) (which corresponds to our $\hat{\phi}$ polarization) they present the formula

$$E_y^s(x',0,z') = -\frac{jka^2\cos\theta}{r}\, e^{-jkr} \qquad (1\text{-}13)$$

$$\left\{ \frac{vJ_1(v+v_o)}{v_o(v+v_o)} + \sum_{n=0}^{\infty} \sum_{m=1}^{\infty} E_{nm}(v)E_{nm}(v_o)(1+\Gamma_{nm}) \left(1 + \frac{jk\cos\theta}{\gamma_{nm}}\right) \right\}$$

where

$v_o = ka\sin\theta_o$ (incident)

$v = ka\sin\theta$ (scattered)

E_{nm} = weighting coefficient for nm-th mode

γ_{nm} = propagation coefficient for nm-th mode

Γ_{nm} = reflection coefficient seen at aperture for nm-th mode.

The work of Weinstein* in many cases predates the works reviewed here. However, most of Weinsteins's papers were published in Russian journals. His book [Weinstein (1969)] contains virtually all of his earlier work, and is readily available. It should simply be noted that Weinstein's work did frequently predate work in the West.

[Weinstein (1969)] has collected all of his earlier work on the Wiener-Hopf technique into a single volume. The book is tutorial in nature, beginning with the simplest problem, diffraction and radiation by a plane parallel plate waveguide. Having developed the basic Wiener-Hopf arguments, he proceeds to analyze circular waveguides, first considering only symmetrical modes (to eliminate azimuthal dependence from the problem). Acoustical problems are then solved, followed by the general problem for electromagnetic waves scattered and radiated by a semi-infinite circular cylinder, including azimuthal dependence. Comparisons with answers obtained via the Kirchoff method are frequent, showing those circumstances under which the Kirchoff method works and those under which it fails. There is a substantial discussion of the relative accuracy of Huygens principle, compared with edge diffraction; a substantial point is made that edge diffraction yields more reliable answers.

[Kao (1970)] presents a completely novel approach to scattering from cylinders. He determines the currents on finite cylinders by using point matching and then calculates radiation patterns from the currents. For the semi-infinite cylinder [1970b] he sets up two sets of points with slightly different interpoint spacing. By various manipulations of these, he determines the magnitude of the traveling wave launched on the cylinder by the incident plane wave, as well as the current in the vicinity of the aperture. However, his analysis is confined to broadside incidence (θ=90^0).

[Bowman (1970)] develops ray-optical diffraction expressions for the scattering from the end (aperture) of the semi-infinite waveguide, and compares these with an asymptotic approximation to the

*Also translated as Vajnshtejin, Wainstein, Vainshtein.

exact Weiner-Hopf solutions. For the asymptotic form of the Wiener-Hopf solution, he obtains, for direct backscatter (θ=0)

$$E^{BS} \sim -\hat{x}\,\frac{a}{2r}\,e^{ikr}\left\{1+\frac{e^{i\pi/4}}{\sqrt{\pi ka}}\sum_{m=1}^{\infty} i^m\, m^{-3/2}\, e^{i2mka}\right\} \qquad (1\text{-}14)$$

whereas by ray optical methods, he obtains

$$E^{BS} \sim -\hat{x}\,\frac{a}{2r}\,e^{ikr}\left\{1+\frac{e^{i\pi/4}}{\sqrt{\pi ka}}\sum_{m=1}^{\infty}\frac{i^m e^{i2mka}}{2^{m-1}\,m}\right\}. \qquad (1\text{-}15)$$

For bistatic scattering with axial incidence he obtains from approximating the Wiener-Hopf solution letting his θ go to $\pi-\theta$ and his ϕ to $2\pi-\phi$

$$E^{S} \sim +\hat{\phi}\,\frac{e^{ikr}}{r}\left(\frac{2a}{\pi k\sin\theta}\right)^{1/2}\frac{\cos(ka\sin\theta-\pi/4)(\sin\phi)}{\cos(\theta/2)}$$

$$\left\{1+\frac{e^{i\pi/4}}{\sqrt{\pi ka}}\,\frac{\cos^2(\theta/2)}{\cos\theta}\sum_{m=1}^{\infty} i^m\, m^{-3/2}\, e^{i2mka}\right\} \qquad (1\text{-}16)$$

From the ray optical approximation he obtains

$$E^{S} \sim +\hat{\phi}\,\frac{e^{ikr}}{r}\left(\frac{2a}{\pi k\sin\theta}\right)^{1/2}\frac{\cos(ka\sin\theta-\pi/4)}{\cos\theta/2}\,\sin\phi$$

$$\left\{1+\frac{e^{i\pi/4}}{\sqrt{\pi ka}}\,\frac{\cos^2(\theta/2)}{\cos\theta}\sum_{m=1}^{\infty}\frac{i^m\, e^{i2mka}}{2^{m-1}\sqrt{m}}\right\}. \qquad (1\text{-}17)$$

In both cases it is seen that the term of $O(ka^{-1/2})$ is identical up to the first two terms in the summation

$$\frac{ie^{i2ka}}{1}+\frac{i^2e^{4ika}}{2^{3/2}}+\frac{i^3e^{i6ka}}{3^{3/2}} \qquad (1\text{-}18a)$$

vs

$$\frac{ie^{i2ka}}{1}+\frac{i^2e^{i4ka}}{2^{3/2}}+\frac{i^3e^{i6ka}}{4\sqrt{3}} \qquad (1\text{-}18b)$$

He attributes this difference to the ray-optical approach, for which he first considered scattering by plane parallel plates; multiple scattering was effected by assuming a cylinder wave was generated from each edge after scattering. This result was then specialized to having a single point participate in the scattering on each edge but not modified to take account of the fact that a cylindrical wave is no longer being emanated from each edge. Beyond this comment, Bowman does not analyze further, since the exact result from the Weiner-Hopf solution instructs us how to modify the ray-optic contribution.

A comparison of Bowman's results with those of Witt and Price is illuminating. If we restrict ourselves to on-axis backscatter and disregard terms due to reflection from the termination, the formula presented by Witt and Price reduces to

$$E^s = -\frac{jka^2}{r} e^{-jkr}\left\{\frac{1}{2} + \sum_{n=0}^{\infty}\sum_{m=1}^{\infty} E_{nm}(v)^2\right\}$$

$$= -jka\ \frac{a}{2r}\ e^{-jkr}\left\{1 + \sum_{n=0}^{\infty}\sum_{m=1}^{\infty} E_{nm}(v)^2\right\}. \qquad (1\text{-}19)$$

We observe that, besides the opposite time convention, there is an additional factor of jka present in the form presented by Witt and Price. They remark that this is recognizable as the physical optics approximation for scattering from a flat conducting disk. Since this is not in agreement with the high frequency behavior of the Weiner-Hopf solution, we conclude that the disk is not a good high frequency model for this problem. In fact, it will be seen later that the disk does adequately model the on-axis scattering of a cylinder terminated by a perfectly conducting plate.

[Moll and Seecamp (1970)] present a more realistic model of the engine geometry. The approach of Witt and Price is used to model the scattering, coupling, and radiation at the duct inlet. The study is confined to TE modes. The termination, however is modeled by two sets of blades, each as shown in Figure 1-4, to simulate the first stage of a compressor. The blades are modeled as being planar (normal to the z axis). The two sets of blades had different numbers of blades and blade widths and assumed varying relative orientations (stator to rotor). The scattering at the termination is modeled by a similar procedure to that at the inlet. The backscattered field is expressed as a sum of modes traveling toward the mouth. The total tangential electric fields must match at points where there are blades. For each incident mode, integrals were taken over the area covered by either set of blades, forcing the fields to vanish. The equations thus obtained are used to solve for the scattering coefficients for modes generated at the termination. Then, the

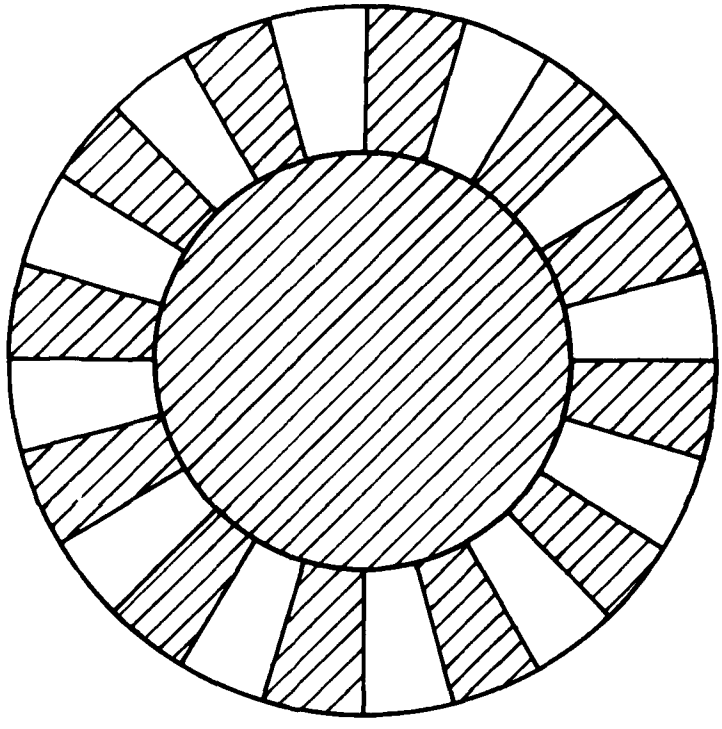

Figure 1-4. Planar engine model used by Moll and Seacamp.

radiation from each mode is computed by matching the radiated field plus the incident field to the internal field at the duct aperture, where the internal field is the sum of the modes traveling down the waveguide plus those scattered back by the termination. The RCS is computed for various orientation of the blade structure and various relative orientations of the two bladed structures, giving a range of modulation of the RCS caused by the rotor motion. They used 31 and 37 blades on the respective blade structures. There is a brief discussion of a non-planar cap in the duct termination, but the idea is not developed.

[Lee et al (1973)] are primarily concerned with the measurement errors made when field strength is measured with a sensor boom. The effect of the presence of the boom is analyzed via the Wiener-Hopf technique, and the relative distortion thus introduced is calculated. The relevant part of this paper deals with the calculation of the Wiener-Hopf factorization functions. Although the general factorization expression is developed (as an infinite product of factors), the general expression is clearly too complex to be useful. A low frequency form is developed for the n=1 case for both L+ and M+ functions. The n=1 case is relevant to low frequencies because the TE_{11} mode has the lowest cutoff frequency, hence is also the slowest decaying evanescent mode when all modes are cut off. Unfortunately the low frequency expression presented do not appear to fit very well with data computed in this dissertation by numerical integration of the exact integral defining the functions. (Lee et al) indicate a constant phase for the low frequency, but it appears that the phase varies rather rapidly as the frequency increases from D.C. The formulas do work out to the correct "DC" form.

[Mittra et al (1974)] present a detailed report which includes reconciliation of the numerical solution with experimental data. The complete Wiener-Hopf solution for the semi-infinite cylinder is presented. There appear to be some errors in the results presented, since the scattering coefficients for direct backscatter (Equation (3-86)) could not be reconciled with those presented by [Bowman (1970)]; also the two direct polarization solutions for $S_{\theta\theta}$ and $S_{\phi\phi}$ do not reduce to the same answer on axis, nor do they reduce to the answer given by [Einarsson et al(1966)] for on axis backscatter (Equation (5-63)). The solution for large pipes is simplified by an asymptotic approximation for the L+ and M+ functions; these are expressed as functions of the series

$$\sum_{m=1}^{\infty} m^{-3/2} e^{im(2ka-n\pi+\pi/2)} \qquad (1\text{-}20)$$

and the same summation, including either even terms or odd terms.

The Generalized Scattering Matrix Technique (GSMT) is used to formulate the problem. Considerable effort is expended expressing the individual elements of the matrix in terms of the Wiener-Hopf solution.

Solutions for other geometries are developed by the ray-optical method. The geometries considered are an ellipsoid, elliptical plate, and semi-infinite elliptical cylinder. The semi-infinite elliptical cylinder is analyzed in terms of diffraction by the edge of the cylinder.

These solutions are then combined to estimate the total RCS for an aircraft. Numerical results were computed for selected fixed frequencies for two aircraft. For calculations involving a termination in the jet intake, this was modeled earlier as a perfect conductor, or as a dielectric plug of infinite depth, or as a dielectric plug of finite depth.

[Chuang et al (1975)] present an extension of the report by [Mittra et al (1973)]. Starting with the exact solution for bistatic scattering from a semi-infinite pipe, they develop approximate high frequency expressions for the factorization function, based on an asymptotic evaluation of the integral defining these functions. Both factorization functions can be rather simply expressed in terms of a third function, called a modified Lerch function of order 3/2,

$$L(x,v) = \sum_{m=1}^{\infty} m^{-v} e^{i2\pi mx} \qquad (1\text{-}21)$$

They then derive via the Mellin transformation a twelve-term series representation with complex coefficients, which enables the computation of this function for $v = 3/2$ to be mechanized trivially. The results thus obtained show excellent agreement with results obtained by direct numerical integration of the defining integral, down to the cutoff frequency of the lowest mode of that order. Finally there is a simplification of the infinite sum which is present in the scattering calculation mode by use of the asymptotic form with one of the Bessel function addition theorems.

There appear to be a few errors in this paper. These are summarized in Appendix B.

[James and Greene (1978)] indicate that both theoretical and experimental results show substantial sensitivity to wall thickness. They indicate that the exact Wiener-Hopf solution based on infinitely thin walls breaks down when the wall thickness is larger than $.01\lambda$. The results of their summary seems to be that the radiation patterns of thick walled pipes are narrower than given by the Wiener-Hopf solution. Beyond noting this effect, we will not further discuss this problem, since it would require an entirely separate study.

CHAPTER II
DISCUSSION OF WIENER-HOPF SOLUTION

The exact Wiener-Hopf solution to the diffraction by a semi-infinite circular waveguide can be found in [Einarsson et al (1966)]. The significant formulas from this report are summarized in Appendix B. The major numerical problem -- that of calculating the factorization functions -- is discussed at length in Appendix A. This chapter discusses the physical significance of some of these formulas. We reiterate that the $e^{-i\omega t}$ time dependence is assumed and suppressed.

The coordinate system is a substantial stumbling block since the incident and scattered field are defined with respect to $\hat{\theta}$ and $\hat{\phi}$ unit vectors which are themselves functions of angle. Further complicating matters, [Einarsson et al (1966)] and [Mittra et al (1974)] use different coordinate systems. This study uses the coordinate system illustrated in Figure 2-1, which is the same as [Mittra et al (1974)], since it forms a self-consistant reference for scattering calculations.

The incident field is assumed to come from the angle $\phi_i=\pi$. Looking in along the y-axis toward the origin, we see Figure 2-2. Looking in along the x-axis toward the origin we see Figure 2-3. Hence we obtain the following unit vectors.

$$\hat{\theta} = -\hat{x}\cos\theta_i - \hat{z}\sin\theta_i \qquad (2\text{-}1a)$$

$$\hat{\phi} = -\hat{y} \quad . \qquad (2\text{-}1b)$$

For the scattered field, we are not necessarily constrained to $\phi_s=\pi$ (for bistatic scattering). Hence, we obtain general formulas for the unit vectors.

$$\hat{\theta} = \hat{x}\cos\theta_s\cos\phi_s + \hat{y}\cos\theta_s\sin\phi_s - \hat{z}\sin\theta_s \qquad (2\text{-}2a)$$

$$\hat{\phi} = -\hat{x}\sin\phi_s + \hat{y}\cos\phi_s \quad . \qquad (2\text{-}2b)$$

In our coordinate system, the incident and scattered fields are in the same coordinate system. In [Einarsson et al (1966)], the direction of the z-axis is reversed, but θ_i and the unit vectors for the inci-

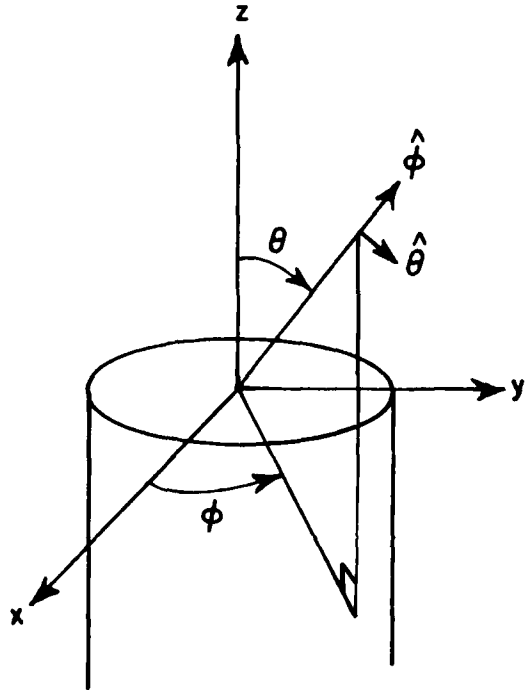

Figure 2-1. Coordinate system for Wiener-Hopf solution to semi-infinite cylinder.

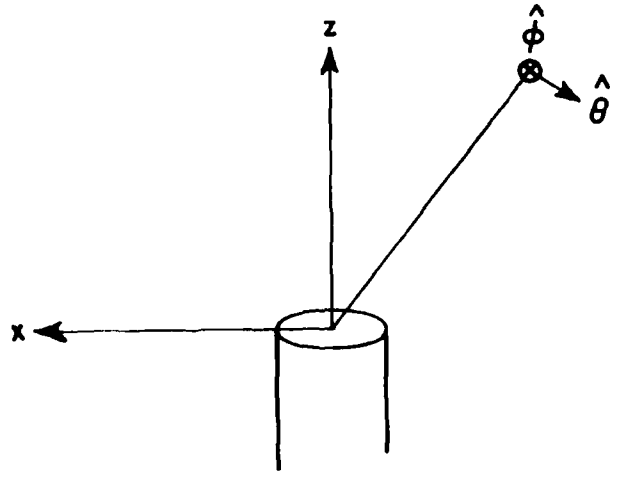

Figure 2-2. Coordinate system looking at origin from positive Y-axis.

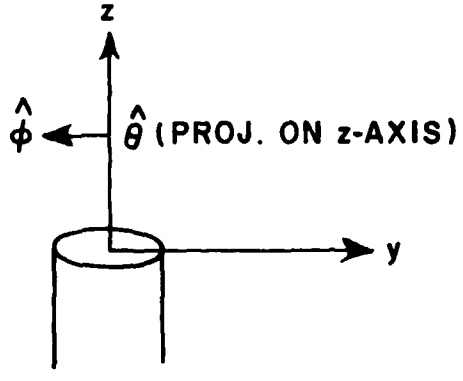

Figure 2-3. Coordinate system looking at origin from positive X-axis.

dent field are defined in such a way that they physically point in the same direction as in our system. Thus $\cos\theta_i$, $\sin\theta_i$, E^i_θ, E^i_ϕ are all the same in Einarsson's and our coordinate systems. (See Figure 2-2 in Einarsson; E^i_θ occurs for $\beta=0$, E^i_ϕ for $\beta = \frac{\pi}{2}$ with α being replaced by θ_i). In the scattered coordinate systems, $\hat{\theta}$ and $\hat{\phi}$ are reversed in sign (hence also E_θ and E_ϕ), and $\cos\theta_s$ has the opposite sign, but $\sin\theta_s$ is unchanged. In addition ϕ_s is replaced by $-\phi_s$ since the x-axis is the same in the two systems.

A. On-axis Results

The most elementary case of the Wiener-Hopf solution can be found by taking the limit as $\theta \to 0$. In taking this limit we will consider both the backscatter and coupling of energy into the waveguide.

Taking the limit of Equation (B-3) (which gives the general bistatic scattering from the rim for $\hat{\theta}$ incident and scattered fields) with $\phi_s=\pi$, $\theta_i=\theta_s=\delta$ (in the limit $\delta\to 0$) we obtain

$$S_{00} = \lim_{\delta\to 0} \frac{-2i}{k} \sum_{n=0}^{\infty} \varepsilon_n (-1)^n \frac{\left[J_n(ka\delta)\right]^2}{\delta^2\left[L_+(k)\right]^2} \left[\frac{\delta^2\cdot\delta^2}{16} - \frac{f_n^2}{1-f_n^2}\right] \quad (2\text{-}3)$$

where

ε_n = Neumann epsilon = 1; n=0
= 2; n≠0

$J_n()$ is the cylindrical bessel function of the first kind

k is the wavenumber = $\frac{2\pi}{\lambda}$

a is the pipe radius.

L+, M+ are the factorization functions; these are functions of (n,α,k); k is always understood and n is usually obvious from the context. Hence the only argument that is explicitly given is α. L+(k) means L+(n,α=k,k)

f_n = nL+(k)/2kaM+(k)

$$S_{00} = \lim_{\delta\to 0} \frac{-2i}{k\delta^2} \sum_{n=1}^{\infty} \frac{2(-1)^n (ka\delta)^{2n}}{2^{2n}\left[L+(k)\right]^2} \left(-\frac{f_n^2}{1-f_n^2}\right) \quad (2\text{-}4a)$$

$$= \frac{2i}{k} \frac{2(-1)(ka)^2}{4\left[L+(k)\right]^2} \frac{f_1^2}{1-f_1^2} \quad (2\text{-}4b)$$

$$= \frac{ia^2k}{4k^2a^2M_+(k)^2 - L_+(k)^2} \quad (n=1 \text{ understood}) \qquad (2\text{-}4c)$$

since f_0 is identically 0.

When combined with Equation (B-2), we obtain

$$\frac{E^s}{E^i} = \frac{e^{ikr}}{r} \cdot \frac{-ia^2k}{4k^2a^2M_+(k)^2 - L_+(k)^2} \quad (n=1 \text{ understood}) \qquad (2\text{-}5)$$

This can be seen to be the same as Equation (5-163) of [Einarsson (1966)] with $r \to z$; the same procedure applied to $S_{\phi\phi}$ (which gives the general bistatic scattering from the rim for $\hat{\phi}$ incident and scattered fields) leads to exactly the same result.

$$S_{\phi\phi} = \lim_{\delta \to 0} \frac{2i}{4k} \sum_{n=0}^{\infty} \varepsilon_n (-1)^n \frac{\left[J_n'(ka\delta)\right]^2}{\left[M_+(k)\right]^2} \left(\frac{2 \cdot 2}{2 \cdot 2} + \frac{f_n^2}{(1-f_n^2)} \right) \qquad (2\text{-}6a)$$

$$= \frac{2i}{4k} 2(-1) \frac{(1/2)^2}{(M_+(k))^2} \left[1 + \frac{f_1^2}{1-f_1^2} \right] \qquad (2\text{-}6b)$$

$$= \frac{-i}{4kM_+(k)^2(1-f_1^2)} \qquad (2\text{-}6c)$$

$$= \frac{-ia^2k}{4k^2a^2M_+(k)^2 - L_+(k)^2} \quad (n=1 \text{ understood}) \qquad (2\text{-}6d)$$

We see immediately from Equations (B-5) and (B-6) (which give the cross-polarized backscatter) that sin $n\pi$=0 so no cross-polarized field is generated.

The radar cross-section is defined by

$$\sigma = \lim_{r \to \infty} 4\pi r^2 \left| \frac{E^s}{E^i} \right|^2 \qquad (2\text{-}7)$$

Applying Equation (2-5), we obtain

$$\sigma = \lim_{r\to\infty} 4\pi r^2 \left| \frac{1}{r} \frac{a^2k}{(4k^2a^2M+(k)^2-L+(k)^2} \right|^2 \qquad (2\text{-}8a)$$

$$= 4\pi \left| \frac{a^2k}{4k^2a^2M+(k)^2-L+(k)^2} \right|^2 \qquad (2\text{-}8b)$$

$$\frac{\sigma}{\pi a^2} = \left| \frac{2ak}{4k^2a^2M+(k)^2-L+(k)^2} \right|^2 \qquad (2\text{-}9)$$

The results of Equation (2-9) are evaluated and plotted in Figure 2-4. It is of interest to note that the normalized cross-section peaks at $D/\lambda=.55$, with $\sigma/\pi a^2=10.4$ dB, and then decreases very rapidly. The lowest order propagating mode (TE11) is enabled at $D/\lambda=.586$; hence this peak occurs just below cutoff for this mode, and as the mode is able to transport energy, the cross section rapidly decreases. The first three peaks and corresponding modes are summarized in Table 2-1.

TABLE 2-1
SUMMARY OF ON-AXIS RCS PEAKS AND MODE ACTIVITY

Location of peak (D/λ)	Height of peak (dB)	Cutoff for mode (D/λ)	Mode
.55	10.4	.586	TE11
1.68	3.5	1.697	TE12
2.69	2.5	2.717	TE13

The rapid variation of cross section in these regions is related to the strong coupling of the normally incident plane wave to the $TE_{l,m}$ modes, as discussed below.

[Bowman (1970)] and [Chuang et al (1975)] use their asymptotic forms for L+ and M+ to obtain a simple form for the on-axis cross section.

$$S_{00} \sim \frac{-a}{2} \left[1 + \frac{e^{i\pi/4}}{\sqrt{\pi ka}} \sum_{n=1}^{\infty} i^m{}_m{}^{-1.5} e^{i2mka} \right] . \qquad (2\text{-}10)$$

This leads to

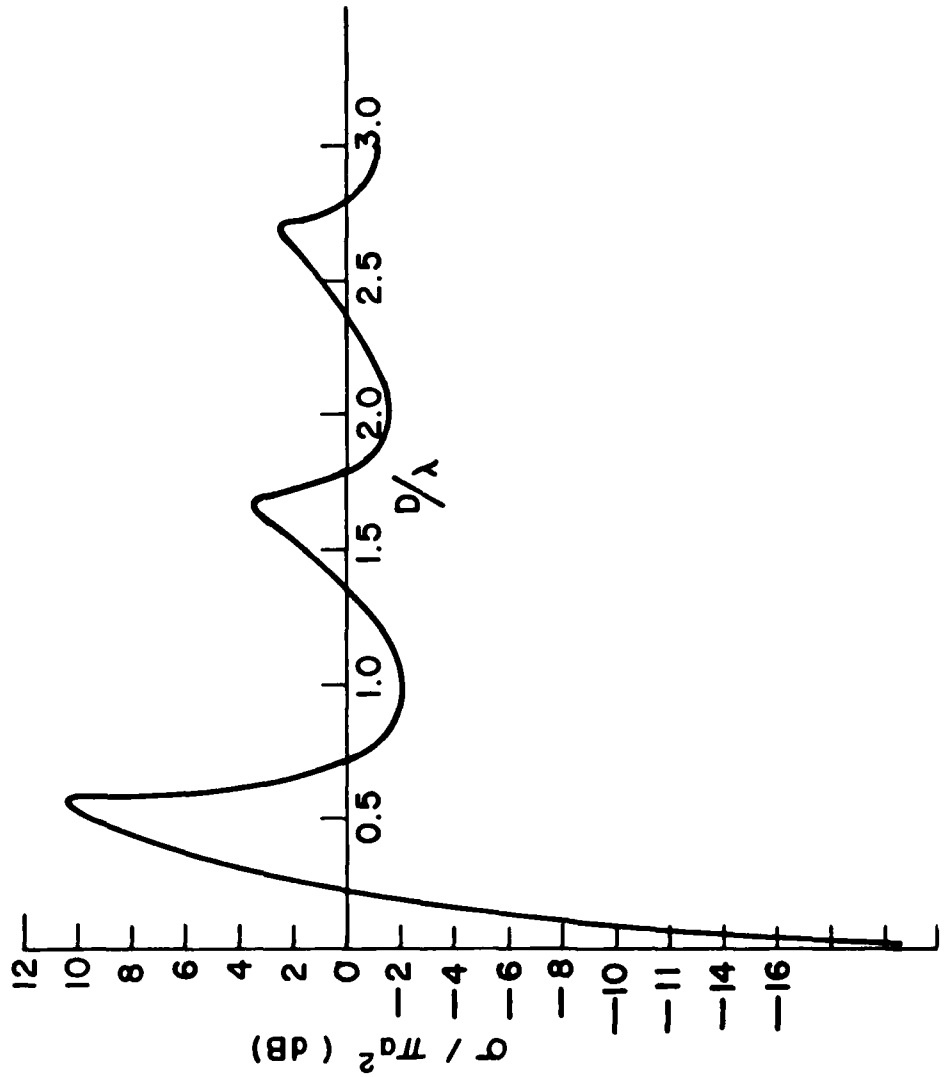

Figure 2-4. On-axis cross section for semi-infinite cylinder exact (from numerical integration).

$$\frac{\sigma}{\pi a^2} \sim \left| 1 + \frac{e^{i\pi/4}}{\sqrt{\pi ka}} \sum_{m=1}^{\infty} i^{m} m^{-1.5} e^{i2mka} \right|^2 \qquad (2\text{-}11)$$

Equation (2-11) is plotted in Figure 2-5 and yields good results for $D/\lambda > 1$.

Taking the inverse Fourier transform of Equation (2-5) with the spatial dependence suppressed, we obtain the time domain response, shown in Figure 2-6. This represents the backscattered field as a time function resulting from a normally incident plane wave, impulsive in time. This result was generated via the discrete Fourier transform of the backscattered formula for $0 < D/\lambda < 3.2$. Naturally the time domain response is dominated by the peak at $D/\lambda = .55$, which results in damped oscillations. The time domain response can be related (perhaps dubiously at low frequencies) to a ray optic model of scattering at the mouth. The optic model was developed by [Bowman (1970)]. For example, if we take the simplest asymptotic approximation for the L+ and M+ functions, given by Equations (A-27), (A-29), (A-31), (A-58) and (A-59), and substitute them into Equation (2-5), suppressing the spatial decay and propagation,

$$\frac{E^s}{E^i} = \frac{1}{4\pi} \frac{-4\pi i a^2 k}{4k^2 a^2 M+(k)^2 - L+(k)^2} \qquad (2\text{-}12)$$

retaining only terms of $O(1)$ and $O(ka^{-1/2})$, with a unit incident field

$$E^s \sim \frac{-a}{2} \left[1 + \frac{e^{i\pi/4}}{\sqrt{\pi ka}} \sum_{m=1}^{\infty} \frac{(-1)^m e^{i2m(ka-\pi/4)}}{m^{3/2}} \right] \qquad (2\text{-}13)$$

$$E^s \sim \frac{-a}{2} \left[1 + \sqrt{\frac{c}{\pi a}} \sum_{m=1}^{\infty} \frac{e^{i\pi/2(m+1/2)} e^{i\frac{2ma\omega}{c}}}{\sqrt{\omega}\ m^{3/2}} \right] \qquad (2\text{-}14)$$

Taking the first few terms of the summation explicitly

$$E^s \sim \frac{-a}{2} \left[1 + \sqrt{\frac{c}{\pi a}} \left(\frac{e^{i\frac{3\pi}{4}} e^{\frac{i2a\omega}{c}}}{\sqrt{\omega}} + \frac{e^{i\frac{5\pi}{4}} e^{\frac{i4a\omega}{c}}}{2\sqrt{2}\sqrt{\omega}} + \frac{e^{i\frac{7\pi}{4}} e^{\frac{i6a\omega}{c}}}{3\sqrt{3}\sqrt{\omega}} \right) \right] \qquad (2\text{-}15)$$

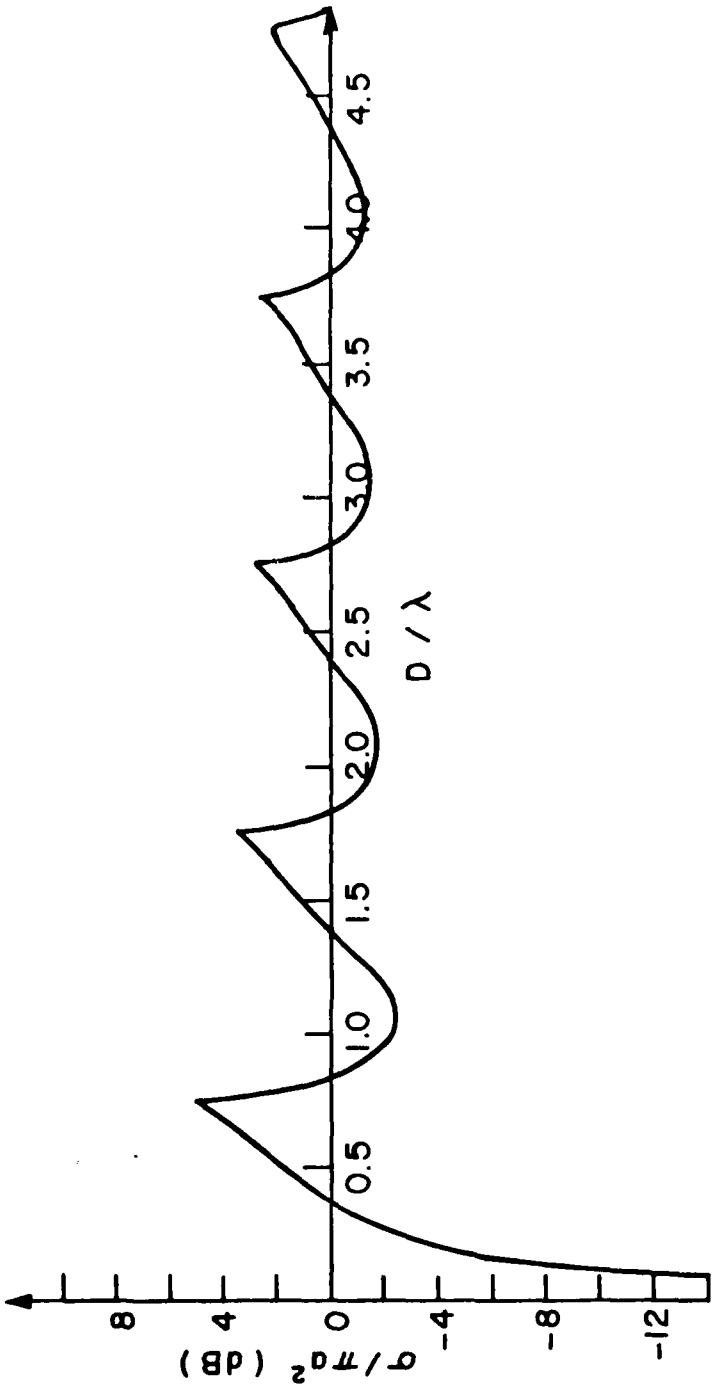

Figure 2-5. On-axis cross section for semi-infinite cylinder based on simple asymptotic approximations.

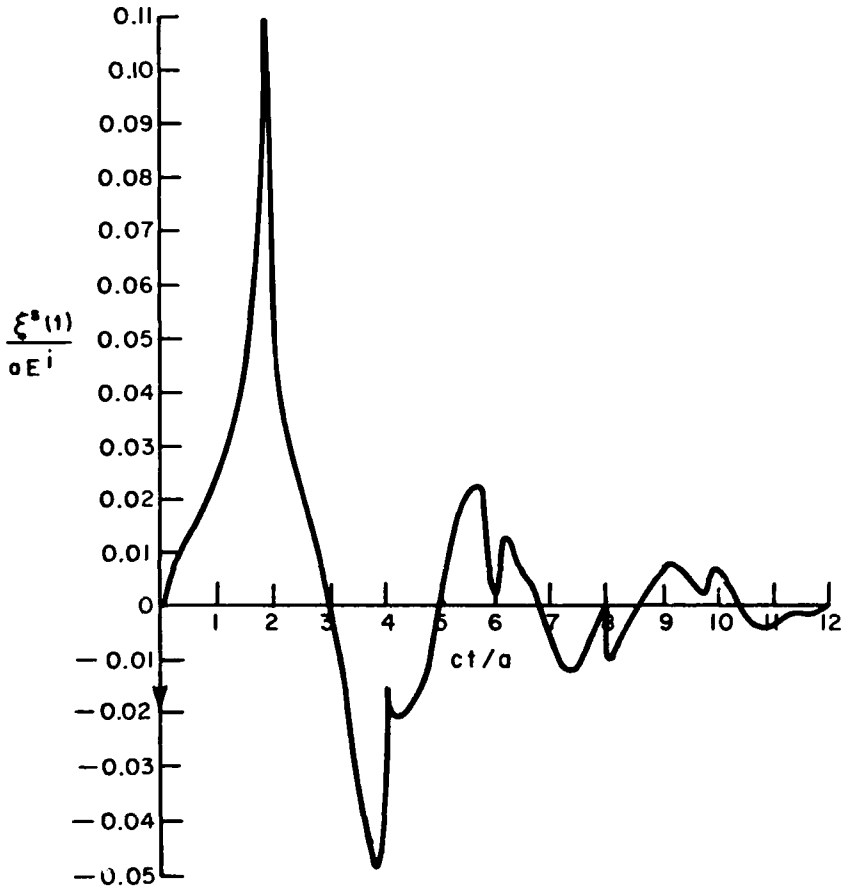

Figure 2-6. Inverse Fourier transform of "exact" on-axis backscatter with weighting to reduce Gibbs-type ringing.

Note that $e^{\frac{i2am\omega}{c}}$ results in a time delay of $\frac{2am}{c}$. We employ the Fourier transform pair

$$\frac{1}{\sqrt{\omega}} \longleftrightarrow \frac{u(t)}{\sqrt{2\pi t}} \tag{2-16a}$$

and its Hilbert transform

$$\frac{i}{\sqrt{\omega}} \longleftrightarrow \frac{-u(-t)}{\sqrt{-2\pi t}} \tag{2-16b}$$

Taking the transform of the frequency domain expression

$$E^S \backsim \frac{-a}{2}\left[1 + \sqrt{\frac{c}{2\pi a}}\left(\frac{(-1+i)}{\sqrt{\omega}} e^{i\frac{2a\omega}{c}} + \frac{(-1-i)}{2\sqrt{2}\sqrt{\omega}} e^{i\frac{4a\omega}{c}} + \frac{(1-i)e^{i\frac{6a\omega}{c}}}{3\sqrt{3}\sqrt{\omega}}\right)\right] \tag{2-17}$$

leads to

$$E^S(t) \backsim \frac{-a}{2}\left[\delta(t) + \frac{1}{2\pi}\sqrt{\frac{c}{a}}\left(-\frac{u(t-\frac{2a}{c})}{\sqrt{t-\frac{2a}{c}}} - \frac{u(\frac{2a}{c}-t)}{\sqrt{\frac{2a}{c}-t}}\right.\right.$$

$$\left.\left. - \frac{u(t-\frac{4a}{c})}{2\sqrt{2}\sqrt{t-\frac{4a}{c}}} + \frac{u(\frac{4a}{c}-t)}{2\sqrt{2}\sqrt{\frac{4a}{c}-t}} + \frac{u(t-\frac{6a}{c})}{3\sqrt{3}\sqrt{t-\frac{6a}{c}}} + \frac{u(\frac{6a}{c}-t)}{3\sqrt{3}\sqrt{\frac{6a}{c}-t}}\right)\right] \tag{2-18}$$

This is plotted in Figure 2-7.

We note in Figure 2-6 that the sharp peaks at $t=m.\frac{2a}{c}$ become almost negligible after m=3, and the response shown in the discrete Fourier transform results seems to be dominated by the ringing associated with the lowest frequency resonance. Since this resonance is not well predicted by the asymptotic forms (compare Figures 2-4 and 2-5) it is not surprising that the long-time or steady-state response is not well predicted. This resonance appears to be related to the currents excited at the mouth, and to some extent, associated with an exterior natural resonance of the cylinder, since all the waveguide modes are evanescent in this region.

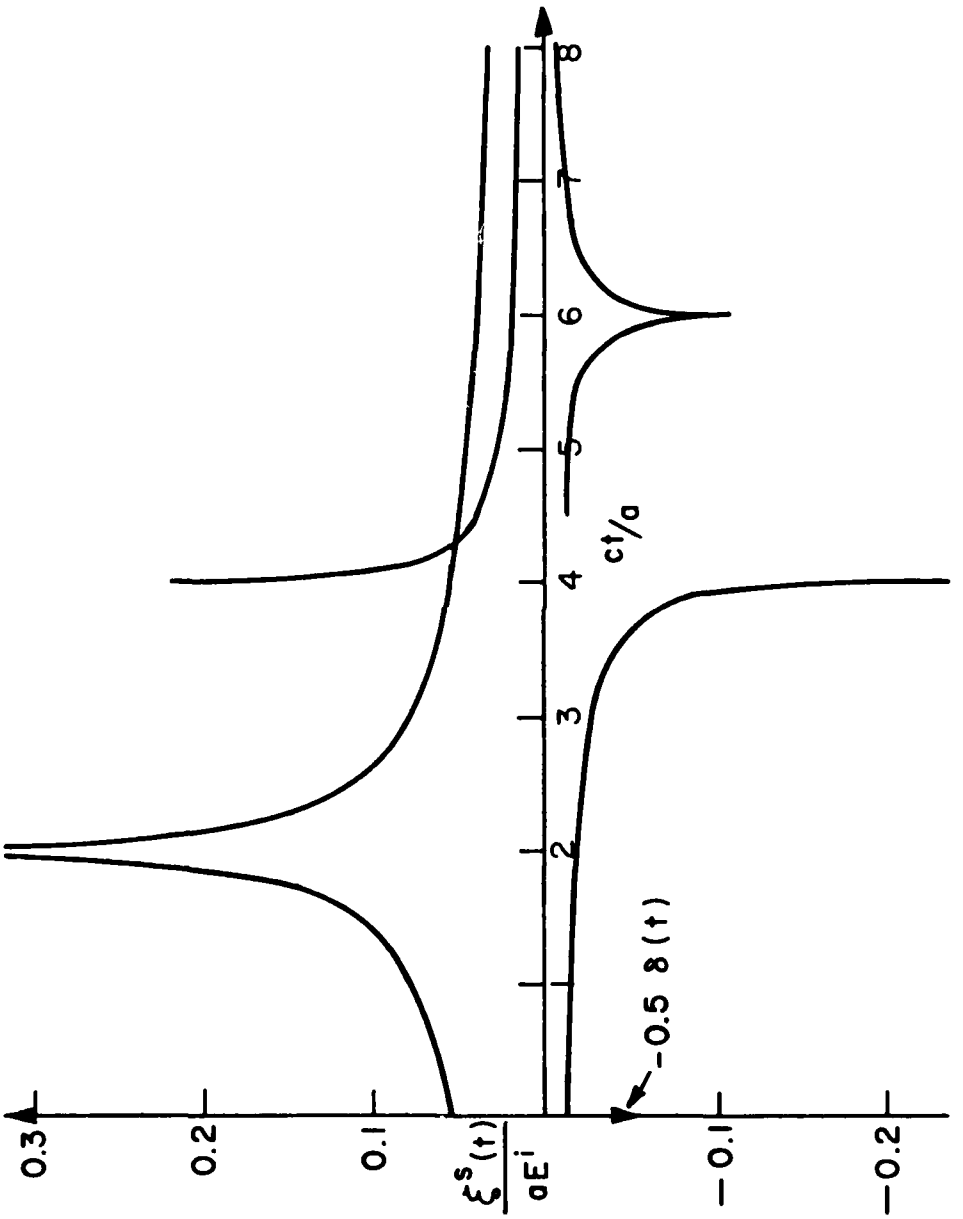

Figure 2-7. Inverse Fourier transform of asymptotic on-axis backscatter.

The coupling of an axially incident plane wave to waveguide modes can be determined from a special case of equations (B-11) thru (B-14) (which give the general coupling coefficients for incident plane waves). Taking $\theta_i \to 0$ we see immediately that only n=1 modes are excited.

$$A^0_{1m} = -\frac{4ij_{nm}L^+(\alpha_{1m})}{\alpha_{1m}aL^+(k)} \cdot \frac{1}{2}\left[\frac{f_1^2}{1-f_1^2}\right] = -\frac{2ij_{1m}L^+(\alpha_{1m})}{\alpha_{1m}aL^+(k)} \cdot \frac{f_1^2}{1-f_1^2} \tag{2-19a}$$

$$A^\phi_{1m} = -\frac{4ij_{nm}L^+(\alpha_{1m})}{k\alpha_{1m}a^2 2M^+(k)} \cdot \frac{1}{2}\,\frac{f_1}{1-f_1^2} = -\frac{2ij_{1m}L^+(\alpha_{1m})}{\alpha_{1m}aL^+(k)} \cdot \frac{f_1^2}{1-f_1^2} \tag{2-19b}$$

$$B^0_{1m} = \frac{4i(k+\alpha'_{1m})}{\alpha'_{1m}\left(1-\frac{1}{j'^2_{1m}}\right)}\;\frac{M^+(\alpha'_{1m})}{L^+(k)}\;\frac{1}{2}\;\frac{f_1}{1-f_1^2}$$

$$= \frac{i(k+\alpha'_{1m})M^+(\alpha'_{1m})}{ka\alpha'_{1m}\left(1-\frac{1}{j'^2_{1m}}\right)M^+(k)} \cdot \frac{1}{1-f_1^2} \tag{2-19c}$$

$$B^\phi_{1m} = -\frac{4i(k+\alpha'_{1m})M^+(\alpha'_{1m})}{k\alpha'_{1m}a\left(1-\frac{1}{j'^2_{1m}}\right)2M^+(k)} \cdot \frac{1}{2}\left[\frac{f_1^2}{1-f_1^2} + \frac{k-\alpha'_{1m}}{k-\alpha'_{1m}}\right]$$

$$= -\frac{i(k+\alpha'_{1m})M^+(\alpha'_{1m})}{k\alpha'_{1m}a\left(1-\frac{1}{j'^2_{1m}}\right)M^+(k)} \cdot \frac{1}{1-f_1^2} \tag{2-19d}$$

In both TE and TM cases, rotation of the incident field from $\hat{\theta}$ to $\hat{\phi}$ corresponds to an equal rotation of the azimuthal dependence of the waveguide mode; otherwise the coupling coefficients are the same.

For purposes of comparing the relative importance of these coupling coefficients, the power flow associated with each of the modes can be computed. For TE modes, with an incident plane wave of unit amplitude based on [Collin (1960), p. 179] the power flow is computed as

$$P = \frac{1}{2}\sqrt{\frac{\mu_o}{\epsilon_o}}\, k\alpha'_{nm}\left(\frac{a}{j'_{nm}}\right)^2 \iint |H_z(\rho,\phi)|^2\, da \qquad (2\text{-}20a)$$

$$= \frac{1}{2}\sqrt{\frac{\mu_o}{\epsilon_o}}\, k\alpha'_{nm}\left(\frac{a}{j'_{nm}}\right)^2 \int_0^{2\pi}\int_0^{a} \frac{\epsilon_o}{\mu_o}\, \frac{J_n(j'_{nm}\rho/a)^2}{J_n(j'_{nm})^2} \cos^2 n\phi\, |B_{nm}|^2 \rho\, d\rho\, d\phi \qquad (2\text{-}20b)$$

$$= \frac{1}{2}\sqrt{\frac{\epsilon_o}{\mu_o}}\, k\alpha'_{nm}\left(\frac{a}{j'_{nm}}\right)^2 |B_{nm}|^2 \pi \frac{}{J_n(j'_{nm})^2} \int_0^{a} J_n(j'_{nm}\rho/a)^2 \rho\, d\rho \qquad (2\text{-}20c)$$

$$= \frac{\pi}{2}\sqrt{\frac{\epsilon_o}{\mu_o}}\, k\alpha'_{nm}\left(\frac{a}{j'_{nm}}\right)^2 |B_{nm}|^2 \frac{}{J_n(j'_{nm})^2} \frac{1}{2}\left[\left(a^2 - \frac{n^2 a^2}{j'^2_{nm}}\right) J_n(j'_{nm})^2\right] \qquad (2\text{-}20d)$$

$$P = \frac{\pi}{4}\sqrt{\frac{\epsilon_o}{\mu_o}}\, \frac{(ka)(\alpha'_{nm}a)a^2}{(j'_{nm})^2}\left(1 - \frac{n^2}{j'^2_{nm}}\right)|B_{nm}|^2 \qquad (2\text{-}20e)$$

We assumed a unit incident field, which has an incident power density of $\frac{1}{2}\sqrt{\frac{\epsilon_o}{\mu_o}}\, E^{i\,2} = \frac{1}{2}\sqrt{\frac{\epsilon_o}{\mu_o}}$, so the normalized power flow becomes (normalized to the average power flow and the area of the waveguide mouth)

$$\frac{P}{\left(\frac{1}{2}\sqrt{\frac{\epsilon_o}{\mu_o}}\right)(\pi a^2)} = \frac{1}{2}\,\frac{(ka)(\alpha'_{nm}a)}{(j'_{nm})^2}\left(1 - \frac{n^2}{j'^2_{nm}}\right)|B_{nm}|^2 \qquad (2\text{-}21)$$

Similarly, for TM modes, we obtain

$$P = \frac{1}{2}\sqrt{\frac{\epsilon_o}{\mu_o}}\, k\alpha_{nm}\left(\frac{a}{j_{nm}}\right)^2 \iint |E_z|^2\, da \tag{2-22a}$$

$$= \frac{1}{2}\sqrt{\frac{\epsilon_o}{\mu_o}}\, k\alpha_{nm}\left(\frac{a}{j_{nm}}\right)^2 \int_0^{2\pi}\int_0^{a} \frac{J_n(j_{nm}\rho/a)^2}{J_n'(j_{nm})^2} \cos^2 n\phi |A_{nm}|^2 \rho d\rho d\phi \tag{2-22b}$$

$$= \frac{1}{2}\sqrt{\frac{\epsilon_o}{\mu_o}}\, \frac{k\alpha_{nm}\left(\frac{a}{j_{nm}}\right)^2 \pi |A_{nm}|^2}{J_n'(j_{nm})^2} \int_0^{a} J_n(j_{nm}\rho/a)^2 \rho d\rho \tag{2-22c}$$

$$= \frac{\pi}{2}\sqrt{\frac{\epsilon_o}{\mu_o}}\, \frac{k\alpha_{nm}\left(\frac{a}{j_{nm}}\right)^2 |A_{nm}|^2}{J_n'(j_{nm})^2}\, \frac{1}{2}\left[a^2 J_n'(j_{nm})^2\right] \tag{2-22d}$$

$$\frac{P}{\left(\frac{1}{2}\sqrt{\frac{\epsilon_o}{\mu_o}}\,(\pi a^2)\right)} = \frac{1}{2}\,\frac{(ka)(\alpha_{nm}a)}{j_{nm}^2}\,|A_{nm}|^2 \tag{2-23}$$

The power flow coefficients are plotted in Figure 2-8 for the first three TE_{1m} and TM_{1m} modes, for axially incident plane waves.

The reason for the behavior of the on-axis cross section becomes somewhat clearer, since we see that the TE_{1m} modes all couple much more strongly to the axially incident plane wave than the TM_{1m} modes. Hence, the region in which they are enabled exhibits a much more dramatic variation due to the size of the change of power absorbed. [Weinstein (1969), p. 151] discusses this behavior and proves that asymptotically the optical cross section equals the sum of the absorption cross sections for the TE_{1m} modes. Figure 2-8 can be compared with Weinstein's Figure 53.

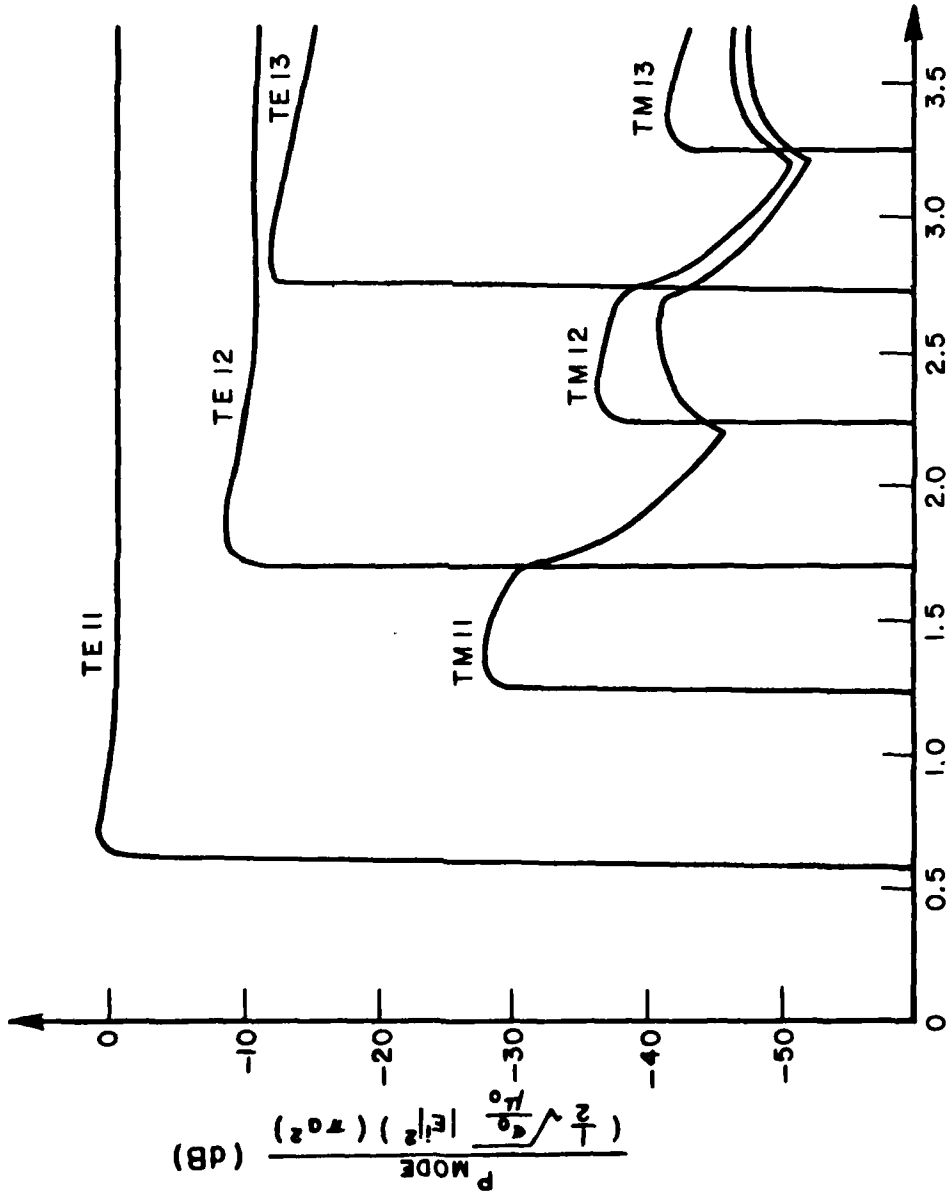

Figure 2-8. Coupling of on-axis incident plane wave to various waveguide modes - normalized power flow.

B. Off-axis Behavior

The radiation patterns of the various waveguide modes have been produced in the literature; all that is produced here are a few curves for comparison. Figures 2-9 and 2-10 with ka=4 can be compared with [Weinstein (1969)] Figures 46 and 48. Figure 2-11 and 2-12 with ka=12.77 can be compared with [Narasimhan (1979)].

Of more practical importance is the relationship of these radiation patterns to radar cross-section. As is discussed in Section II-C, the radiation pattern of a single waveguide mode in a certain direction can be seen, by reciprocity, to be directly proportional to the coupling of an incident plane wave from that direction to the appropriate waveguide mode. If, for the moment, we assume that the cylinder is terminated with a perfectly conducting flat wall, each propagating mode will be reflected back to the waveguide mouth unattenuated. For a monostatic radar system, this will mean that at some angle, which happens to couple well to a particular waveguide mode, that waveguide mode will radiate equally well in that direction. Therefore, it becomes of considerable importance to know the directions and relative strengths of the coupling coefficients of the various waveguide modes. Obviously, for θ=0, we can see from Figure 2-8 that the TE_{11} mode dominates all others. From Table 1-1 we see that, for increasing waveguide diameters, the TM_{01}, TE_{21}, TM_{11}, TE_{01} are the next modes to propagate. In a manner analogous to Figure 2-8, the relative importance to radar cross-section for these modes is shown in Figure 2-13. However, Figure 2-13 differs in that the direction is varied for each mode so that the incident field is assumed to come from the optimum direction. This direction is plotted in Figure 2-14. For example, for D/λ=1.5, the TE_{01} has a maximum for E_ϕ at 30^o, the TM_{01} and TE_{21} modes also have maxima at 30^o, but for E_θ. However, the relative magnitudes are 0.7, -6.8, and 1.0 dB, respectively. Figure 2-13 might be termed the cavity cross-section, since it is the contribution to the RCS which coupling to and radiation from a single mode would produce, assuming that only that mode contributed to backscatter. Naturally, this is not true, as other modes will contribute to some extent, as well as the direct backscatter from the rim. We see that for on-axis scattering, the "cavity cross-section" produced by the TE_{11} mode is remarkably similar to that of the disk.

For an incident plane wave, we have from Equations (B-9) and (B-10) (which give the coupling of incident plane waves to the axial waveguide field)

$$\begin{Bmatrix} E_z/E_i \\ \sqrt{\frac{\mu_o}{\epsilon_o}}\, H_z/E_i \end{Bmatrix} = \begin{Bmatrix} A_{nm}^{\theta,\phi}(\theta_i,\phi_i) f(\rho,\phi,z) \\ B_{nm}^{\theta,\phi}(\theta_i,\phi_i) g(\rho,\phi,z) \end{Bmatrix} \qquad (2\text{-}24)$$

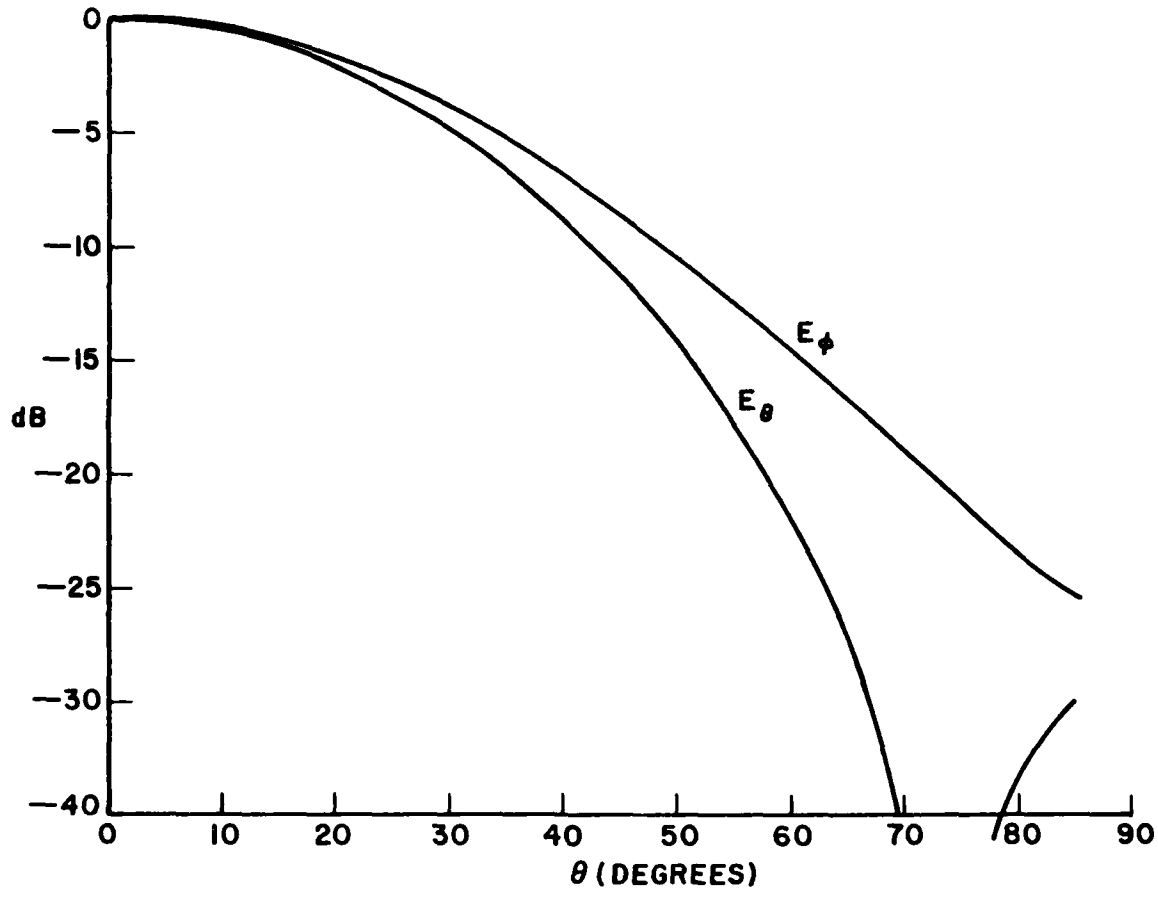

Figure 2-9. Radiation pattern for TE_{11} mode with ka=4 (D/λ=1.273).

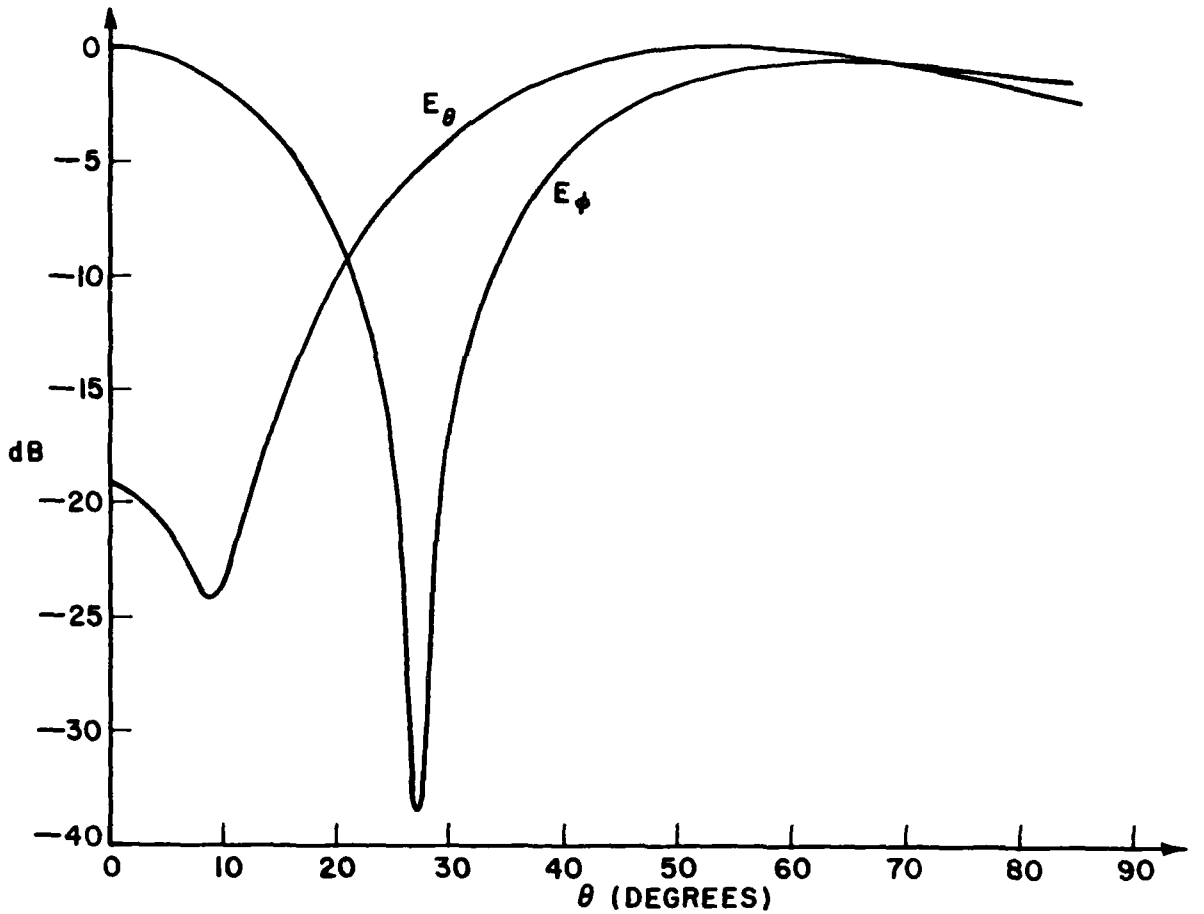

Figure 2-10. Radiation pattern for TM_{11} mode with ka=4 (D/λ=1.273).

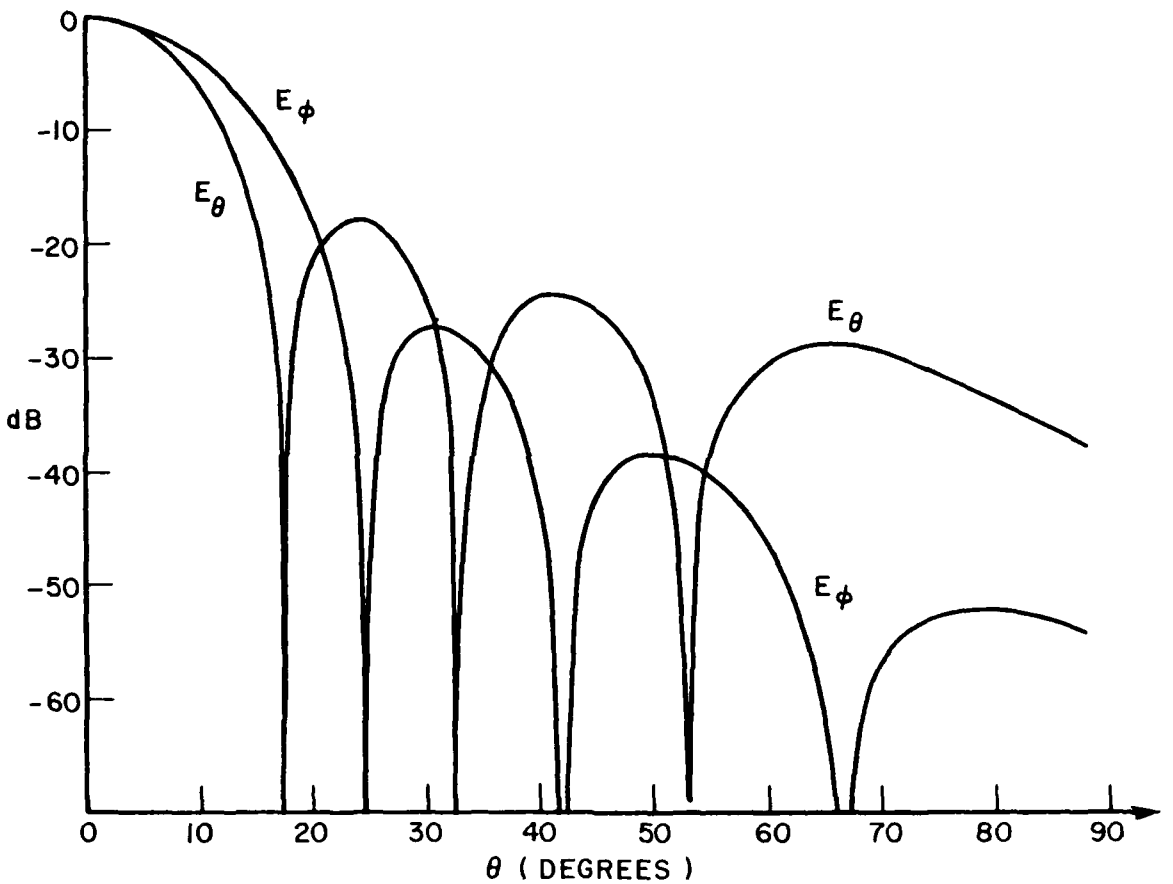

Figure 2-11. Radiation pattern for TE_{11} mode with ka=12.77 (D/λ=4.065).

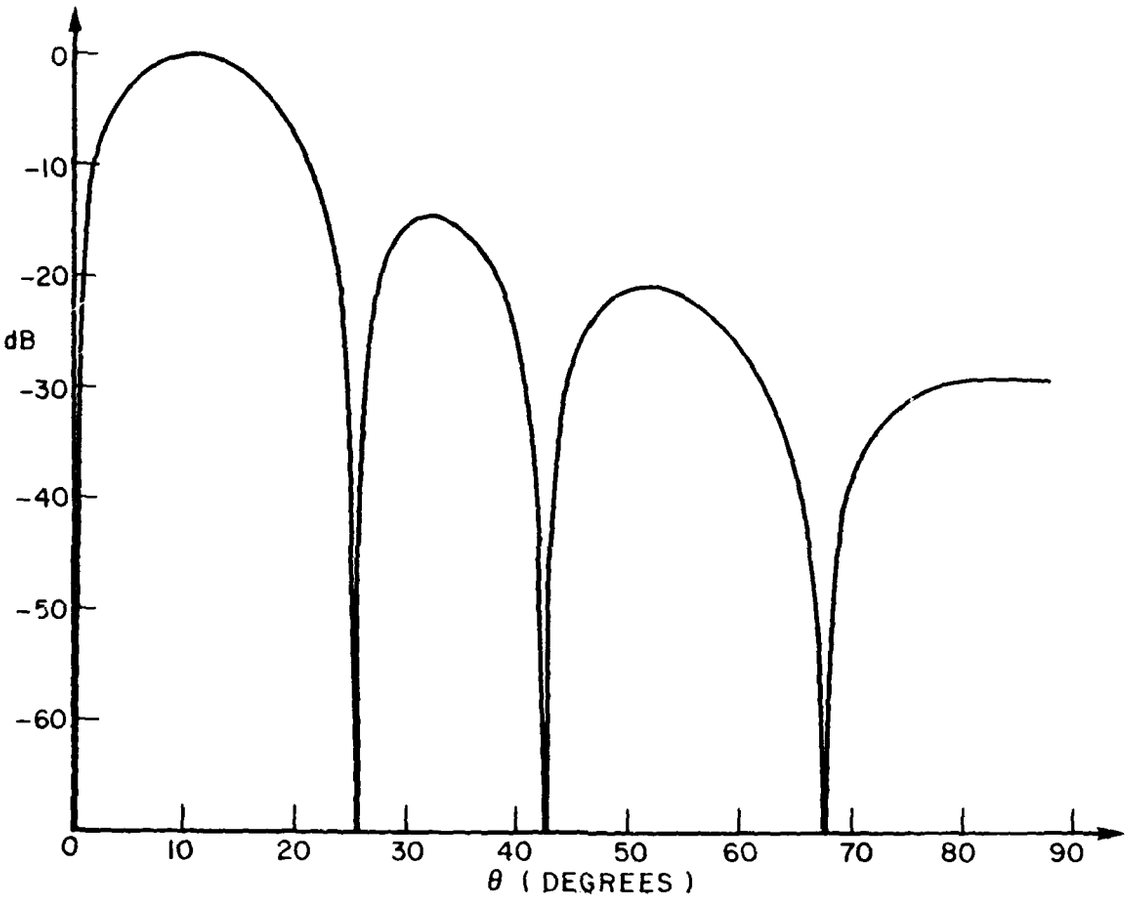

Figure 2-12. Radiation pattern for TM_{01} mode with ka=12.77 (D/λ=4.065).

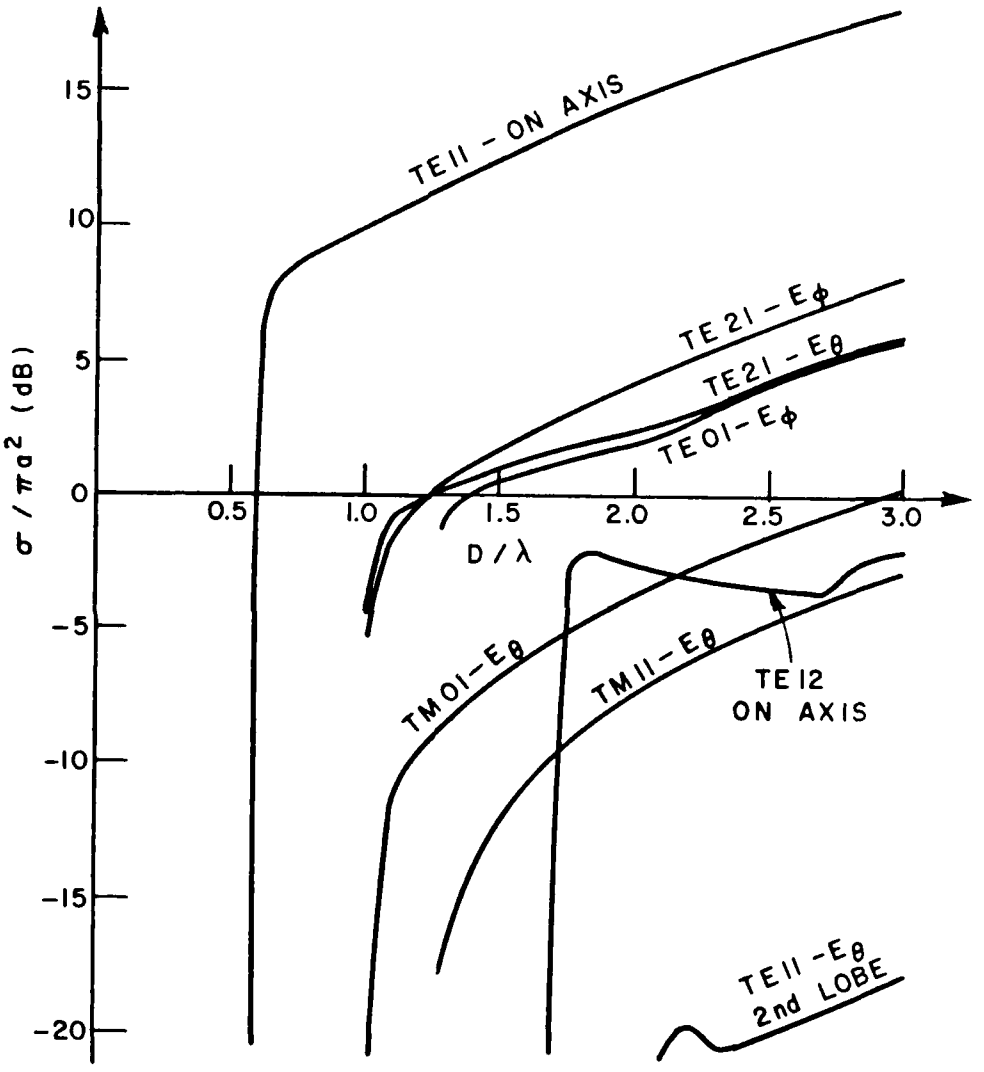

Figure 2-13. "Cavity cross-section" for six lowest order waveguide modes.

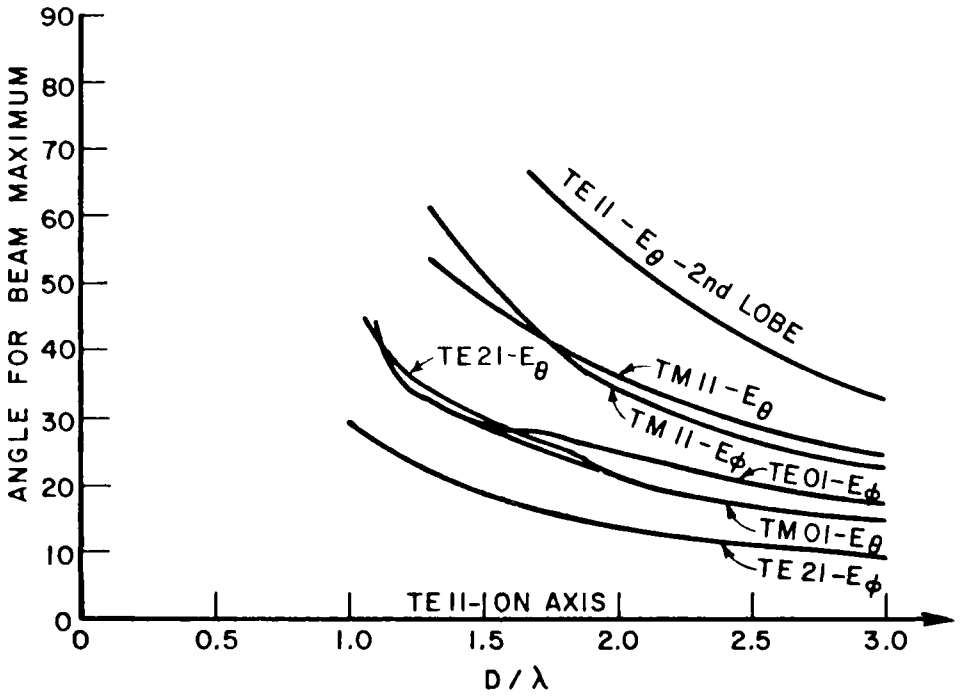

Figure 2-14. Angle for beam maximum for six lowest-order waveguide modes.

From Equation (B-17), (which give the radiation patterns for the waveguide modes) we obtain scattered fields of the form

$$\begin{bmatrix} E_\theta^s \\ E_\phi^s \end{bmatrix} = \begin{bmatrix} C_{\theta E}(\theta_s,\phi_s) & C_{\theta H}(\theta_s,\phi_s) \\ C_{\phi E}(\theta_s,\phi_s) & C_{\phi H}(\theta_s,\phi_s) \end{bmatrix} \begin{bmatrix} E_{nm} \\ \sqrt{\frac{\mu_o}{\epsilon_o}}\, H_{nm} \end{bmatrix} \frac{e^{ikr}}{r} \qquad (2\text{-}25)$$

Consider first the topline of Equation (B-9).

$$\frac{E_z}{E^i} = A_{nm}^{\theta}(\theta_i,\phi_i)\cos n\phi \, \frac{J_n(j_{nm}\,\rho/a)}{J_n'(j_{nm})} \, e^{-i\alpha_{nm}z} \qquad (2\text{-}26)$$

This gives us $\Gamma_{nm}^{\theta} = A_{nm}^{\theta}(\theta_i,\phi_i)$ in Equation (B-15) except for the direction of propagation. If we assume perfect reflection, and ignore the sign change, (since we are interested only in magnitude) this leads to

$$\frac{E_\theta^s}{E^i} = C_{\theta E}(\theta_s,\phi_s)A_{nm}^{\theta}(\theta_i,\phi_i) \, \frac{e^{ikr}}{r} \qquad (2\text{-}27)$$

The RCS becomes

$$\sigma = \lim_{r\to\infty} 4\pi r^2 \left|\frac{E^s}{E^i}\right|^2 \qquad (2\text{-}28a)$$

$$= 4\pi \left|C_{\theta E}(\theta_s,\phi_s)\right|^2 \left|A_{nm}^{\theta}(\theta_i,\phi_i)\right|^2 \qquad (2\text{-}28b)$$

Since we chose $\phi_i = \pi$, we likewise set $\phi_s = \pi$ and vary $\theta = \theta_i = \theta_s$ to its optimum value. Note that for computations involving A_{nm}^{ϕ} and B_{nm}^{θ}, there is a sin $n\phi$ dependence in the modal fields. To adjust this to conform with Equations (B-15) and (B-16), it is necessary to rotate the coordinate system. This results in radiation patterns evaluated at $\phi_s = \frac{\pi}{2}$. Hence, we obtain, for the remaining three cases:

$$\sigma = 4\pi \left|C_{\theta H}(\theta_s,\phi_s)\right|^2 \left|B_{nm}^{\theta}(\theta_i,\phi_i)\right|^2$$
$$\phi_s = \pi/2,\ \phi_i = \pi\ , \quad \theta_s = \theta_i = \theta \qquad (2\text{-}29)$$

$$\sigma = 4\pi \left|C_{\phi E}(\theta_s,\phi_s)\right|^2 \left|A^{\phi}_{nm}(\theta_i,\phi_i)\right|^2$$

$$\phi_s = \pi/2, \quad \phi_i = \pi, \quad \theta_s = \theta_i = \theta \tag{2-30}$$

$$\sigma = 4\pi \left|C_{\phi H}(\theta_s,\phi_s)\right|^2 \left|B_{nm}(\theta_i,\phi_i)\right|^2$$

$$\phi_s = \phi_i = \pi, \quad \theta_s = \theta_i = \theta \tag{2-31}$$

The backscatter directly from the rim is discussed by [Chaung et al (1975)]. They used a pulse radar and extracted the RCS of the rim based on the first return pulse. The agreement between theory and experiment is better in some cases than others, but fails to match the detailed pattern. The normalized RCS can be derived from Equations (B-1) through (B-4) as follows.

$$E^s_\theta = S_{\theta\theta}\, E^i_\theta\, \frac{e^{ikr}}{r} \tag{2-32}$$

$$\sigma = \lim_{r\to\infty} 4\pi r^2 \left|\frac{E^s_\theta}{E^i_\theta}\right|^2 \tag{2-33a}$$

$$= 4\pi \left|S_{\theta\theta}\right|^2 \tag{2-33b}$$

$$\frac{\sigma}{\pi a^2} = \frac{4}{a^2}\left|S_{00}\right|^2 = \left|\frac{2}{a}\, S_{00}\right|^2 \tag{2-34}$$

Similarly

$$\frac{\sigma}{\pi a^2} = \left|\frac{2}{a}\, S_{\phi\phi}\right|^2 \tag{2-35}$$

Comparison of Figures 2-15 and 2-16 with Figures 2 through 5 of [Chuang et al (1975)] reveals that despite use of the complex scattering form, and more accurate computation of the factorization functions, some substantial discrepancies still exist between theory and experiment. Possibly the explanation is that any real cylinder must, of necessity, have a finite wall thickness. [James and Greene (1978)] showed that this leads to substantially different results than obtained with the infinitely thin "knife-edge". Of course, the accuracy of the measured results is a possible source of discrepancy.

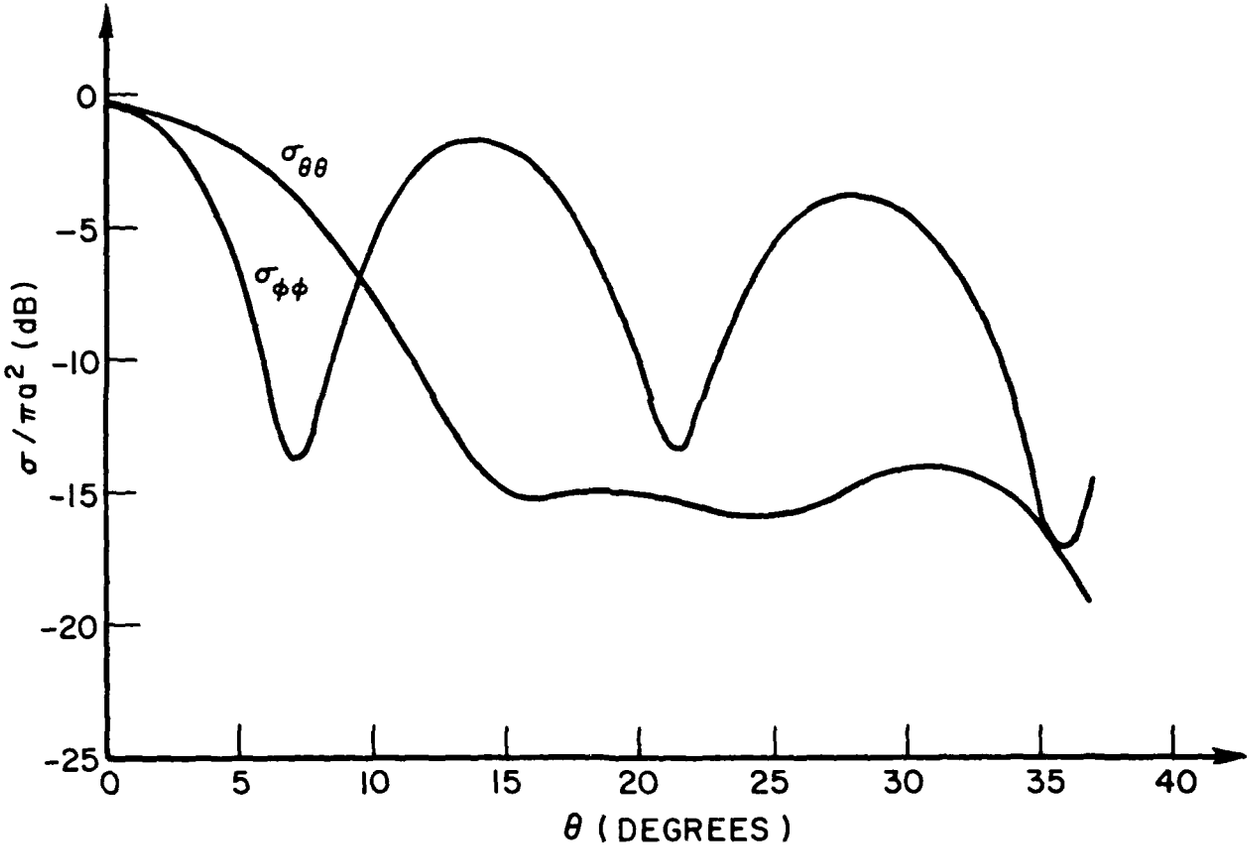

Figure 2-15. Rim backscatter cross-section for semi-infinite cylinder with ka=7.261 (D/λ=2.311).

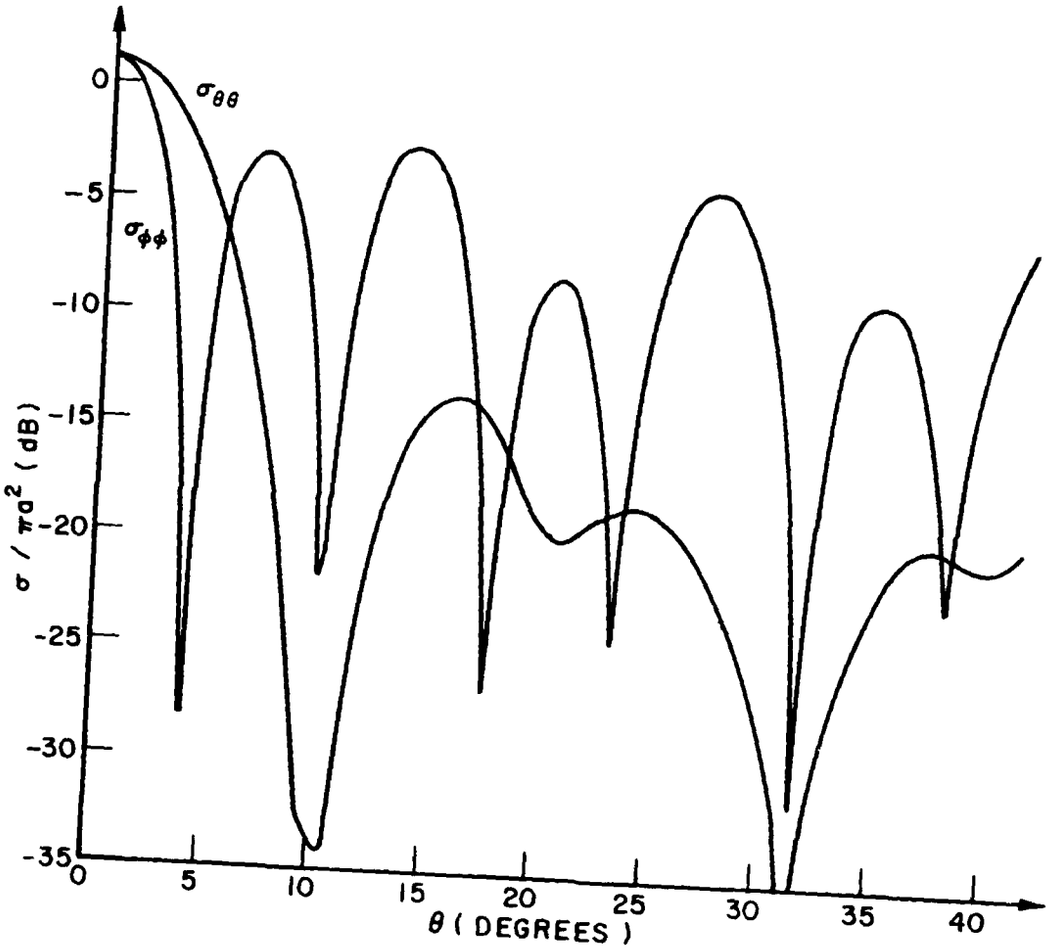

Figure 2-16. Rim backscatter cross-section for semi-infinite cylinder with ka=14.4 (D/λ=4.584).

C. Reciprocity Considerations

It is evident from physical considerations that there must be some relationship between the coupling of an incident plane wave to a waveguide mode, and the waveguide radiation pattern of that mode. This will be shown by the reciprocity theorem.

From [Harrington (1969), p. 116-117], if the current J^a produces fields (E^a,H^a), and current J^b produces fields (E^b,H^b), then

$$-\oint\!\!\!\oint_S (\overline{E^a} \times \overline{H^b} - \overline{E^b} \times \overline{H^a})\cdot ds = \iiint_V (\overline{E^a}\cdot\overline{J^b} - \overline{E^b}\cdot\overline{J^a})dv \qquad (2\text{-}36)$$

where the surface and volume are of finite extent. Generally speaking, reciprocity is applied to sources and matter of finite extent. In this case, however, the matter is of semi-infinite extent. Usually, it is shown that the surface integral vanishes far from all matter and sources. In this case, we will assume that it vanishes external to the waveguide, and thus need only evaluate the 'power flow' $(\overline{E^a} \times \overline{H^b})$ inside the waveguide.

First, we apply reciprocity to determine what source will produce a plane wave incident on the waveguide. We assume that there exists a current dipole, impulsive in space, of either $\hat{\theta}$ or $\hat{\phi}$ orientation, located by $\bar{R}_o = (\theta=\theta_o,\ \phi=\pi,\ r=R_o)$, where $R_o >> a$, $R_o >> \lambda$, as shown in Figure 2-17. This dipole produces a far-field at the origin of

$$E_x = \sqrt{\frac{\mu_o}{\epsilon_o}}\ \frac{ikI\ell}{4\pi|\bar{r}-\bar{R}_o|}\ e^{ik|\bar{r}-\bar{R}_o|}\ \begin{Bmatrix} -\cos\theta_o \\ 0 \end{Bmatrix} \qquad (2\text{-}37a)$$

$$E_y = \sqrt{\frac{\mu_o}{\epsilon_o}}\ \frac{ikI\ell}{4\pi|\bar{r}-\bar{R}_o|}\ e^{ik|\bar{r}-\bar{R}_o|}\ \begin{Bmatrix} 0 \\ -1 \end{Bmatrix} \qquad (2\text{-}37b)$$

$$E_z = \sqrt{\frac{\mu_o}{\epsilon_o}}\ \frac{ikI\ell}{4\pi|\bar{r}-\bar{R}_o|}\ e^{ik|\bar{r}-\bar{R}_o|}\ \begin{Bmatrix} -\sin\theta_o \\ 0 \end{Bmatrix} \qquad (2\text{-}37c)$$

for $\hat{\theta}$ or $\hat{\phi}$ source unit vectors, respectively. Hence, to produce a 'plane wave' of unit amplitude in the vicinity of the origin, it is necessary to set

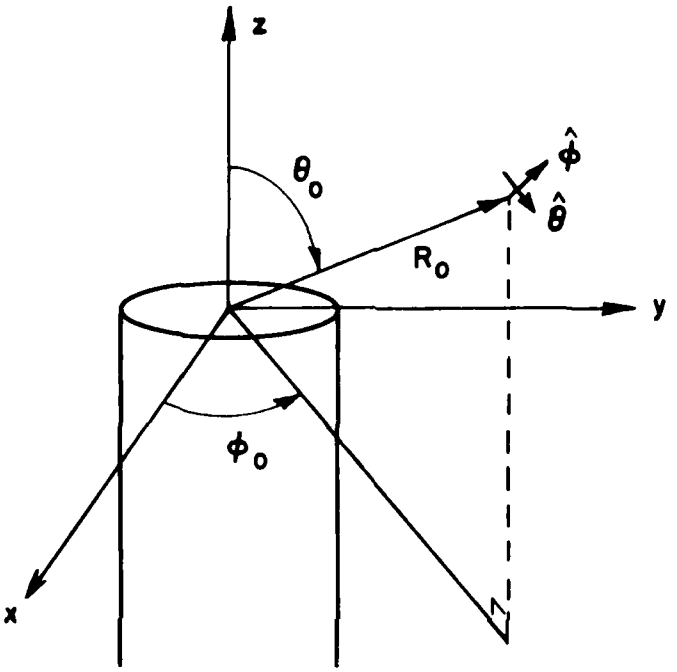

Figure 2-17. Sources for incident "plane-wave".

$$I = -\sqrt{\frac{\mu_o}{\epsilon_o}}\ \frac{ikI\ell}{4\pi R_o}\ e^{ikR_o} \tag{2-38a}$$

$$I\ell = \sqrt{\frac{\epsilon_o}{\mu_o}}\ \frac{i4\pi R_o}{k}\ e^{-ikR_o} \tag{2-38b}$$

For source a we choose

$$\overline{J^a} = \sqrt{\frac{\epsilon_o}{\mu_o}}\ \frac{i4\pi R_o}{k}\ e^{-ikR_o}\ \delta(\bar{r}-\bar{R}_o)\ \begin{Bmatrix}\hat{\theta}\\ \hat{\phi}\end{Bmatrix} \tag{2-39}$$

where

$$\delta(\bar{r}-\bar{R}_o) = \frac{\delta(\theta-\theta_o)\ \delta(\phi-\pi)\ \delta(r-R_o)}{r^2\sin\theta} \tag{2-40}$$

Let us first consider TE modes. These have fields given by

$$H_z = \sqrt{\frac{\epsilon_o}{\mu_o}}\ \frac{J_n(j'_{nm}\rho/a)}{J_n(j'_{nm})}\ \begin{pmatrix}\cos n\phi\\ \sin n\phi\end{pmatrix} e^{\pm i\alpha'_{nm}z} \tag{2-41a}$$

$$E_\rho = \frac{ikna^2}{j'^2_{nm}}\ \frac{J_n(j'_{nm}\rho/a)}{\rho J_n(j'_{nm})}\ \begin{pmatrix}-\sin n\phi\\ \cos n\phi\end{pmatrix} e^{\pm i\alpha'_{nm}z} \tag{2-41b}$$

$$E_\phi = \frac{-ika}{j'_{nm}}\ \frac{J'_n(j'_{nm}\rho/a)}{J_n(j'_{nm})}\ \begin{pmatrix}\cos n\phi\\ \sin n\phi\end{pmatrix} e^{\pm i\alpha'_{nm}z} \tag{2-41c}$$

$$E_z = 0 \tag{2-41d}$$

$$H_\rho = \pm\sqrt{\frac{\epsilon_o}{\mu_o}}\ \frac{i\alpha'_{nm}a}{j'_{nm}}\ \frac{J'_n(j'_{nm}\rho/a)}{J_n(j'_{nm})}\ \begin{pmatrix}\cos n\phi\\ \sin n\phi\end{pmatrix} e^{\pm i\alpha'_{nm}z} \tag{2-41e}$$

$$H_\phi = \pm\sqrt{\frac{\epsilon_o}{\mu_o}}\ \frac{i\alpha'_{nm}a^2}{j'^2_{nm}}\ \frac{n}{\rho}\ \frac{J_n(j'_{nm}\rho/a)}{aJ_n(j'_{nm})}\ \begin{pmatrix}-\sin n\phi\\ \cos n\phi\end{pmatrix} e^{\mp i\alpha'_{nm}z} \qquad (2\text{-}41f)$$

where $e^{+i\alpha'_{nm}z}$ means the fields propagate toward the waveguide mouth

$e^{-i\alpha'_{nm}z}$ means the fields propagate toward - ∞.

Let the b source be located within the guide at z = -L, as shown in Figure 2-18.

$$\overline{J^b} = 2\sqrt{\frac{\epsilon_o}{\mu_o}}\ \frac{i\alpha'_{nm}a}{j'_{nm}}\ e^{-i\alpha'_{nm}L}\left\{\hat\phi\ \frac{J'_n(j'_{nm}\rho/a)}{J_n(j'_{nm})}\ \begin{pmatrix}\cos n\phi\\ \sin n\phi\end{pmatrix}\right.$$

$$\left. -\hat\rho\ \frac{na}{j'_{nm}}\ \frac{J_n(j'_{nm}\rho/a)}{\rho J_n(j'_{nm})}\ \begin{pmatrix}-\sin n\phi\\ \cos n\phi\end{pmatrix}\right\}\delta(z+L) \qquad (2\text{-}42)$$

This current source will generate the appropriate TE mode of unit amplitude propagating toward the waveguide mouth. It will generate the same mode, of equal amplitude, propagating toward the infinite recesses of the waveguide. Note that since the leading sign on H_ρ and H_ϕ changes with direction of propagation, the discontinuity in tangential H exactly matches the surface current. However, E_ρ E_ϕ and H_z are all properly continuous.

Next, according to Equation (B-10), an incident plane wave with $\begin{pmatrix}\hat\theta\\ \hat\phi\end{pmatrix}$ polarization produces a field inside the guide.

$$H_z^a = \sqrt{\frac{\epsilon_o}{\mu_o}}\ \sum_n\ \sum_m \begin{Bmatrix}B^\theta_{nm}\sin n\phi\\ B^\phi_{nm}\cos n\phi\end{Bmatrix}\frac{J_n(j'_{nm}\rho/a)}{J_n(j'_{nm})}\ e^{-i\alpha'_{nm}z} \qquad (2\text{-}43)$$

According to Equation (B-17), the TE_{nm} mode propagating toward the waveguide mouth produces a far-field pattern

$$\begin{Bmatrix}E^b_\theta\\ E^b_\phi\end{Bmatrix} = \begin{Bmatrix}C_{\theta H}\\ C_{\phi H}\end{Bmatrix}\ \frac{e^{ikr}}{r}\ \sqrt{\frac{\mu_o}{\epsilon_o}}\ H_{nm}\ . \qquad (2\text{-}44)$$

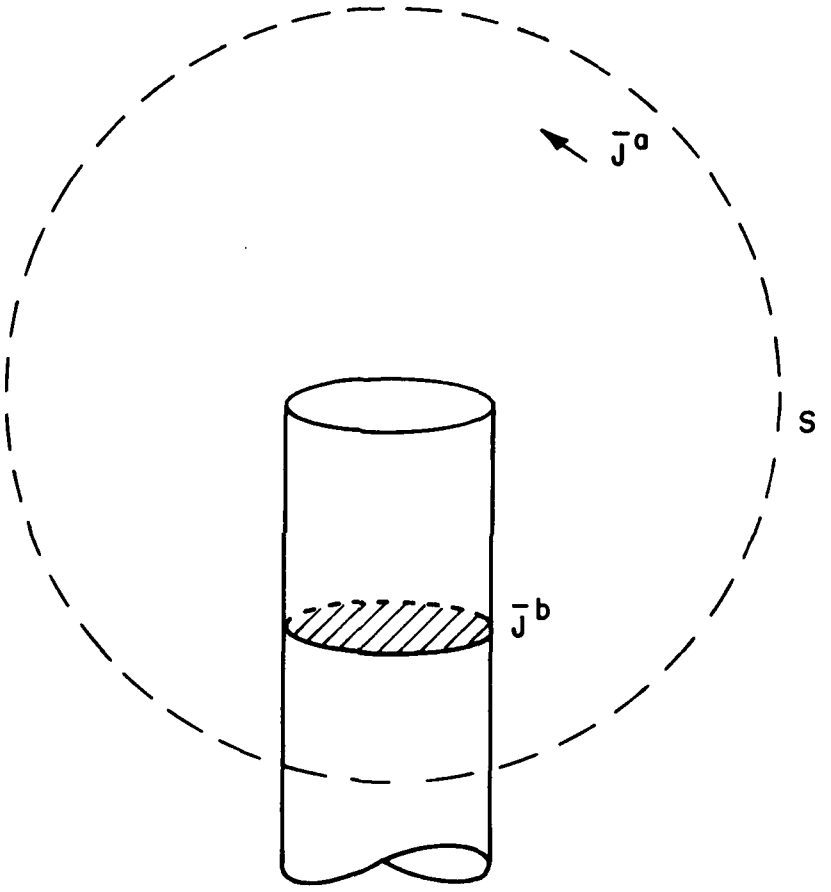

Figure 2-18. Sources for reciprocity theorem.

Plugging the currents and fields into the reciprocity equation, taking the surface and volume indicated in Figure 2-18, we obtain the following result. For $\hat{\theta}$ incidence, H_z^a has sin $n\phi$ dependence, so we take the bottom line of Equations (2-41) and (2-42).

$$\iiint_V \overline{E^a}\cdot\overline{J^b}\,dv = \sum_n \sum_m \int_{-\infty}^{0} \int_0^{2\pi} \int_0^a B_{nm}^{\theta} \frac{ika}{j'_{nm}} e^{-i\alpha'_{nm}z}$$

$$\left(\hat{\rho}\,\frac{na}{j'_{nm}}\,\frac{J_n(j'_{nm}\rho/a)}{\rho J_n(j'_{nm})}\cos n\phi - \hat{\phi}\,\frac{J'_n(j'_{nm}\rho/a)}{J_n(j'_{nm})}\sin n\phi\right)\cdot$$

$$2\sqrt{\frac{\epsilon_o}{\mu_o}}\,\frac{i\alpha'_{nm}a}{j'_{nm}}\,e^{-i\alpha'_{nm}L}\left(-\hat{\rho}\,\frac{an}{j'_{nm}}\,\frac{J_n(j'_{nm}\rho/a)}{\rho J_n(j'_{nm})}\cos n\phi\right.$$

$$\left. + \hat{\phi}\,\frac{J'_n(j'_{nm}\rho/a)}{J_n(j'_{nm})}\sin n\phi\right)\delta(z+L)\rho d\rho d\phi dz \qquad (2\text{-}45)$$

We invoke the orthogonality of modes to assert that the summation reduces to a single term, as this integral vanishes except when the mode and current have the same radial wavenumbers and azimuthal dependence. When this is satisfied,

$$\int_0^{2\pi} \cos^2 n\phi d\phi = \int_0^{2\pi} \sin^2 n\phi d\phi = \pi \qquad (2\text{-}46)$$

$$\iiint_V \overline{E}^a\cdot\overline{J}^b dv = B_{nm}^{\theta}\,\frac{ika}{j'_{nm}}\,e^{i\alpha'_{nm}L}\cdot 2\sqrt{\frac{\epsilon_o}{\mu_o}}\,\frac{i\alpha'_{nm}a}{j'_{nm}}\,e^{-i\alpha'_{nm}L}\cdot\pi$$

$$\int_0^a -\left(\frac{na}{j'_{nm}}\right)^2\left(\frac{J_n(j'_{nm}\rho/a)}{\rho J_n(j'_{nm})}\right)^2 - \left(\frac{J'_n(j'_{nm}\rho/a)}{J_n(j'_{nm})}\right)^2 \rho d\rho \qquad (2\text{-}47a)$$

$$= \frac{2\pi B_{nm}^{\theta} ka\alpha'_{nm}a}{J_n(j'_{nm})^2 j'^2_{nm}} 2\sqrt{\frac{\epsilon_o}{\mu_o}} \int_0^a \left(\frac{n^2a^2}{j'^2_{nm}}\,\frac{J_n(j'_{nm}\rho/a)^2}{\rho} + J'_n(j'_{nm}\rho/a)^2\rho\right)d\rho \qquad (2\text{-}47b)$$

$$= \frac{2\pi B_{nm}^{k} a\alpha'_{nm} a}{J_n(j'_{nm})^2 j'_{nm}} 2\sqrt{\frac{\epsilon_o}{\mu_o}} \int_o^a \rho J_n(j'_{nm}/a)^2 d\rho \qquad (2\text{-}47c)$$

$$= \frac{\pi B^{0}_{nm} k\alpha'_{nm} a^4}{j'^{4}_{nm}} (j'^{2}_{nm} - n^2)\sqrt{\frac{\epsilon_o}{\mu_o}} \qquad (2\text{-}47d)$$

Since E^b is generated by a field with a sin $n\phi$ dependence, this will rotate the radiated field generated by $C_{\theta H}$ by $\pi/2$. Hence, we evaluate $C_{\theta H}$ with a cos $n\phi_s$ dependence.

$$\iiint_V \overline{E^b} \cdot \overline{J^a}\, dv = \iiint_V \begin{Bmatrix} \hat{\theta}\, C_{\theta H} \\ \hat{\phi}\, C_{\phi H} \end{Bmatrix} \frac{e^{ikr}}{r}\sqrt{\frac{\epsilon_o}{\mu_o}} \cdot \frac{i4\pi R_o}{k} e^{-ikR_o} \delta(\bar{r}-\bar{R}_o)\hat{e}\, dv \qquad (2\text{-}48a)$$

$$= \sqrt{\frac{\epsilon_o}{\mu_o}}\; C_{\theta H}\; \frac{e^{ikR_o}}{R_o}\; \frac{i4\pi R_o}{k} e^{-ikR_o} \qquad (2\text{-}48b)$$

$$= \frac{4\pi i}{k}\sqrt{\frac{\epsilon_o}{\mu_o}}\; C_{\theta H} \qquad (2\text{-}48c)$$

This surface integral within the waveguide becomes

$$\oiint_S (\overline{E^a} \times \overline{H^b} - \overline{E^b} \times \overline{H^a}) \cdot ds$$

$$= \int_o^{2\pi} \int_o^a (\overline{E^a} \times \overline{H^b} - \overline{E^b} \times \overline{H^a}) \cdot \hat{z}\rho d\rho d\phi \qquad \text{as } z \to -\infty \qquad (2\text{-}49a)$$

$$= \int_o^{2\pi} \int_o^a \left[(E^a_\rho H^b_\phi - E^a_\phi H^b_\rho) - (E^b_\rho H^a_\phi - E^b_\phi H^a_\rho)\right] \rho d\rho d\phi \qquad (2\text{-}49b)$$

We observe that $H^a_z = B_{nm} H^b_z$.

Then, since each of E_ρ, E_ϕ, H_ρ, and H_ϕ are based on H_z, the fact that they are scalar multiples forces the integral to vanish identically. Thus we are left with

$$\frac{\pi k a \alpha'_{nm} a \, a^2 (j'^2_{nm} - n^2)}{j'^4_{nm}} \sqrt{\frac{\epsilon_o}{\mu_o}} \; B^{\theta}_{nm} = \frac{4\pi i}{k} \sqrt{\frac{\epsilon_o}{\mu_o}} \; C_{\theta H} \tag{2-50a}$$

$$C_{\theta H} = -\frac{ik}{4} k a \alpha'_{nm} a \, a^2 \frac{(j'^2_{nm} - n^2)}{j'^4_{nm}} \; B^{\theta}_{nm} \tag{2-50b}$$

which can be seen to be satisfied by some simple algebraic manipulations.

For a $\hat{\phi}$ incident plane wave, we note that H^a_z has a cos $n\phi$ dependence, so we take the top lines of Equations (2-41) and (2-42) for both the current and waveguide fields. This results in exactly the same integrals for both $\overline{E^a}.\overline{J^b}$ and $\overline{E^b}.\overline{J^a}$, with $\theta \rightarrow \phi$ so that

$$C_{\phi H} = -\frac{ik^2}{4} \; \alpha'_{nm} a^4 \; \frac{(j'^2_{nm} - n^2)}{j'^4_{nm}} \; B^{\phi}_{nm} \tag{2-51}$$

which is satisfied identically.

For TM modes, we begin with

$$E_z = \frac{J_n(j_{nm}\rho/a)}{J'_n(j_{nm})} \begin{Bmatrix} \cos n\phi \\ \sin n\phi \end{Bmatrix} e^{\pm i\alpha_{nm} z} \tag{2-52a}$$

$$E_\rho = \pm i\alpha_{nm} \frac{a}{j_{nm}} \frac{J'_n(j_{nm}\rho/a)}{J'_n(j_{nm})} \begin{Bmatrix} \cos n\phi \\ \sin n\phi \end{Bmatrix} e^{\pm i\alpha_{nm} z} \tag{2-52b}$$

$$E_\phi = \pm i\alpha_{nm} \frac{na^2}{j^2_{nm}} \frac{J_n(j_{nm}\rho/a)}{\rho J'_n(j_{nm})} \begin{Bmatrix} -\sin n\phi \\ \cos n\phi \end{Bmatrix} e^{\pm i\alpha_{nm} z} \tag{2-52c}$$

$$H_\rho = -\frac{ikna^2}{j_{nm}^2}\sqrt{\frac{\epsilon_o}{\mu_o}}\ \frac{J_n(j_{nm}\rho/a)}{\rho J_n'(j_{nm})}\ \begin{Bmatrix}-\sin n\phi\\ \cos n\phi\end{Bmatrix} e^{\pm i\alpha_{nm}z} \qquad (2\text{-}52d)$$

$$H_\phi = \frac{ika}{j_{nm}}\sqrt{\frac{\epsilon_o}{\mu_o}}\ \frac{J_n'(j_{nm}\rho/a)}{J_n'(j_{nm})}\ \begin{Bmatrix}\cos n\phi\\ \sin n\phi\end{Bmatrix} e^{\pm i\alpha_{nm}z} \qquad (2\text{-}52e)$$

$$H_z = 0$$

$e^{+i\alpha_{nm}z}$ propagates toward mouth (2-52f)

$e^{-i\alpha_{nm}z}$ propagates toward $-\infty$.

Let

$$J^b = 2\sqrt{\frac{\epsilon_o}{\mu_o}}\ \frac{ikae^{-i\alpha_{nm}L}}{j_{nm}J_n'(j_{nm})}\left[-\hat{\phi}\,\frac{na}{j_{nm}}\ \frac{J_n(j_{nm}\rho/a)}{\rho}\ \begin{Bmatrix}-\sin n\phi\\ \cos n\phi\end{Bmatrix}\right.$$

$$\left. -\hat{\rho}\,J_n'(j_{nm}\rho/a)\ \begin{Bmatrix}\cos n\phi\\ \sin n\phi\end{Bmatrix}\right]\delta(z+L) \qquad (2\text{-}53)$$

This will generate the appropriate field traveling toward the waveguide mouth. However, to generate the discontinuity in tangential H, the leading sign on all terms must be reversed for the mode traveling toward the infinite recesses of the tube. However, as before, this is of little importance since it contributes nothing to the reciprocity integral.

The incident plane wave generates fields

$$E_z^a = \begin{Bmatrix}A_{nm}^\theta\cos n\phi\\ A_{nm}^\phi\sin n\phi\end{Bmatrix}\ \frac{J_n(j_{nm}\rho/a)}{J_n'(j_{nm})}\ e^{-i\alpha_{nm}z} \qquad (2\text{-}54)$$

The modal fields radiate

$$\begin{Bmatrix} E_\theta^b \\ E_\phi^b \end{Bmatrix} = \begin{Bmatrix} C_{\theta E} \\ C_{\phi E} \end{Bmatrix} E_{nm} \frac{e^{ikr}}{r} \tag{2-55}$$

For the $\hat{\theta}$ incident field we obtain

$$\iiint_V \overline{E^a}.\overline{J^b}\,d = \int_{-\infty}^{0} \int_0^{2\pi} \int_0^a \frac{A_{nm}^{\theta} i\alpha_{nm} a e^{-i\alpha_{nm} z}}{j_{nm} J_n'(j_{nm})} \left(-\hat{\rho} J_n'(j_{nm}\rho/a)\cos n\phi + \hat{\phi} \frac{na}{j_{nm}} \frac{J_n(j_{nm}\rho/a)}{\rho} \sin n\phi\right) \cdot 2\sqrt{\frac{\varepsilon_0}{\mu_0}} \frac{ika}{j_{nm}} \frac{e^{-i\alpha_{nm} L}}{J_n'(j_{nm})}$$

$$\left(\hat{\phi} \frac{na}{j_{nm}} \frac{J_n(j_{nm}\rho/a)}{\rho} \sin n\phi - \hat{\rho}\, J_n'(j_{nm}\rho/a)\cos n\phi\right) \delta(z+L)$$

$$\rho\, d\rho\, d\phi\, dz \tag{2-56a}$$

$$= 2\pi\sqrt{\frac{\varepsilon_0}{\mu_0}} A_{nm}^{\theta} \frac{i\alpha_{nm} a}{j_{nm}} \frac{e^{i\alpha_{nm} L}}{J_n'(j_{nm})^2} \frac{ika}{j_{nm}} e^{-i\alpha_{nm} L}$$

$$\int_0^a \left(J_n'(j_{nm}\rho/a)^2 + \frac{n^2 a^2}{j_{nm}^2} \frac{J_n(j_{nm}\rho/a)^2}{\rho^2}\right) \rho\, d\rho \tag{2-56b}$$

$$= -2\pi\sqrt{\frac{\varepsilon_0}{\mu_0}} \frac{A_{nm}^{\theta} k\alpha_{nm} a^2}{j_{nm}^2 J_n'(j_{nm})^2} \int_0^a \rho\, J_n(j_{nm}\rho/a)^2\, d\rho \tag{2-56c}$$

$$= -2\pi\sqrt{\frac{\varepsilon_0}{\mu_0}} A_{nm}^{\theta} \frac{k\alpha_{nm} a^2}{j_{nm}^2 J_n'(j_{nm})^2} \cdot \frac{1}{2} a^2 J_n'(j_{nm})^2 \tag{2-56d}$$

$$= -\pi\sqrt{\frac{\epsilon_o}{\mu_o}}\ \frac{A^{0}_{nm} k\alpha_{nm} a^4}{j_{nm}^2} \qquad (2\text{-}56e)$$

$$\iiint_V \overline{E^b}\cdot\overline{J^a}\,dv = \iiint_V (\hat{\theta}C_{\theta E}+\hat{\phi}C_{\phi E})\ \frac{e^{ikr}}{r}\cdot\hat{\theta}\sqrt{\frac{\epsilon_o}{\mu_o}}\ \frac{i4\pi R_o}{k}\ e^{-ikR_o}\delta(\bar{r}-\bar{R}_o)\,dv \qquad (2\text{-}57a)$$

$$=\sqrt{\frac{\epsilon_o}{\mu_o}}\ C_{\theta E}\ \frac{4\pi i}{k} \qquad (2\text{-}57b)$$

Equating these leads to

$$-\pi\sqrt{\frac{\epsilon_o}{\mu_o}}\ A^{0}_{nm}\ \frac{k\alpha_{nm}a^4}{j_{nm}^2} = \sqrt{\frac{\epsilon_o}{\mu_o}}\ C_{\theta E}\ \frac{4\pi i}{k} \qquad (2\text{-}58a)$$

$$C_{\theta E} = \frac{ik^2\alpha_{nm}a^4}{4j_{nm}^2}\ A^{\theta}_{nm} \qquad (2\text{-}58b)$$

Finally, for $\hat{\phi}$ incidence, the field generated has sin $n\phi$ dependence, forcing us to the bottom line of the current and field distributions (Equations (2-52) and (2-53)). The integrals all end up the same, resulting in

$$C_{\phi E} = \frac{ik^2\alpha_{nm}a^4}{4j_{nm}^2}\ A^{\phi}_{nm} \qquad (2\text{-}59)$$

Therefore, we have demonstrated the relationship between coupling of incident plane waves to waveguide modes and the radiation patterns of waveguide modes.

CHAPTER III
SCATTERING BY A REPRESENTATIVE ENGINE-LIKE OBSTACLE IN A WAVEGUIDE

This chapter is concerned with scattering by a simplified model representing an engine geometry in the intake duct. The model consists of an infinite circular waveguide housing an axially symmetric cone centered on a flat plate, both perfectly conducting, as shown in Figure 3-1. This model is based to some extent on observation of the Pratt-Whitney J-57 turbofan jet engine, on display at the Air Force Museum, Wright-Patterson AFB, Ohio. In this study, it is assumed that the TE_{11} mode is incident; similar procedures could be followed for any other incident mode. The coordinate system is centered at the base of the cone, as shown in Figure 3-2.

The calculation of fields scattered by the cone in situ would be known completely if one knew the exact currents on the obstacle. The scattered fields can be obtained straightforwardly from the dyadic electric Green's function and the dyadic magnetic Green's function, based on the integrals given by [Tai (1973), p. 9].

$$\bar{E}(\bar{R}) = i\omega\mu_o \iiint \bar{\bar{G}}_{e1}(\bar{R},\bar{R}')\cdot\bar{J}(\bar{R}')\, dv' \qquad (3\text{-}1)$$

$$\bar{H}(\bar{R}) = \iiint \bar{\bar{G}}_{m2}(\bar{R},\bar{R}')\cdot\bar{J}(\bar{R}')\, dv' \quad . \qquad (3\text{-}2)$$

Although the source singular term for the dyadic electric Green's function is still being discussed in the literature by [Yaghjian (1980)] and others, the Green's functions at points not near the source can be obtained unambiguously from residue series expansions. These expansions consist of a double summation over n(azimuthal index) and m(radial index) of terms representing TE and TM fields, both propagating and evanescent. Hence the coupling to a given mode can be determined by a single integral, allowing one to obtain either E_z or H_z, based on known currents. Mathematically this can be expressed as follows: Omitting the source singular term, one can write (using Tai's notation)

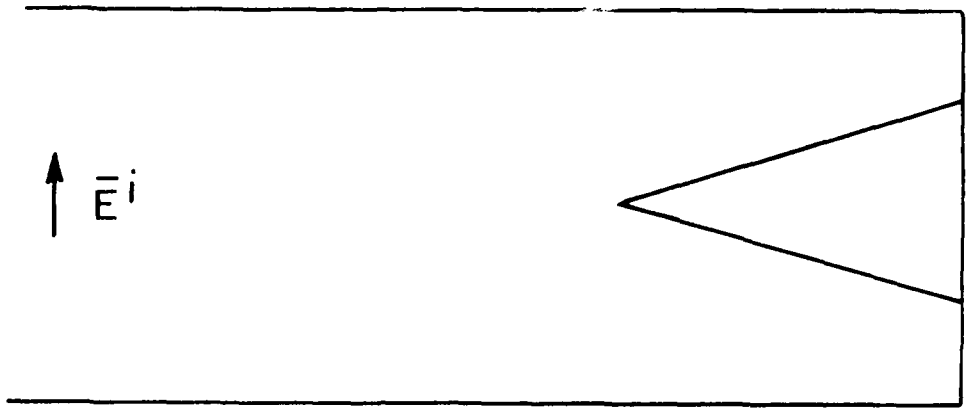

Figure 3-1. Basic geometry for engine scattering model.

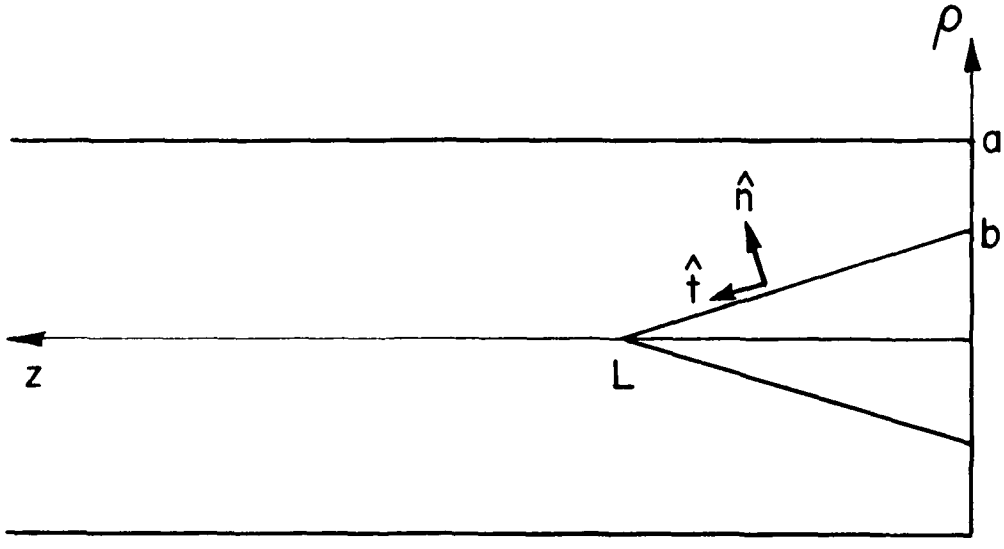

Figure 3-2. Coordinates system and dimensions for scattering from an axial conducting cone.

$$\bar{\bar{G}}_e(\bar{R},\bar{R}') = \frac{i}{4\pi}\sum_{n=0}^{\infty}\sum_{m=1}^{\infty}\varepsilon_n\left\{\frac{1}{\lambda^2 k_\lambda I_\lambda}\bar{N}e_{o\,n\lambda}(\pm k_\lambda)\bar{N}e'_{o\,n}(\mp k_\lambda) + \right.$$

$$\left. + \frac{1}{\mu^2 k_\mu I_\mu}\bar{M}e_{o\,n\mu}(\pm k_\mu)\bar{M}e'_{o\,n\mu}(\mp k_\mu)\right\}$$

$$\text{for } z \gtrless z' \qquad (3\text{-}3)$$

$$\bar{\bar{G}}_{m2}(\bar{R},\bar{R}') = \nabla \times \bar{\bar{G}}_{e1}(\bar{R},\bar{R}')$$

$$= \frac{i}{4\pi}\sum_{n=0}^{\infty}\sum_{m=1}^{\infty}\varepsilon_n\left\{\frac{\kappa_\lambda}{\lambda^2 k_\lambda I_\lambda}\bar{M}e_{o\,n\lambda}(\pm k_\lambda)\bar{N}e'_{o\,n\lambda}(\mp k_\lambda)\right.$$

$$\left. + \frac{\kappa_\lambda}{\mu^2 k_\mu I_\mu}\bar{N}e_{o\,n\mu}(\pm k_\mu)\bar{N}e'_{n\mu}(\mp k_\mu)\right\}$$

$$\text{for } z \gtrless z' \qquad (3\text{-}4)$$

where

$$\mu = j'_{nm}/a \qquad \lambda = j_{nm}/a$$

$$k_\mu = \sqrt{k^2-\mu^2} = \alpha'_{nm} \qquad k_\lambda = \sqrt{k^2-\lambda^2} = \alpha_{nm}$$

$$I_\mu = \tfrac{1}{2}a^2(1-n^2/j'^2_{nm})J_n(j'_{nm})^2 \qquad I_\lambda = \tfrac{1}{2}a^2 J'_n(j_{nm})^2$$

$$\kappa_\mu = k \qquad \kappa_\lambda = k$$

$$\varepsilon_n = \begin{cases} 1 & n=0 \\ 2 & n=1,2,3\ldots \end{cases}$$

$\bar{N}(h)$ represents TM electric fields or TE magnetic fields; $\bar{N}$ contains an axial component

$\bar{M}(h)$ represents TE electric fields or TM magnetic fields so that $\bar{M}$ is purely transverse.

For example, for a single II mode, we can obtain

$$H_{z,n,m} = \hat{z} \cdot \iiint \bar{\bar{G}}_{m2}(\bar{R},\bar{R}') \cdot \bar{J}(\bar{R}')\, dv'$$

$$= \frac{i\varepsilon_n}{4\pi\mu^2 k_\mu I_\mu} \hat{z} \cdot \bar{N}e_{o\,n\mu}(\mp k_\mu) \iiint \bar{M}e_{o\,n\mu}(\mp k_\mu) \cdot \bar{J}(\bar{R}')\, dv' \quad (3\text{-}5)$$

and similarly calculate E_z using $\bar{\bar{G}}_{e1}$. The elements of $\bar{\bar{G}}_{e1}$ and $\bar{\bar{G}}_{m2}$ are written out in Appendix C.

Because of the difficulty of and restrictions on previous solutions for current, a new technique of solving for currents was explored. A few cases have been previously solved with great effort. For example, [Tesche (1972)] solved the problem of a skewed wire between parallel plates by using images. [Wang (1978)] used the dyadic electric Green's function to solve for the currents in an arbitrarily shaped dielectric body inside a rectangular waveguide. [Harrington (1961), pp. 402-406] gives a variational technique to find stationary formulas for scattering using approximate current distributions. He applies this to a post in a parallel-plate guide. Unfortunately, this method requires computing the self-reaction of the assumed current distribution, which in most cases is equally as difficult as solving the problem exactly, since it requires computing the electric field generated by the assumed current in the source region. Hence, no computational advantage is obtained over solving directly for the actual current by the method of moments, or some similar technique.

In principle, the problem can be solved by the method of moments by assuming the current distribution to be a collection of a series of pulses with unknown weighting coefficients, calculating the electric fields generated by these pulses, and adusting the coefficients such that the tangential electric field vanishes as the surface of the obstacle. The problem with this approach, as pointed out by [Wang (1978)], is that for coplanar field and source, the dyadic electric Green's function converges extremely slowly, if at all, in addition to the problems involved with the source singular term. Convergence of the residue series is enforced by the axial propagation factor $e^{i\alpha_{nm}|z-z'|}$, which becomes $e^{-\alpha_{nm}|z-z'|}$, for large enough m. For coplanar source and field, this factor becomes unity. In Wang's case the problem was solved by summing the resultant series (without the convergence factor) in closed form. In the case of the circular waveguide, we have a Fourier-Bessel series whose summation in closed form is not readily apparent. For example, the z component of $\bar{\bar{G}}_{e1}$ is given by

$$\bar{\bar{G}}_{elz,z} = \frac{i}{4\pi}\sum_{n=0}^{\infty}\sum_{m=1}^{\infty}\varepsilon_n \frac{e^{i\alpha_{nm}|z-z'|}}{\alpha_{nm}k^2 J_n'(j_{nm})^2 a}\, 4 J_n(j_{nm}\rho/a) J_n(j_{nm}\rho'/a)\cos n\phi \cos n\phi'. \tag{3-6}$$

Taking asymptotic forms for j_{nm} and $J_n(\ )$, assuming n=1, for coplanar source and field point, we obtain

$$j_{1m} \sim (m+\tfrac{1}{4})\pi \tag{3-7}$$

$$J_1(x) \sim \sqrt{\frac{2}{\pi x}}\cos(x-3\pi/4) \tag{3-7}$$

$$\bar{\bar{G}}_{elz,z} \sim \frac{-\cos\phi\ \cos\phi'}{k^2a^2}\sum_{m=1}^{\infty}\frac{(m+\frac{1}{4})}{\sqrt{\rho\rho'}}\cos((m+\tfrac{1}{4})\pi\rho/a-3\pi/4)\ \cos((m+\tfrac{1}{4})\pi\rho'/a-3\pi/4). \tag{3-8}$$

It seems that even if ρ and ρ' are different, this series does not converge. The series does converge for real objects after integrating over volume currents of finite extent, since integration over ρ' results in dividing the asymptotic terms by $(m+\frac{1}{4})\pi$, and integration over z multiplies the element by the differential dz, forcing the coplanar elements to make an infinitesimal contribution. The reminder of the integral is well behaved, due to the convergence factor for noncoplanar points.

This extremely cumbersome process seemingly cannot be avoided. However, poor convergence in the source region suggests a similar problem in free-space scattering, and the superior convergence of the magnetic field integral equation (MFIE) over the electric field integral equation (EFIE) for most obstacle scattering problems. We therefore proceed, analogous to the MFIE to force $\bar{J}_s = \hat{n} \times \bar{H}^{total}$ just outside the surface of the conducting body and $\hat{n} \times \bar{H}^{total}=0$ just inside the surface. As with the MFIE, taking the mean at the surface results in dividing the current by two. Assume the current consists of a collection of pulses of arbitrary weighting

$$\bar{J}_s = \sum_k a_k p(\bar{r} - \bar{r}_k)\hat{u}_k \tag{3-9}$$

where $\hat{u}_k$ is a unit vector tangent at the surface at $\bar{r}_k$, and $p(\bar{r}-\bar{r}_k)$ is localized near r_k. Then

$$\bar{H}^s(\bar{R}) = \iiint \bar{\bar{G}}_{m2}(\bar{R},\bar{R}')\cdot\bar{J}_s(\bar{R}')\ dv'$$

$$= \sum_k a_k \iint \bar{\bar{G}}_{m2}(\bar{R},\bar{R}')\cdot\hat{u}_k p(\bar{R}'-\bar{r}_k)\ ds' \quad . \tag{3-10}$$

Enforcing the boundary condition

$$\tfrac{1}{2}\bar{J}_s = \hat{n} \times \bar{H}^{total} = \hat{n} \times \bar{H}^i + \hat{n} \times \bar{H}^s$$

$$\hat{n} \times \bar{H}^i = \tfrac{1}{2}\bar{J}_s - \hat{n} \times \bar{H}^s$$

$$\hat{n} \times \bar{H}^i(\bar{R}) = \sum_k a_k \left\{ \tfrac{1}{2}\hat{u}_k - \hat{n} \times \iint \bar{\bar{G}}_{m2}(\bar{R},\bar{R}')\cdot\hat{u}_k p(\bar{R}'-\bar{r}_k)\ ds' \right\} \quad . \tag{3-11}$$

We can then enforce this condition as many times as necessary to obtain the required number of equations to solve for the a_k's. The advantage of this approach is found only by careful examination of the convergence properties of $\bar{\bar{G}}_{el}$ and $\bar{\bar{G}}_{m2}$. The least convergent term in $\bar{\bar{G}}_{el}$ goes asymptotically as m sin mx, but the least convergent term in $\bar{\bar{G}}_{m2}$ goes as 1 sin mx. After integrating over the surface, we obtain $\frac{\sin mx}{m}$ or $\frac{\cos mx}{m}$, which are convergent. Hence, we can work with surface, rather than volume currents, and construct a relatively simple code. Additionally, there appears to be no dispute concerning the behavior of $\bar{\bar{G}}_{m2}$ in the source region.

With the geometry shown in Figure 3-2, we define

$$\hat{n} = \frac{L\hat{\rho} + b\,\hat{z}}{\sqrt{L^2 + b^2}}$$

$$\hat{t} = \hat{n} \times \hat{\phi} = \frac{1}{\sqrt{L^2 + b^2}} \begin{vmatrix} \hat{\rho} & \hat{\phi} & z \\ L & 0 & b \\ 0 & 1 & 0 \end{vmatrix} = \frac{-b\hat{\rho} + L\,\hat{z}}{\sqrt{L^2 + b^2}} \tag{3-12}$$

Assume the current consists of the sum of pulses

$$J_s = \sum_{k=1}^{N} a_k \hat{t}\, p(\rho-\rho_k) + \sum_{k=1}^{N} b_k\, \hat{\phi}\, p(\rho-\rho_k) \qquad (3\text{-}13)$$

where $p(\rho)$ is a triangular pulse function. This current distribution is shown in Figure 3-3. Then using Equation (3-11), we obtain

$$n \times H^i = \sum_k a_k \left[\hat{t}\, p(\rho-\rho_k) - \hat{n} \times \iint \bar{\bar{G}}_{m2}(\bar{R},\bar{R}') \cdot \hat{t}\, p(\bar{R}'-\bar{R}_k)\, ds' \right]$$

$$+ \sum_k b_k \left[\hat{\phi}\, p(\rho-\rho_k) - \hat{n} \times \iint \bar{\bar{G}}_{m2}(\bar{R},\bar{R}') \cdot \hat{\phi}\, p(\bar{R}'-\bar{r}_k)\, ds' \right]. \qquad (3\text{-}14)$$

Next, to employ Galerkin's method, we generate 2N equations by multiplying through by each basis function and integrating over the surface S, to obtain

$$\hat{u}_i \cdot \hat{n} \times \iint \bar{H}^i(\bar{R}) p(\bar{R}-\bar{r}\,)\, ds =$$

$$\sum_{k=1}^{N} a_k \left[\tfrac{1}{2} \iint p(\bar{R}-\bar{r}_k) p(\bar{R}-\bar{r}_q) ds (\hat{u}_i \cdot \hat{t}) - \hat{u}_i \cdot \hat{n} \times \iiint\!\!\iint p(\bar{R}-\bar{r}_q) \bar{\bar{G}}_{m2}(\bar{R},\bar{R}') \cdot \right.$$

$$\left. \cdot \hat{t}\, p(\bar{R}'-\bar{r}_k) ds ds' \right]$$

$$+ \sum_{k=1}^{N} b_k \left[\tfrac{1}{2} \iint p(\bar{R}-\bar{r}_k) p(\bar{R}-\bar{r}_q) ds (\hat{u}_i \cdot \hat{\phi}) - \hat{u}_i \cdot \hat{n} \times \iiint\!\!\iint p(\bar{R}-\bar{r}_q) \bar{\bar{G}}_{m2}(\bar{R},\bar{R}') \cdot \right.$$

$$\left. \cdot \hat{\phi}\, p(\bar{R}'-\bar{r}_k) ds ds' \right] \qquad (3\text{-}15)$$

$q = 1,2,\ldots N$

$i = 1,2$

where $\hat{u}_1 = \hat{\phi} \quad \hat{u}_2 = \hat{t}$.

Thus 2N linear equations for the 2N unknown coefficients a_k and b_k can be obtained, which can be straightforwardly solved by linear algebra.

In order to further speed computation, elimination of unknown currents in the backplane can be obtained by using the method of images. Instead of the original problem, we introduce an image such

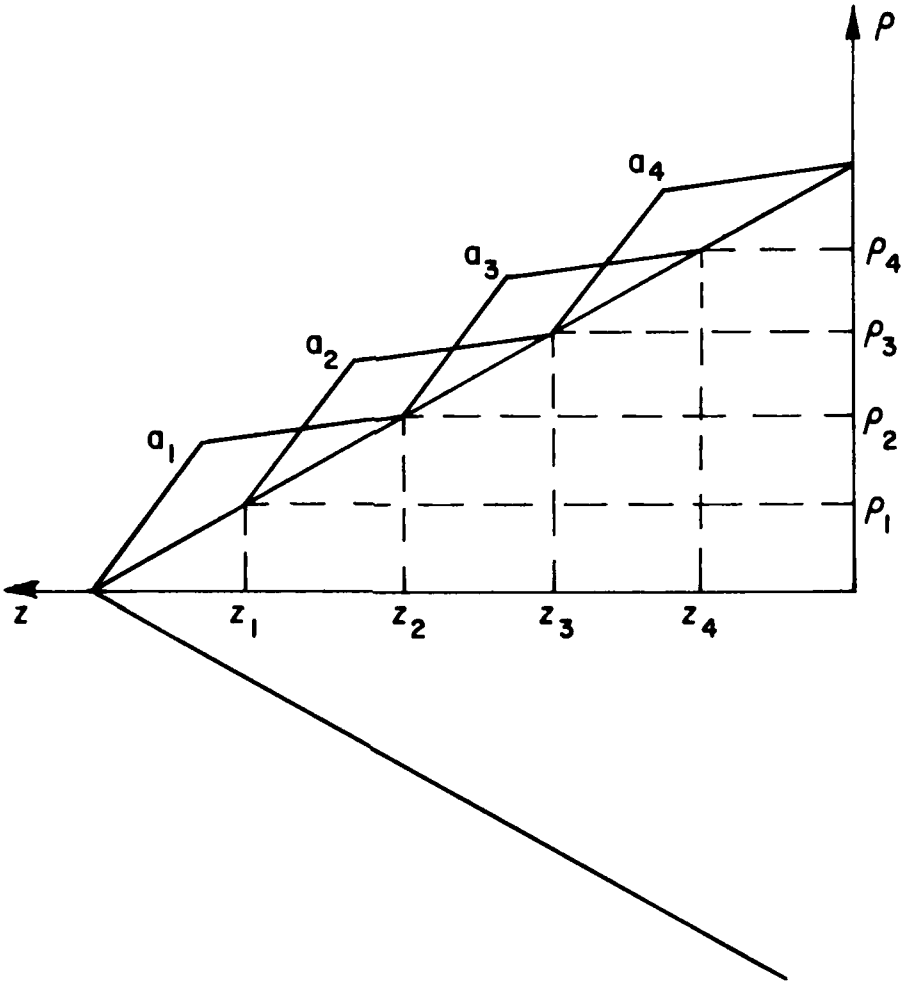

Figure 3-3. Current pulses for moment method solution of scattering by cone.

that the image of the cone has image currents on it, and the image incident field is assumed to be present, as shown in Figure 3-4. This automatically forces $\hat{n}\times\bar{E}^{total}=0$ and $n\cdot\bar{H}^{total}=0$ in the backplane, hence reducing the amount of coplanar integration necessary. With this technique, we obtain a solution for the currents on the cone, then integrate these with $\bar{\bar{G}}_{m?}$ to obtain the H-field in the backplane, hence the currents in the backplane. The current distribution thus obtained is shown in Figure 3-5. It would be extremely difficult to measure this experimentally, and constraints of time and money prohibit this verification.

The fields in the region of the cone-base termination can be approximated in the spirit of the WKB approximation, if the cone is slender enough, and the cone diameter varies slowly enough with axial position. At each axial position on the cone, it is assumed that appropriate TE fields exist for an infinite coaxial line of the same inner diameter. Since $E_z=0$, this guarantees $\hat{n} \times \bar{E} = 0$ on the cone and outer waveguide walls. The radial wavenumber is then computed by solving the characteristic equation

$$J_n'(\mu b)\, Y_n'(\mu a) - Y_n'(\mu b)\, J_n'(\mu a) = 0 \tag{3-16}$$

for the smallest positive μ, with b the inner diameter and a the outer diameter. The values of μ are plotted in Figure 3-6. Next, the scalar wave equation for H_z is approximated by assuming that $\mu(z)$ varies slowly enough so that we can neglect the coupling of $\mu(z)$ through the radial function. Suppressing the azimuthal dependence, let $H_z = R(\rho,z)\, Z(z)$. The scalar wave equation

$$\frac{1}{\rho}\frac{\partial}{\partial\rho}\left(\frac{\partial H_z}{\partial\rho}\right) - \frac{n^2}{\rho^2} H_z + \frac{\partial^2 H_z}{\partial z^2} + k^2 H_z = 0 \tag{3-17}$$

is approximated by setting

$$\frac{\partial}{\partial z} R(\rho,z) = 0 \tag{3-18}$$

so that the wave equation reduces to

$$\left[\frac{\partial^2 R}{\partial\rho^2} + \frac{1}{\rho}\frac{\partial R}{\partial\rho} + (\mu^2 - \frac{n^2}{\rho^2})R\right] Z(z) + (k^2-\mu^2)R(\rho)Z(z) + R(\rho)\,\frac{\partial^2 Z(z)}{\partial z^2} = 0. \tag{3-19}$$

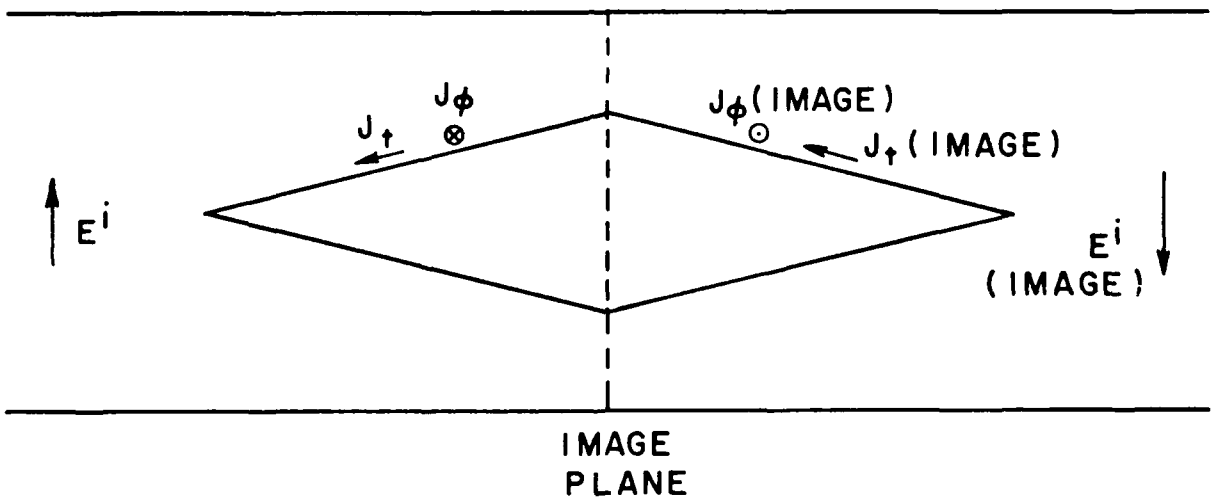

Figure 3-4. Geometry for cone scattering using images.

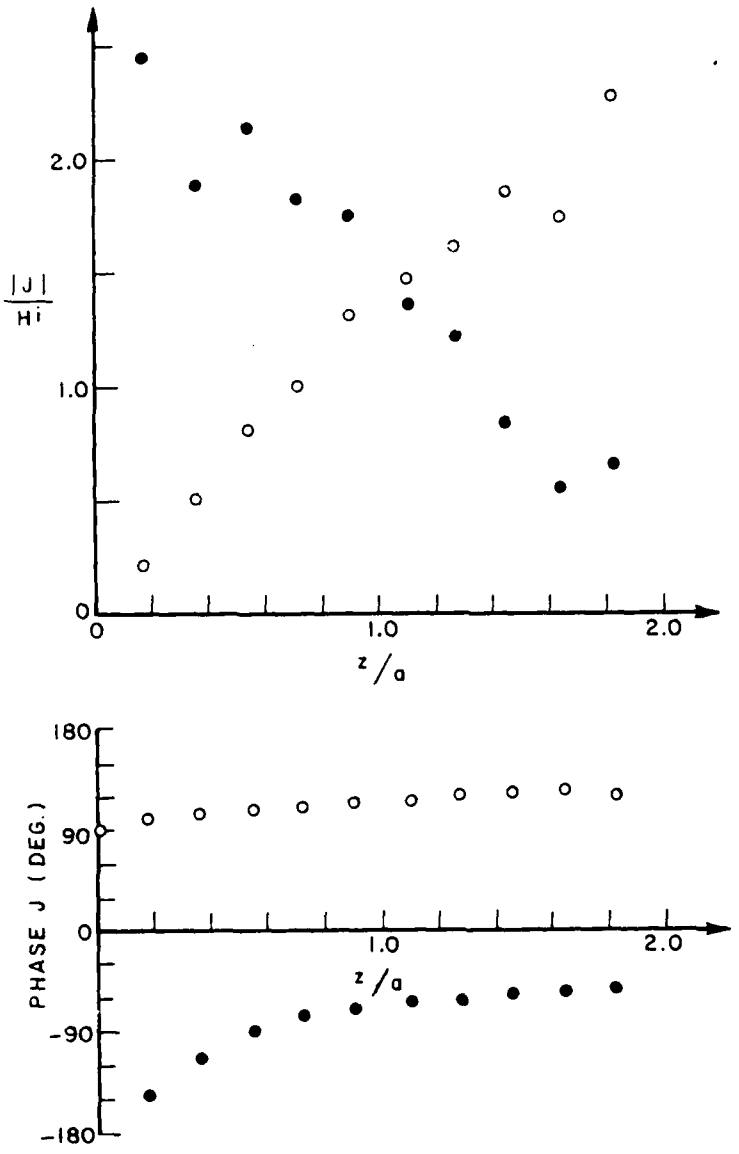

Figure 3-5. Currents induced on cone in circular waveguide with incident TE_{11} mode, L/a=2.0, b/a=0.5, ka=2.0 solution by dyadic magnetic Green's function.

● - J_{tan}

o - J_{ϕ}

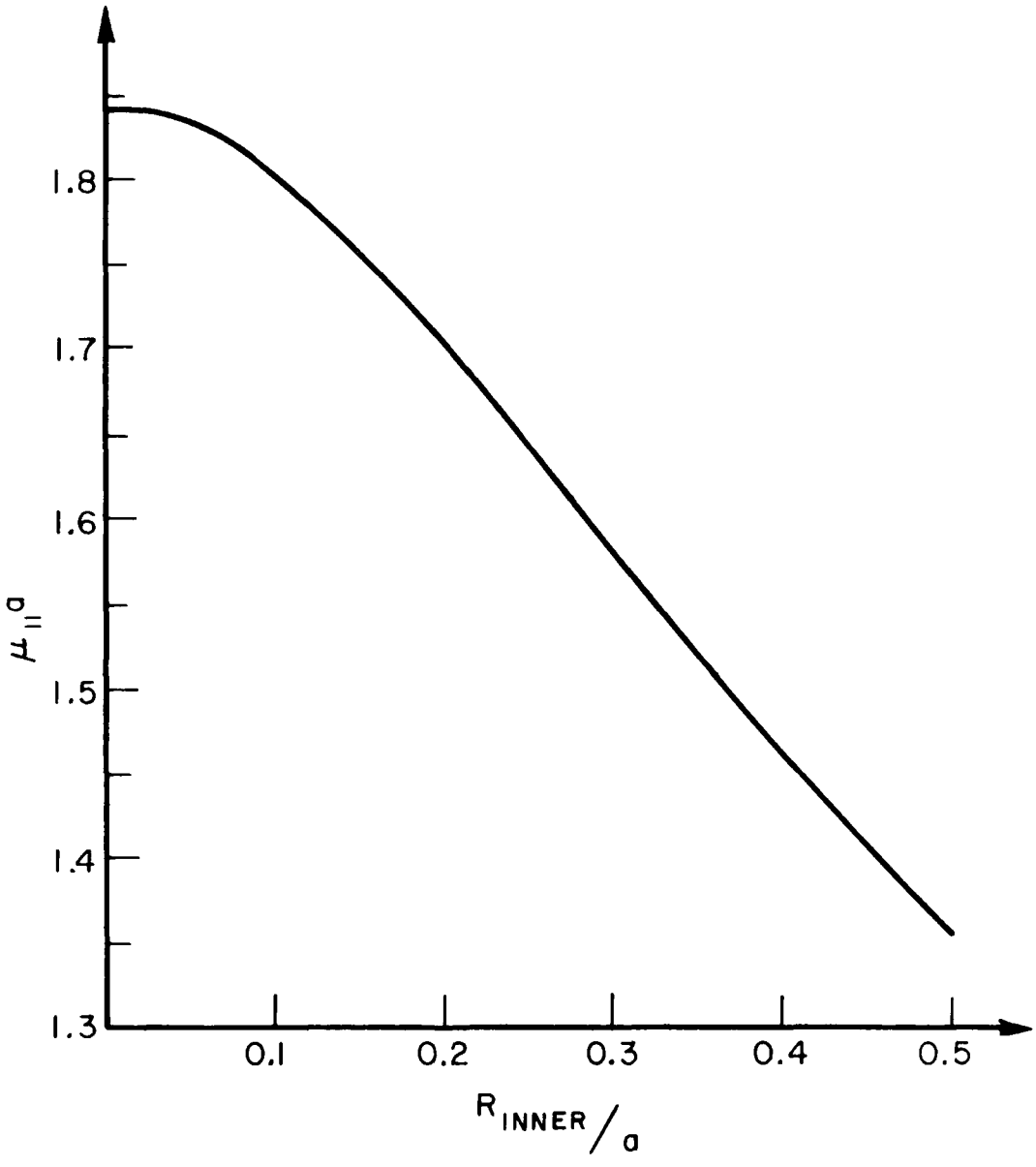

Figure 3-6. Eigenvalue of TE_{11} mode for coaxial waveguide as a function of inner conductor radius.

Since it was assumed that $R(\rho)$ was an appropriate combination of Bessel functions, this reduces to

$$\frac{\partial^2 Z}{\partial z^2} + (k^2-\mu^2)Z = 0 \quad . \tag{3-20}$$

Since $\mu(z)$ is a known function, based on the local radius, this equation can be integrated numerically to obtain $Z(z)$. The results of this numerical integration are given in Figure 3-7. Finally, to normalize the radial function properly, $\int|R(\rho,z)|^2$ da must be constant locally at all cross-sectional planes. Subsequently, H_ρ, H_ϕ, and H_z can be determined at the inner conductor, and hence the surface currents J_{tan} and J_ϕ, which are shown in Figure 3-8.

There are several limitations to this approach. Since $H_\rho = 0$ on the inner conductor but $H_z \neq 0$, $\hat{n} \cdot \bar{H} \neq 0$. Maxwell's equations are only satisfied approximately, not exactly, since the coupling of $\mu(z)$ through the radial functions was neglected. The behavior of the fields near the tip of the cone was approximated very loosely since it was assumed that the field consisted only of incident and scattered TE_{11} modes immediately beyond the tip.

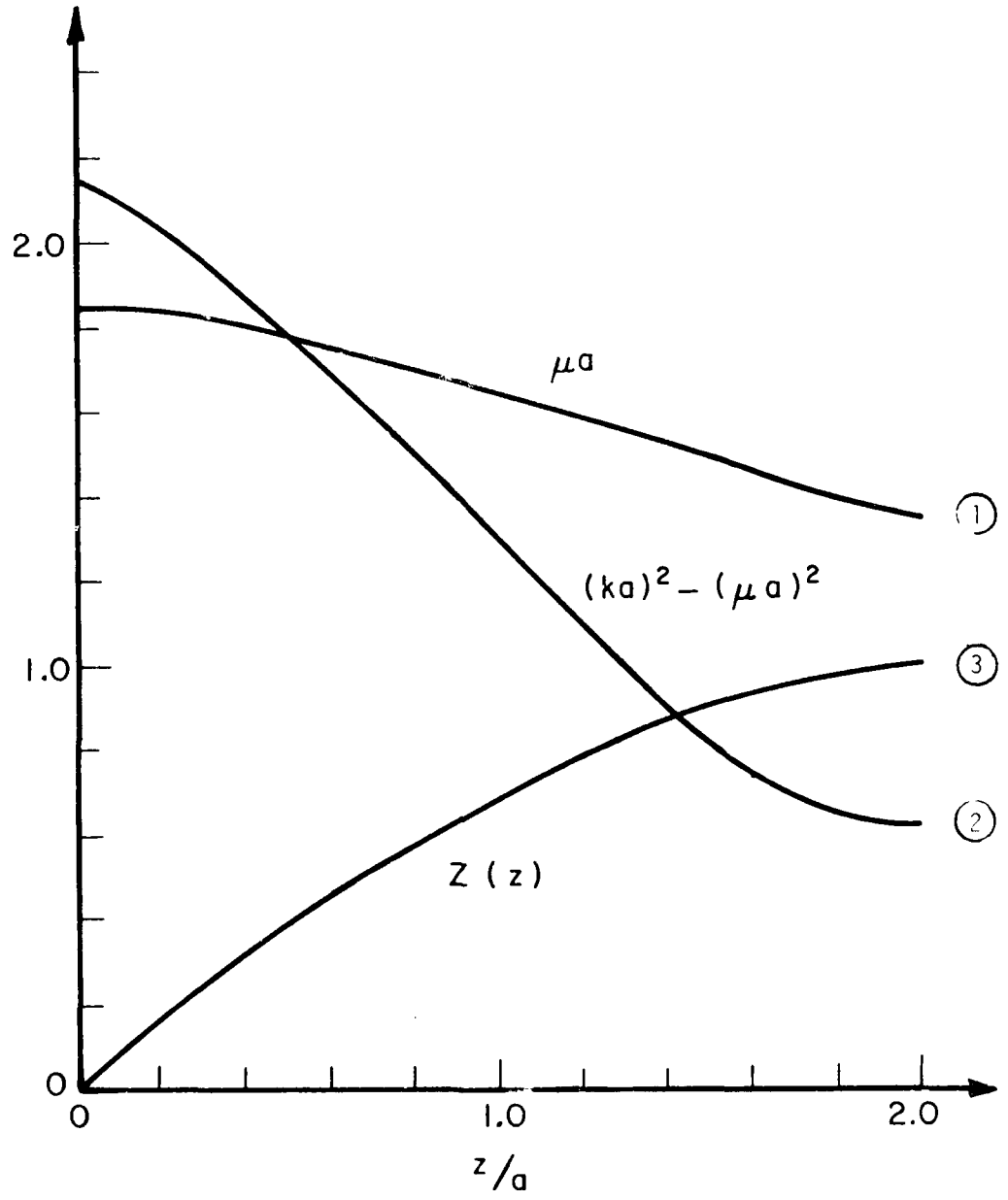

Figure 3-7. Solution for axial variation of fields for TE_{11} mode in circular waveguide with cone. L/a=?.0, b/a=0.5, ka=?.0.

① = μa

② = $(ka)^2 - (\mu a)^2$

③ = Z(z)

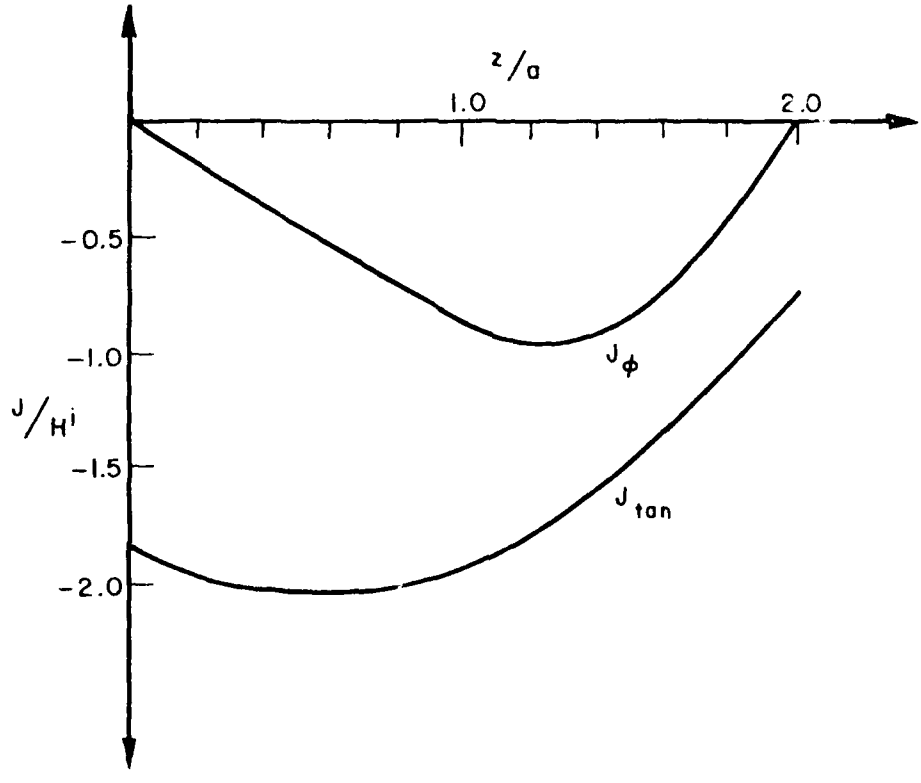

Figure 3-8. Currents induced on cone in circular waveguide with incident TE_{11} mode, L/a=2.0, b/a=0.5, ka=2.0, solution by coaxial approximation with slowly varying center conductor.

CHAPTER IV
CONCLUSIONS AND DISCUSSION

The problem of predicting the radar cross section of jet intake cavities in a spectral region where the cavity aperture is of resonant dimension has been approached via the exact Wiener-Hopf solution for a semi-infinite waveguide. Exact (numerical integration) RCS computations have been presented for the semi-infinite circular waveguide for electrical diameters from zero to three wavelengths. These computations smoothly join high frequency asymptotic results and also serve to define the region of validity for the simpler asymptotic models. Therefore one of the matrices in a generalized scattering matrix development of the scattering by a finite loaded circular waveguide has been completed. In the process, the nontrivial relationships between two earlier studies of the semi-infinite cylinder have been developed and certain errors in a publication from one of these studies have been corrected.

The coupling coefficients relating an incident plane wave to internal waveguide modes have been extracted from earlier studies, recast in a more convenient form, and evaluated in the resonance region. The predominance of the TE modes over the TM modes in power absorption for axial incidence has been demonstrated. The relative importance of the five lowest order modes for non-axial incidence has been demonstrated graphically. The relationship between the coupling coefficients and the radiation patterns of the waveguide modes has been established via the Lorentz reciprocity theorem. The relationship thus demonstrated is that the radiation pattern and the coupling coefficient for a given mode at a given frequency and polarization are proportional. This is of particular importance to RCS calculation since a given waveguide mode will couple to and radiate efficiently in the same direction and with the same polarization.

Modelling of the leading surface of a jet engine as a cone on a flat plate inside a circular waveguide, we have computed the currents on this obstacle, by using the method of moments and the dyadic magnetic Green's function appropriate to the interior of a circular waveguide. The reflection coefficient for an incident TE_{11} mode has been calculated based on these currents at selected fixed frequencies.

It therefore remains to apply these results to Equation (1-8) to solve the radar scattering problem in a self-consistent

fashion. This is done for some illustrative cases. First, fixing a perfectly conducting flat plate at ten radii down the waveguide from the mouth as shown in Figure 4-1, the RCS has been computed while varying the diameter from zero to 1.5 wavelengths. The normalized RCS is shown in Figure 4-2. In Figure 4-3, the normalized RCS is shown for the case when the waveguide diameter is one wavelength and the flat plate varies from two to ten radii down the waveguide.

Discussion

The calculation of scattering from the inlet mouth and coupling to internal modes has been performed modelling the inlet as a circular duct with infinitely thin walls and a knife-edge rim. In practice inlet rims have a finite wedge angle, and are very rarely circular. The major inadequacy encountered in calculating rim scattering for the knife edge by ray optics proved to be the underestimate of the peak just above cutoff of the lowest order propagating mode (comparing Figures 2-4 and 2-5). Unfortunately, for arbitrary geometries, there seems to be no simple way to patch up ray-optics to solve this problem. Since the frequency range this occurs in is low, it may be possible to evaluate this region by moment method techniques. Although this was not done in this study, we can see that the ray optics approximation does work well provided we are sufficiently above cutoff of the lowest order mode. For circular geometries, this condition is that the diameter is greater than one wavelength.

Because of the reciprocity relations demonstrated in Section II-C, it is clear that discussion of radiation patterns and coupling coefficients are redundant. The calculation of radiation patterns has been discussed by [Weinstein (1969), pp. 139-150]. Weinstein's comments on the use of Huygen's principle for calculation of radiation patterns indicates that in the transition region (near cutoff) Huygen's principle performs poorly, and worse for TM modes than TE modes. As Figures 2-13 and 2-14 indicate, the relative importance of TM modes to backscattering from cavities is very far below that of TE modes, and limited to angle far from the forward direction. For all practical purposes, forward scattering in the transition region can be calculated using the TE_{11} mode, adding the TE_{21} and TE_{01} modes as requirements may dictate. The reason for this can be grasped physically by considering Figure 1-3. For modes higher than m=1 and for all TM modes, the oscillation in sign across the waveguide cross-section forces the average interaction to a very small value, regardless of incidence angle. For m=1 modes, the variation due to cos nφ dependence can be seen to lead to an optimum angle, from which the aperture fields appear to be nearly of the same sign.

For non-circular geometries, the primary conclusion we might draw is that the appropriate low-order TE modes will dominate scattering in the forward direction. Since Wiener-Hopf solutions are

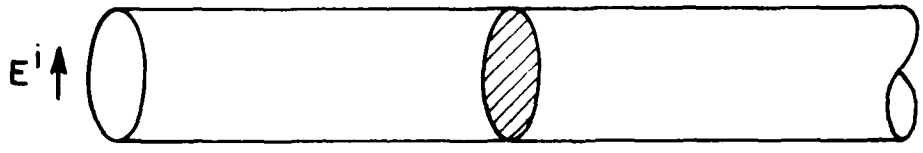

Figure 4-1. Geometry for self-consistent scattering problem using flat plate.

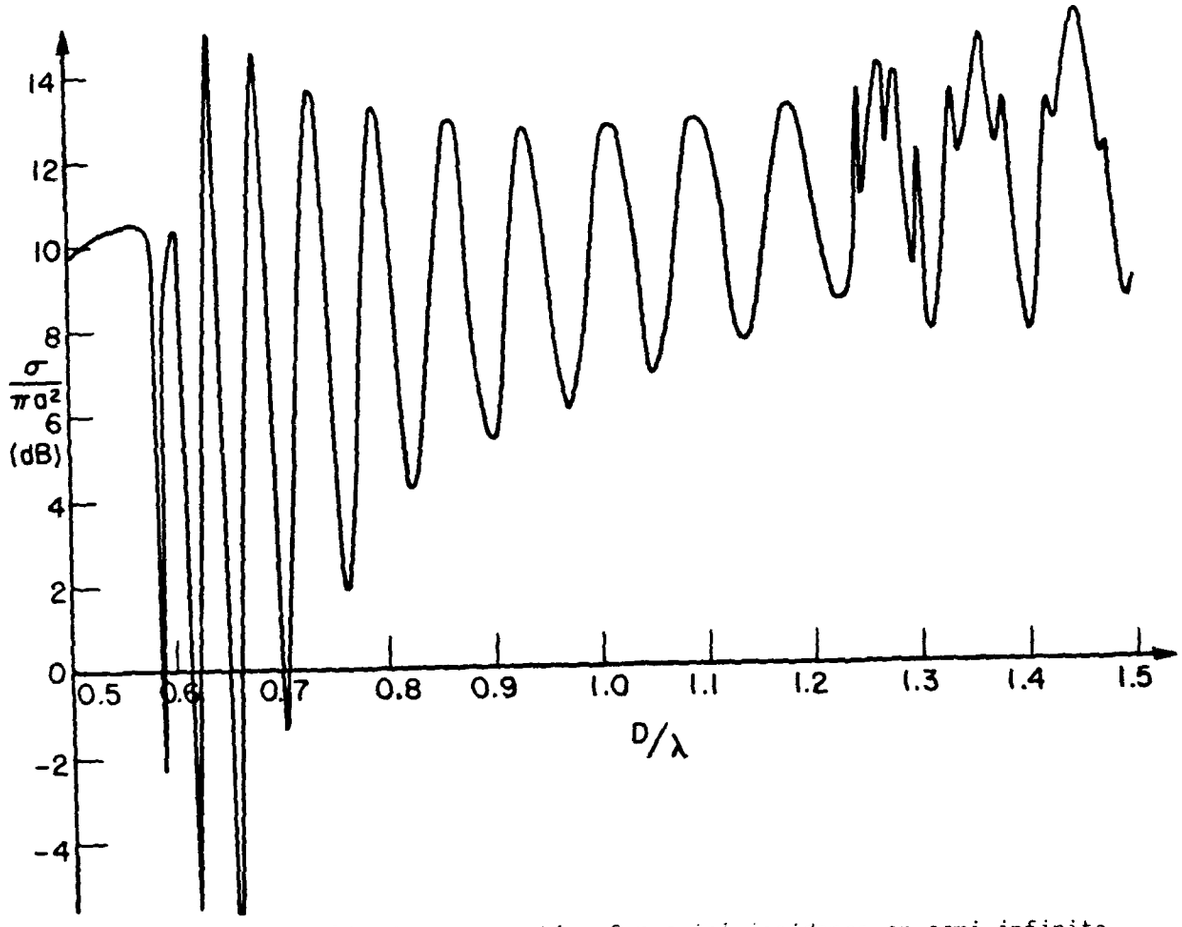

Figure 4-2. Normalized cross-section for axial incidence on semi-infinite circular waveguide with conducting plate 10 radii down the guide, varying waveguide diameter.

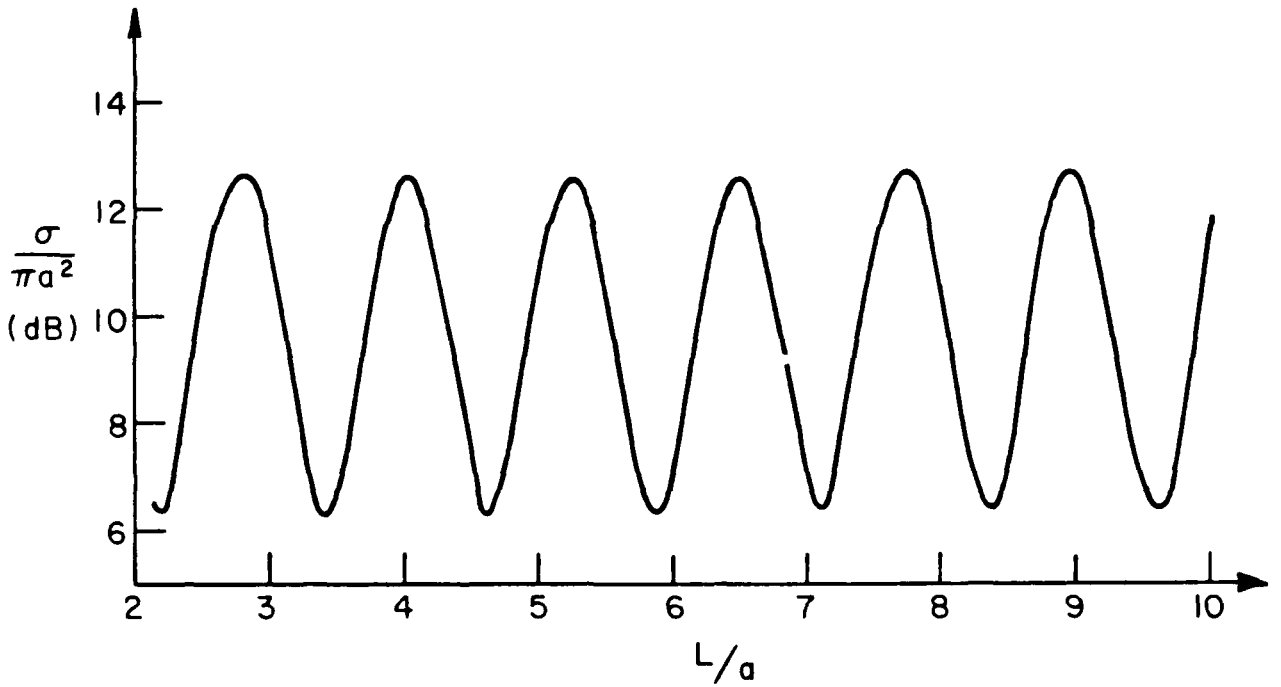

Figure 4-3. Cross section of semi-infinite circular waveguide for axial incidence, $D/\lambda=1.0$, with flat plate at two to ten radii down guide.

not available for these arbitrary geometries, it will probably be necessary to construct moment method solutions for near cutoff frequencies. Higher frequencies can probably be adequately approximated by ray-optic solutions as done by [Pathak and Huang (1980)], for example.

The impulse response waveform given by Figure 2-6 indicates that rim backscatter is really only significant for times of $t<5a/c$. Furthermore, this short time response can be reasonably approximated ray-optically, confirming our earlier statement that high-frequency scattering can be adequately modelled ray-optically. The low-frequency scattering, which is not ray-optic, corresponds to the long-time response, which is typically of little interest.

Having enumerated the difficulties in calculating scattering coefficients for object inside waveguides, it becomes clear that much work remains to be done. The use of the magnetic field dyadic Green's function and appropriate boundary conditions provide some improvement over use of the dyadic electric Green's function, but it is still very expensive computationally. The possibility of azimuthal asymmetry (for example, a blade structure) has not yet been addressed. One might model the blade structure axisymmetrically by using boundary conditions in the backplane $E_\rho = 0$ and $J_\phi = H_\rho = 0$ and at the outer wall $J_\rho(\rho=a) = - H_\phi(\rho=a) = 0$. This allows radial currents and azimuthal E-fields to exist, but not radial E-fields or azimuthal currents. It further forces the axial current to vanish at the tip of the blades. For a structure with 28 blades, for example, it would require an extremely large diameter waveguide before significant azimuthal currents could flow on the blades. One problem in implementing this study would be that the image procedure used in Chapter III to eliminate coplanar integrations could not be used, and it would be necessary to integrate coplanar source and field points. Another approach would be the use of the free-space Green's function, to analyze the structure. In this case it would be necessary to also set up currents and enforce boundary conditions at the waveguide walls, thus vastly increasing the number of current elements required. Another possible approach is to segment the obstacle structure and use waveguide modes appropriate to coaxial waveguides near the obstacle. However, the convergence properties of this approach are unknown.

REFERENCES

Abramowitz, Milton and Irene A. Stegun, (1964) Handbook of Mathematic Functions, U.S. Government Printing Office, Washington, D.C.

Bowman, John J., (1970) "Comparison of Ray Theory with Exact Theory for Scattering by Open Waveguides," SIAM J. Appl. Math., 18(4), pp. 818-829.

Chu, L.J., (1940) "Calculations of the Radiation Properties of Hollow Pipes and Horns," J. Appl. Phys., 11, pp. 603-610.

Chuang, C.A., C.S. Liang, and Shung-Wu Lee, (1975) "High-Frequency Scattering from an Open-Ended Semi-Infinite Cylinder," IEEE Trans. Ant. Prop., AP-23(6), pp. 770-776.

Collin, Robert E., (1960) Field Theory of Guided Waves, McGraw-Hill Book Co., New York.

Einarsson, O., R.E. Kleinman, P. Laurin, and P.L.E. Uslenghi, (1966) "Studies in Radar Cross Sections L - Diffraction and Scattering by Regular Bodies IV: The Circular Cylinder," Radiation Laboratory, University of Michigan, Ann Arbor, DDC #AD-635186.

Harrington, Roger F., (1961) Time-Harmonic Electromagnetic Fields, McGraw-Hill Book Co., New York.

James, G.L. and C.J. Greene, (1978) "Effect of Wall Thickness on Radiation from Circular Waveguides," Electronics Letters, 14(4), pp. 90-91.

Jones, D.S., (1955) "The Scattering of a Scalar Wave by a Semi-Infini Rod of Circular Cross-Section," Phil. Trans. Roy. Soc. London, ser A., 247, 499-528.

Jones, D.S., (1964) The Theory of Electromagnetism, Pergamon Press, MacMillan Company, New York, pp. 594-602.

Kao, Cheng C., (1970a) "Electromagnetic Scattering from a Finite Tubular Cylinder: Numerical Solutions," Radio Science, 5(3), pp. 617-624.

Kao, Cheng C., (1970b) "Currents on a Semi-Infinite Tube Illuminated by Electromagnetic Waves," Radio Science, 5(5), pp. 853-859.

Kouyoumjian, R.G., and P.H. Pathak, (1974) "A Uniform Geometrical Theory of Diffraction of an Edge in a Perfectly Conducting Surface," Proc. IEEE, 62(11), pp. 1448-1461.

Lee, Shung-Wu, Vahraz Jamnejad, and Raj Mittra, (1973) "Near Field of Scattering by a Hollow Semi-Infinite Cylinder and Its Application to Sensor Booms," IEEE Trans. Ant. Prop., AP-21(2), pp. 182-188.

Levine, H. and J. Schwinger, (1948) "On the Radiation of Sound From an Unflanged Circular Pipe," Phys, Rev. 2nd ser., 73(4), pp. 383-406.

Mittra, Raj and S.W. Lee, (1971) Analytic Techniques in the Theory of Guided Waves, MacMillan Company, New York, pp. 107-108.

MIttra, R., S.W. Lee, and C.A. Chuang, (1974) "Analytic Modelling of the Radar Scattering Characteristics of Aircraft," Univ. of Illinois Electromagnetics Laboratory, Urbana, DDC #AD-773685.

Moll, John W. and Rolf G. Seecamp, (1970) "Calculation of Radar Reflecting Properties of Jet Engine Intakes Using a Waveguide Model," IEEE Trans. Aero. Elec. Sys., AES-6(5), pp. 675-683.

Morse, P.M. and Herman Feshbach, (1953) Methods of Theoretical Physics Part I, McGraw-Hill Book Co., New York, pp. 978-992.

Narasimhan, M.S., (1979) "A GTD Analysis of the Radiation Patterns of Open-Ended Circular Cylindrical Waveguide Horns," IEEE Trans. Ant. Prop., AP-27(3), pp. 438-441.

Noble, B. (1958) Methods Based on the Wiener-Hopf Technique, Pergamon Press, Los Angeles.

Pathak, P.H. and C.C. Huang, (1980) "An Analysis of the Electromagnetic Fields Backscattered From a Jet Intake Configuration," Proceedings of the 1980 Radar Camouflage Symposium, 18-20 November 1980, sponsored by USAF Avionics Laboratory and Martin Marietta Corp.

Pearson, J.D., (1953) "The Diffraction of Electromagnetic Waves by a Semi-Infinite Circular Waveguide," Proc. Cambridge Phil. Soc., 49(4), pp. 659-667.

Tai, Chen-To, (1971) Dyadic Green's Functions in Electromagnetic Theory Intext Educational Publishers, Scranton, Pa.

Tai, Chen-To, (1973) "Eigen-Function Expansions of Dyadic Green's Functions," Math. Note 28, Univ. of Michigan Radiation Laboratory, Ann Arbor.

Tesche, F.M., (1972) "On the Behavior of Thin-Wire Antennas and Scatterers Arbitrarily Located Within a Parallel-Plate Region," IEEE Trans. Ant. Prop., AP-20(4), pp. 482-486.

Wang, Johnson J.H., (1978) "Analysis of a Three-Dimensional Arbi
trarily Shaped Dielectric or Biological Body Inside a Rectangula
Waveguide," IEEE Trans. Micro. Th. Tech., MTT-26(7), pp. 457-462

Weinstein, L.A., (1969) The Theory of Diffraction and the Factor
Method, Golem Press, Boulder, Colo.

Witt, H.R. and E.L. Price, (1968) "Scattering From Hollow Conduc
Cylinders," Proc. IEE (London), 115(1), pp. 94-99.

Yaghjian, A.D., (1980) "Electric Dyadic Green's Functions in the
Source Region," Proc. IEEE, 68(2), pp. 248-263.

APPENDIX A
EVALUATION OF WIENER-HOPF FACTORIZATION FUNCTIONS

The factorization functions $L_+(\alpha)$, and $M_+(\alpha)$, are defined as being functions which are analytic in the upper half of the complex α-plane, which also satisfy the equations

$$L_+(\alpha)L_+(-\alpha) = \pi i J_n(\gamma a)H_n^{(1)}(\gamma a) \tag{A-1}$$

$$M_+(\alpha)M_+(-\alpha) = \pi i J_n'(\gamma a)H_n^{(1)\prime}(\gamma a) \tag{A-2}$$

where $\gamma = \sqrt{k^2 - \alpha^2}$ (Einarsson et al, Equations (5-33), (5-34)). The exact function can be evaluated by numerical integration [Mittra and Lee, (1971), p. 107, Eqs. (9.8)]. The approximate evaluation of these functions proceeds in two different regions, for which the Bessel functions are approximated differently. Section A-1 deals with exact numerical integration. Section A-2 deals with low-freque approximations. Section A-3 deals with high-frequency approximation

A-1. Exact Numerical Integration

The exact expression for $L_+(\alpha)$, is given by

$$L_+(\alpha) = \exp\left\{ \frac{1}{2\pi i} \int_{-\infty+ic}^{\infty+ic} \frac{\ln\left[\pi i J_n(a\sqrt{k^2-z^2})H_n^{(1)}(a\sqrt{k^2-z^2})\right]dz}{z-\alpha} \right\} \tag{A-3}$$

where $-Im(k) < c < Im(\alpha) < Im(k)$.

Before proceeding further, however, we note that it would be very beneficial to not have to integrate out to ∞. We note that, for $Re(z)>Re(k)$, the arguments of the Bessel functions become essentiall imaginary. From Abramowitz, Equations (9.6.3) and (9.6.4)

$$H_n^{(1)}(ia\sqrt{z^2-k^2}) = \frac{2}{\pi i} e^{\frac{-in\pi}{2}} K_n(a\sqrt{z^2-k^2}) \tag{A-4}$$

$$J_n(ia\sqrt{z^2-k^2}) = e^{\frac{in\pi}{2}} I_n(a\sqrt{z^2-k^2})$$

where $K_n(\ )$ and $I_n(\ )$ are modified Bessel Functions.

Taking asymptotic forms (Abramowitz Equations (9.7.1) and (

$$\pi i \frac{2}{\pi i} e^{-\frac{in\pi}{2}} K_n(a\sqrt{z^2-k^2})\, e^{\frac{in\pi}{2}} I_n(a\sqrt{z^2-k^2})$$

$$\sim 2\, e^{-a\sqrt{z^2-k^2}} \sqrt{\frac{\pi}{2a\sqrt{z^2-k^2}}} \cdot \frac{e^{a\sqrt{z^2-k^2}}}{2\pi a\sqrt{z^2-k^2}}$$

$$\sim \frac{1}{a\sqrt{z^2-k^2}}$$

We are integrating $\ln(a\sqrt{z^2-k^2})$ from k to ∞, but would prefer grate $\ln(1)$ from k to ∞, since it is trivial. Hence, we for equation

$$-ia\sqrt{k^2-\alpha^2}L_+(\alpha)L_+(-\alpha) = \pi\gamma a J_n(\gamma a)H_n^{(1)}(\gamma a)$$

$$\sqrt{-ia(k+\alpha)}L_+(\alpha)\sqrt{-ia(k-\alpha)}L_+(-\alpha) = \pi\gamma a J_n(\gamma a)H_n^{(1)}(\gamma a)$$

We can evaluate this by the same integral, except that the a of the logarithm becomes very close to 1 for Re(z)>Re(k). T $c\to 0$

$$\sqrt{-ia(k+\alpha)}L_+(\alpha) = \exp\left\{\frac{1}{2\pi i}\int_{-\infty}^{\infty} \frac{\ln\left[\pi a\sqrt{k^2-z^2}J_n(a\sqrt{k^2-z^2}H_n^{(1)}(a\sqrt{k^2-z^2})\right.}{z-\alpha}\right.$$

Similarly

$$\sqrt{-\frac{1}{a}}(k+\alpha)M_+(\alpha)=\exp\left\{\frac{1}{2\pi i}\int_{-\infty}^{\infty}\frac{\ln\left[\pi a\sqrt{k^2-z^2}J_n'(a\sqrt{k^2-z^2})H_n^{(1)'}(a\sqrt{k^2-z^2})\right]}{z-\alpha}\right\}$$

These integrals have the advantage that we can essentially inte on the range where $-(ka+C) < z < (ka+C)$ and the total error thu introduced can be made negligible by proper choice of C.

The complex value of k requires some thought. The argume introducing this imaginary part is given by [Einarsson (1966), p. 147]. The correct answer is defined as the one obtained in limit where $\mathrm{Im}(k) \to 0$. For the purpose of numerical integratic two routes present themselves. We can either allow k and α to small but finite imaginary parts, or we can attempt to integra in a symmetric fashion about the singularities at $z=\alpha$ and $z=k$, they lie on the path of integration, and add in the appropriate residues. In fact, the first alternative was chosen. It was that the factorization functions must be smooth, hence slowly as functions of complex k and α. Also, experimentation with va of loss tangent indicated the results were relatively insensiti to the loss tangent. Hence, for purposes of numerical integra complex values of k and α (being k_0 and α_0) are defined by

$$k_0 = (1 + i.005)k$$

$$\alpha_0 = \alpha + i.005\, k$$

The results of numerical integration for values of n (the orde the Bessel functions listed as n in Table A-1) ranging from 0 3 are presented in Table A-1. It was found, by way of confirm that there was excellent agreement with both DC and asymptotic The $\$M_+$ function is defined by

$$\$M_+(\alpha) = a(k + \alpha)M_+(\alpha) \quad .$$

It remains finite as $\kappa \to 0$.

AD-A095 554 OHIO STATE UNIV COLUMBUS ELECTROSCIENCE LAB F/G 20/14
ELECTROMAGNETIC SCATTERING BY OPEN CIRCULAR WAVEGUIDES,(U)
DEC 80 T W JOHNSON, D L MOFFATT N00014-78-C-0049
UNCLASSIFIED ESL-710816-9 NL

2 OF 2
AD A095554

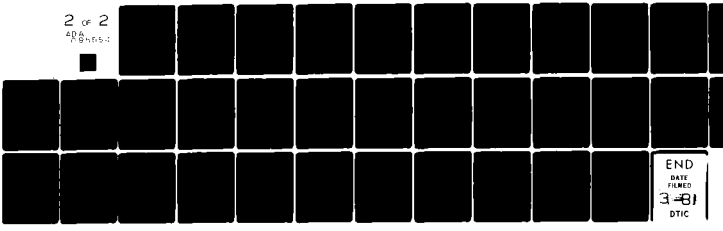

END
DATE FILMED
3-81
DTIC

Table A-1
VALUES OF FACTORIZATION FUNCTIONS L+ AND M+ COMPUTED BY NUMERICAL INTEGRATION

n	D/λ	α/k	Re L+	Im	Re M+	Im
0	0.1	0.0	1.7539	0.8444	1.0355	0.0355
0	0.1	0.2	1.5063	0.8585	1.0238	0.0718
0	0.1	0.4	1.4783	0.8615	1.0095	0.1038
0	0.1	0.6	1.3591	0.8575	0.9941	0.1329
0	0.1	0.8	1.2749	0.8495	0.9772	0.1589
0	0.1	1.0	1.1929	0.8365	0.9595	0.1825
0	0.2	0.0	1.3144	0.9595	1.0727	0.1303
0	0.2	0.2	1.1435	0.9319	1.0516	0.1678
0	0.2	0.4	1.0103	0.8585	0.9884	0.2335
0	0.2	0.6	0.9061	0.8441	0.9451	0.2704
0	0.2	0.8	0.8223	0.8079	0.9327	0.2991
0	0.2	1.0	0.7544	0.7601	0.9520	0.3214
0	0.3	0.0	0.9654	1.0095	1.0775	0.2562
0	0.3	0.2	0.8105	0.9179	0.9992	0.3169
0	0.3	0.4	0.7015	0.8355	0.9252	0.3577
0	0.3	0.6	0.6230	0.7639	0.8574	0.3839
0	0.3	0.8	0.5553	0.7025	0.7953	0.3996
0	0.3	1.0	0.5212	0.6504	0.7420	0.4077
0	0.4	0.0	0.6634	0.9745	1.0599	0.3923
0	0.4	0.2	0.5510	0.8420	0.9255	0.4359
0	0.4	0.4	0.4817	0.7377	0.8294	0.4571
0	0.4	0.6	0.4372	0.6563	0.7475	0.4622
0	0.4	0.8	0.4072	0.5927	0.6793	0.4582
0	0.4	1.0	0.3857	0.5424	0.6225	0.4490
0	0.5	0.0	0.4052	0.8592	0.9595	0.5197
0	0.5	0.2	0.3530	0.7180	0.8219	0.5326
0	0.5	0.4	0.3296	0.6125	0.7142	0.5235
0	0.5	0.6	0.3132	0.5379	0.6308	0.5042
0	0.5	0.8	0.3117	0.4840	0.5660	0.4810
0	0.5	1.0	0.3067	0.4439	0.5151	0.4572
0	0.6	0.0	0.1986	0.6932	0.8424	0.6235
0	0.6	0.2	0.2153	0.5537	0.6963	0.5949
0	0.6	0.4	0.2351	0.4589	0.5927	0.5545
0	0.6	0.6	0.2500	0.4152	0.5181	0.5140
0	0.6	0.8	0.2595	0.3795	0.4644	0.4763
0	0.6	1.0	0.2642	0.3541	0.4243	0.4432
0	0.7	0.0	0.1536	0.4265	0.6973	0.6918
0	0.7	0.2	0.1435	0.3400	0.5519	0.6200
0	0.7	0.4	0.1957	0.3003	0.4734	0.5533
0	0.7	0.6	0.2282	0.2815	0.4173	0.4970
0	0.7	0.8	0.2447	0.2718	0.3789	0.4515
0	0.7	1.0	0.2521	0.2645	0.3512	0.4149

n	D/λ	α/k	Re L+	Im	Re M+	Im
1	0.1	0.0	1.0355	0.0356	0.1419	3.0738
1	0.1	0.2	1.0238	0.0718	0.2022	2.5830
1	0.1	0.4	1.0048	0.1038	0.2420	2.2331
1	0.1	0.6	0.9941	0.1328	0.2694	1.9709
1	0.1	0.8	0.9772	0.1589	0.2890	1.7570
1	0.1	1.0	0.9595	0.1825	0.3033	1.6039
1	0.2	0.0	1.0727	0.1303	0.2021	1.5047
1	0.2	0.2	1.0515	0.1878	0.2352	1.2795
1	0.2	0.4	0.9884	0.2338	0.2565	1.1169
1	0.2	0.6	0.9451	0.2704	0.2713	0.9938
1	0.2	0.8	0.9027	0.2991	0.2821	0.8976
1	0.2	1.0	0.8670	0.3214	0.2902	0.8205
1	0.3	0.0	1.0775	0.2562	0.1895	1.0155
1	0.3	0.2	0.9992	0.3169	0.2148	0.8614
1	0.3	0.4	0.9252	0.3577	0.2342	0.7506
1	0.3	0.6	0.8574	0.3839	0.2496	0.6581
1	0.3	0.8	0.7963	0.3996	0.2618	0.6052
1	0.3	1.0	0.7420	0.4077	0.2712	0.5551
1	0.4	0.0	1.0399	0.3923	0.1240	0.7390
1	0.4	0.2	0.9265	0.4369	0.1660	0.6173
1	0.4	0.4	0.8294	0.4571	0.1991	0.5351
1	0.4	0.6	0.7475	0.4624	0.2242	0.4790
1	0.4	0.8	0.6793	0.4582	0.2427	0.4371
1	0.4	1.0	0.6229	0.4490	0.2558	0.4069
1	0.5	0.0	0.9595	0.5197	0.0496	0.4751
1	0.5	0.2	0.8219	0.5325	0.1250	0.3925
1	0.5	0.4	0.7142	0.5235	0.1797	0.3456
1	0.5	0.6	0.6330	0.5042	0.2160	0.3185
1	0.5	0.8	0.5660	0.4810	0.2395	0.3020
1	0.5	1.0	0.5151	0.4572	0.2542	0.2913
1	0.6	0.0	0.8424	0.6235	0.1814	0.0234
1	0.6	0.2	0.6953	0.5948	0.2742	0.0526
1	0.6	0.4	0.5927	0.5546	0.3234	0.0880
1	0.6	0.6	0.5180	0.5140	0.3465	0.1195
1	0.6	0.8	0.4644	0.4762	0.3537	0.1454
1	0.6	1.0	0.4243	0.4432	0.3523	0.1648
1	0.7	0.0	0.6973	0.5918	0.4512	0.0715
1	0.7	0.2	0.5819	0.6200	0.4962	0.1344
1	0.7	0.4	0.4933	0.5533	0.4955	0.1795
1	0.7	0.6	0.4173	0.4970	0.4821	0.2098
1	0.7	0.8	0.3739	0.4515	0.4357	0.2293
1	0.7	1.0	0.3512	0.4149	0.4099	0.2384

n	D/λ	α/k	Re L+	Im	Re M+	Im
2	0.1	0.0	0.7131	0.0004	0.0359	4.4533
2	0.1	0.2	0.7125	0.0124	0.0575	3.7204
2	0.1	0.4	0.7115	0.0243	0.1253	3.1912
2	0.1	0.6	0.7097	0.0359	0.1538	2.7953
2	0.1	0.8	0.7073	0.0474	0.1750	2.4893
2	0.1	1.0	0.7044	0.0585	0.1936	2.2434
2	0.2	0.0	0.7327	0.0061	0.0327	2.1703
2	0.2	0.2	0.7294	0.0310	0.0893	1.8136
2	0.2	0.4	0.7235	0.0555	0.1298	1.5510
2	0.2	0.6	0.7155	0.0785	0.1573	1.3731
2	0.2	0.8	0.7057	0.0995	0.1785	1.2279
2	0.2	1.0	0.6945	0.1183	0.1945	1.1126
2	0.3	0.0	0.7545	0.0222	0.0577	1.8839
2	0.3	0.2	0.7534	0.0834	0.1107	1.1647
2	0.3	0.4	0.7372	0.0999	0.1459	1.0099
2	0.3	0.6	0.7177	0.1316	0.1702	0.8948
2	0.3	0.8	0.6961	0.1586	0.1876	0.8060
2	0.3	1.0	0.6734	0.1813	0.2004	0.7353
2	0.4	0.0	0.8020	0.0587	0.0972	0.9923
2	0.4	0.2	0.7755	0.1137	0.1394	0.8443
2	0.4	0.4	0.7483	0.1581	0.1654	0.7388
2	0.4	0.6	0.7205	0.1930	0.1846	0.6598
2	0.4	0.8	0.6933	0.2197	0.1974	0.5985
2	0.4	1.0	0.6680	0.2396	0.2067	0.5496
2	0.5	0.0	0.8347	0.1171	0.1311	0.7768
2	0.5	0.2	0.7952	0.1804	0.1503	0.6559
2	0.5	0.4	0.7542	0.2257	0.1794	0.5656
2	0.5	0.6	0.7132	0.2557	0.1929	0.5253
2	0.5	0.8	0.6757	0.2759	0.2026	0.4786
2	0.5	1.0	0.6425	0.2890	0.2097	0.4418
2	0.6	0.0	0.8537	0.1945	0.1381	0.6487
2	0.6	0.2	0.7783	0.2671	0.1608	0.5541
2	0.6	0.4	0.7053	0.2947	0.1779	0.4862
2	0.6	0.6	0.6412	0.3157	0.1915	0.4362
2	0.6	0.8	0.5853	0.3245	0.2013	0.3988
2	0.6	1.0	0.5378	0.3262	0.2081	0.3700
2	0.7	0.0	0.8508	0.2860	0.1147	0.5503
2	0.7	0.2	0.7485	0.3354	0.1428	0.4634
2	0.7	0.4	0.6598	0.3590	0.1558	0.4047
2	0.7	0.6	0.5856	0.3636	0.1641	0.3641
2	0.7	0.8	0.5257	0.3598	0.1961	0.3351
2	0.7	1.0	0.4792	0.3494	0.2041	0.3137

n	D/λ	α/k	Re L+	Im	Re M+	Im
2	0.5	0.0	0.8199	0.3846	0.0738	0.4423
2	0.5	0.2	0.6948	0.4097	0.1192	0.3671
2	0.5	0.4	0.5973	0.4095	0.1535	0.3215
2	0.5	0.6	0.5229	0.3961	0.1771	0.2935
2	0.5	0.8	0.4553	0.3781	0.1922	0.2753
2	0.5	1.0	0.4226	0.3592	0.2012	0.2625
2	0.7	0.0	0.7625	0.4636	0.0291	0.2900
2	0.7	0.2	0.6250	0.4550	0.1037	0.2414
2	0.7	0.4	0.5269	0.4409	0.1521	0.2210
2	0.7	0.6	0.4572	0.4111	0.1814	0.2131
2	0.7	0.8	0.4072	0.3824	0.1978	0.2095
2	0.7	1.0	0.3688	0.3565	0.2070	0.2082
2	1.0	0.0	0.5729	0.5460	0.1783	0.0219
2	1.0	0.2	0.5365	0.5058	0.2514	0.0569
2	1.0	0.4	0.4459	0.4545	0.2844	0.0943
2	1.0	0.6	0.3891	0.4115	0.2934	0.1232
2	1.0	0.8	0.3485	0.3754	0.2911	0.1435
2	1.0	1.0	0.3211	0.3459	0.2836	0.1570
2	1.1	0.0	0.5545	0.5902	0.3707	0.0514
2	1.1	0.2	0.4418	0.5157	0.3577	0.1199
2	1.1	0.4	0.3715	0.4499	0.3762	0.1602
2	1.1	0.6	0.3285	0.3974	0.3558	0.1843
2	1.1	0.8	0.3005	0.3582	0.3329	0.1970
2	1.1	1.0	0.2804	0.3290	0.3120	0.2032
2	1.2	0.0	0.4410	0.5073	0.4575	0.1305
2	1.2	0.2	0.3479	0.5021	0.4403	0.1904
2	1.2	0.4	0.3017	0.4255	0.4007	0.2206
2	1.2	0.6	0.2758	0.3715	0.3535	0.2324
2	1.2	0.8	0.2591	0.3334	0.3320	0.2342
2	1.2	1.0	0.2447	0.3052	0.3063	0.2313
2	1.3	0.0	0.3152	0.5370	0.5117	0.2128
2	1.3	0.2	0.2528	0.4641	0.4486	0.2579
2	1.3	0.4	0.2435	0.3865	0.3918	0.2702
2	1.3	0.6	0.2339	0.3364	0.3479	0.2577
2	1.3	0.8	0.2272	0.3030	0.3142	0.2589
2	1.3	1.0	0.2209	0.2789	0.2884	0.2484

n	D/λ	α/k	Re L+	Im	Re M+	Im
3	0.1	0.0	0.5791	0.0000	0.0414	5.4965
3	0.1	0.2	0.5790	0.0052	0.0775	4.5505
3	0.1	0.4	0.5787	0.0124	0.1049	3.9268
3	0.1	0.6	0.5781	0.0185	0.1260	3.4371
3	0.1	0.8	0.5774	0.0247	0.1429	3.0566
3	0.1	1.0	0.5765	0.0307	0.1566	2.7525
3	0.2	0.0	0.5847	0.0071	0.0211	2.7215
3	0.2	0.2	0.5842	0.0130	0.0644	2.2685
3	0.2	0.4	0.5829	0.0256	0.0959	1.9451
3	0.2	0.6	0.5806	0.0381	0.1196	1.7053
3	0.2	0.8	0.5776	0.0502	0.1380	1.5186
3	0.2	1.0	0.5738	0.0619	0.1525	1.3703
3	0.3	0.0	0.5956	0.0039	0.0162	1.7817
3	0.3	0.2	0.5938	0.0213	0.0627	1.4563
3	0.3	0.4	0.5902	0.0411	0.0955	1.2772
3	0.3	0.6	0.5847	0.0599	0.1202	1.1218
3	0.3	0.8	0.5776	0.0775	0.1387	1.0020
3	0.3	1.0	0.5691	0.0940	0.1529	0.9069
3	0.4	0.0	0.6120	0.0040	0.0190	1.2996
3	0.4	0.2	0.6081	0.0333	0.0672	1.0859
3	0.4	0.4	0.6003	0.0608	0.1006	0.9363
3	0.4	0.6	0.5894	0.0858	0.1246	0.8257
3	0.4	0.8	0.5762	0.1080	0.1422	0.7407
3	0.4	1.0	0.5614	0.1274	0.1554	0.6736
3	0.5	0.0	0.6353	0.0124	0.0304	0.9987
3	0.5	0.2	0.6265	0.0520	0.0781	0.8393
3	0.5	0.4	0.6117	0.0871	0.1100	0.7279
3	0.5	0.6	0.5928	0.1170	0.1321	0.6457
3	0.5	0.8	0.5717	0.1419	0.1480	0.5827
3	0.5	1.0	0.5495	0.1620	0.1595	0.5329
3	0.6	0.0	0.6547	0.0298	0.0510	0.7941
3	0.6	0.2	0.6465	0.0800	0.0946	0.6735
3	0.6	0.4	0.6211	0.1213	0.1228	0.5888
3	0.6	0.6	0.5917	0.1544	0.1424	0.5261
3	0.6	0.8	0.5615	0.1789	0.1557	0.4778
3	0.6	1.0	0.5317	0.1959	0.1651	0.4395
3	0.7	0.0	0.6965	0.0501	0.0778	0.6527
3	0.7	0.2	0.6843	0.1193	0.1137	0.5592
3	0.7	0.4	0.6548	0.1635	0.1365	0.4930
3	0.7	0.6	0.6131	0.1956	0.1529	0.4434
3	0.7	0.8	0.5638	0.2167	0.1633	0.4050
3	0.7	1.0	0.5076	0.2294	0.1707	0.3747

n	D/λ	α/k	Re L+	Im	Re M+	Im
3	0.3	0.0	0.7255	0.1073	0.1031	0.5580
3	0.3	0.2	0.5733	0.1697	0.1293	0.4819
3	0.3	0.4	0.5185	0.2119	0.1468	0.4261
3	0.3	0.6	0.5864	0.2376	0.1591	0.3845
3	0.3	0.8	0.5195	0.2519	0.1678	0.3527
3	0.3	1.0	0.4785	0.2584	0.1738	0.3278
3	0.7	0.0	0.7453	0.1607	0.1089	0.4964
3	0.7	0.2	0.5721	0.2237	0.1311	0.4255
3	0.7	0.4	0.5020	0.2590	0.1474	0.3764
3	0.7	0.6	0.5491	0.2757	0.1595	0.3401
3	0.7	0.8	0.4982	0.2811	0.1682	0.3130
3	0.7	1.0	0.4438	0.2[illegible]	0.1747	0.2928
3	1.0	0.0	0.7488	0.2335	0.1018	0.4452
3	1.0	0.2	0.6039	0.2570	0.1252	0.3768
3	1.0	0.4	0.5719	0.3094	0.1439	0.3301
3	1.0	0.6	0.5019	0.3102	0.1582	0.3009
3	1.0	0.8	0.4487	0.3052	0.1678	0.2785
3	1.0	1.0	0.4057	0.2950	0.1737	0.2619
3	1.1	0.0	0.7332	0.3053	0.0751	0.3893
3	1.1	0.2	0.6141	0.3419	0.1103	0.3240
3	1.1	0.4	0.5279	0.3463	0.1355	0.2845
3	1.1	0.6	0.4590	0.3356	0.1548	0.2604
3	1.1	0.8	0.4078	0.3205	0.1661	0.2441
3	1.1	1.0	0.3683	0.3043	0.1725	0.2325
3	1.2	0.0	0.6973	0.3819	0.0435	0.3071
3	1.2	0.2	0.5885	0.3913	0.0969	0.2536
3	1.2	0.4	0.4755	0.3753	0.1332	0.2273
3	1.2	0.6	0.4119	0.3517	0.1554	0.2139
3	1.2	0.8	0.3655	0.3277	0.1681	0.2062
3	1.2	1.0	0.3315	0.3050	0.1743	0.2008
3	1.3	0.0	0.5428	0.4517	0.0203	0.1645
3	1.3	0.2	0.5091	0.4302	0.0996	0.1430
3	1.3	0.4	0.4222	0.3939	0.1455	0.1433
3	1.3	0.6	0.3640	0.3573	0.1703	0.1496
3	1.3	0.8	0.3252	0.3269	0.1816	0.1553
3	1.3	1.0	0.2972	0.3017	0.1859	0.1592
3	1.4	0.0	0.5651	0.5061	0.2114	0.0261
3	1.4	0.2	0.4390	0.4519	0.2621	0.0703
3	1.4	0.4	0.3545	0.3934	0.2758	0.1072
3	1.4	0.6	0.3175	0.3532	0.2730	0.1325
3	1.4	0.8	0.2873	0.3185	0.2627	0.1478
3	1.4	1.0	0.2659	0.2926	0.2507	0.1562

n	D/λ	α/k	Re L+	Im	Re M+	Im
3	1.5	0.0	0.4714	0.5383	0.3339	0.0655
3	1.5	0.2	0.3635	0.4542	0.3418	0.1233
3	1.5	0.4	0.3054	0.3878	0.3248	0.1583
3	1.5	0.6	0.2746	0.3390	0.3019	0.1761
3	1.5	0.8	0.2537	0.3045	0.2800	0.1835
3	1.5	1.0	0.2385	0.2794	0.2609	0.1854
3	1.5	0.0	0.3707	0.5462	0.4030	0.1249
3	1.5	0.2	0.2904	0.4381	0.3752	0.1799
3	1.5	0.4	0.2561	0.3655	0.3370	0.2039
3	1.5	0.6	0.2375	0.3191	0.3036	0.2107
3	1.5	0.8	0.2253	0.2852	0.2755	0.2095
3	1.5	1.0	0.2156	0.2613	0.2551	0.2049
3	1.7	0.0	0.2642	0.5207	0.4384	0.1939
3	1.7	0.2	0.2247	0.4015	0.3795	0.2341
3	1.7	0.4	0.2135	0.3320	0.3286	0.2429
3	1.7	0.6	0.2075	0.2902	0.2911	0.2365
3	1.7	0.8	0.2029	0.2617	0.2634	0.2275
3	1.7	1.0	0.1973	0.2415	0.2425	0.2175

A-2. Low-Frequency Approximations

Derivation of 'DC' forms for the factorization functions is not difficult. They can be obtained directly from the small argument approximations for Bessel and Hankel functions. For $n \neq 0$, we get (Abramowitz, Equations (9.1.7) and (9.1.9))

$$L_+(\alpha)L_+(-\alpha) = \pi i J_n(\gamma a)H_n^{(1)}(\gamma a) \tag{A-13a}$$

$$\sim \pi i \frac{(\frac{\gamma a}{2})^n}{n!} \cdot \frac{-i(n-1)!}{\pi(\frac{\gamma a}{2})^n} \tag{A-13b}$$

$$\sim \frac{1}{n} \tag{A-13c}$$

$$L_+(\alpha) \sim \frac{1}{\sqrt{n}} \tag{A-14}$$

$$M_+(\alpha)M_+(-\alpha) = \pi i J_n'(\gamma a)H_n^{(1)\prime}(\gamma a) \tag{A-15a}$$

$$\sim \pi i \frac{\frac{1}{2}(\frac{\gamma a}{2})^{n-1}}{(n-1)!} \cdot \frac{i}{2} \frac{n!}{(\frac{\gamma a}{2})^{n+1}} \sim -\frac{n}{(\gamma a)^2} \tag{A-15b}$$

$$\sim \frac{-n}{a^2(k^2-\alpha^2)} \tag{A-15c}$$

$$M_+(\alpha) \sim \frac{i\sqrt{n}}{a(k+\alpha)} \tag{A-16}$$

For $n = 0$, we note that

$$J_0'(z) = -J_1(z) \tag{A-17a}$$

$$H_0^{(1)\prime}(z) = -H_1^{(1)}(z) \tag{A-17b}$$

Hence,

$$M_+(n=0,k,\alpha) = L_+(n=1,k,\alpha) \tag{A-18}$$

From Abramowitz Equations (9.1.7) and (9.1.8), for n = 0

$$L_+(\alpha)L_+(-\alpha) = \pi i J_0(\gamma a)H_0^{(1)}(\gamma a) \tag{A-19a}$$

$$\approx \pi i \cdot 1 \cdot \frac{2i}{\pi} \ln(\gamma a) \approx -2\ln \gamma a \tag{A-19b}$$

$$\approx -\ln(a^2(k^2-\alpha^2)) \tag{A-19c}$$

The factorization of this DC form is non-trivial. Based on [Weinstein (1969), p. 335-36] we may approximate $L_+(\alpha) \approx i\sqrt{2}\ \frac{\ln a\sqrt{2k(k+\alpha)}}{\sqrt{\ln(2ka)}}$ for $\alpha << k << 1$.

Having thus obtained the first low-frequency approximation with ease, it is extraordinarily difficult to obtain a better approximation analytically. Lee, Jamnejad, and Mittra present a simple derivation. Unfortunately it does not agree with the results of numerical integration. This can be seen by comparison of their formulas with the plot in Figure A-1, which shows the trajectories of $L_+(k)$ and $M_+(k)$ for n=1 computed by numerical integration. The inclusion of additional terms from the small argument approximation does not improve matters. The approach taken, therefore, is that for small values of ka, the values of L_+ and M_+ are computed by numerical integration, and interpolation is used.

It turns out that, for $L_+(n=1,\alpha=k)$, the values over a surprisingly large range ($0 \leq ka < 2$) can be approximated by

$$L_+ \approx \frac{(1-i.0584\ ka)}{(1+i.68\ ka)} \tag{A-20}$$

However, this does not admit any generalization, nor does it possess any theoretical justification.

A-3. High Frequency Asymptotic Approximations

Using the large argument approximations for Bessel and Hankel functions, we obtain (from Abramowitz Equations (9.2.17) through (9.2.20))

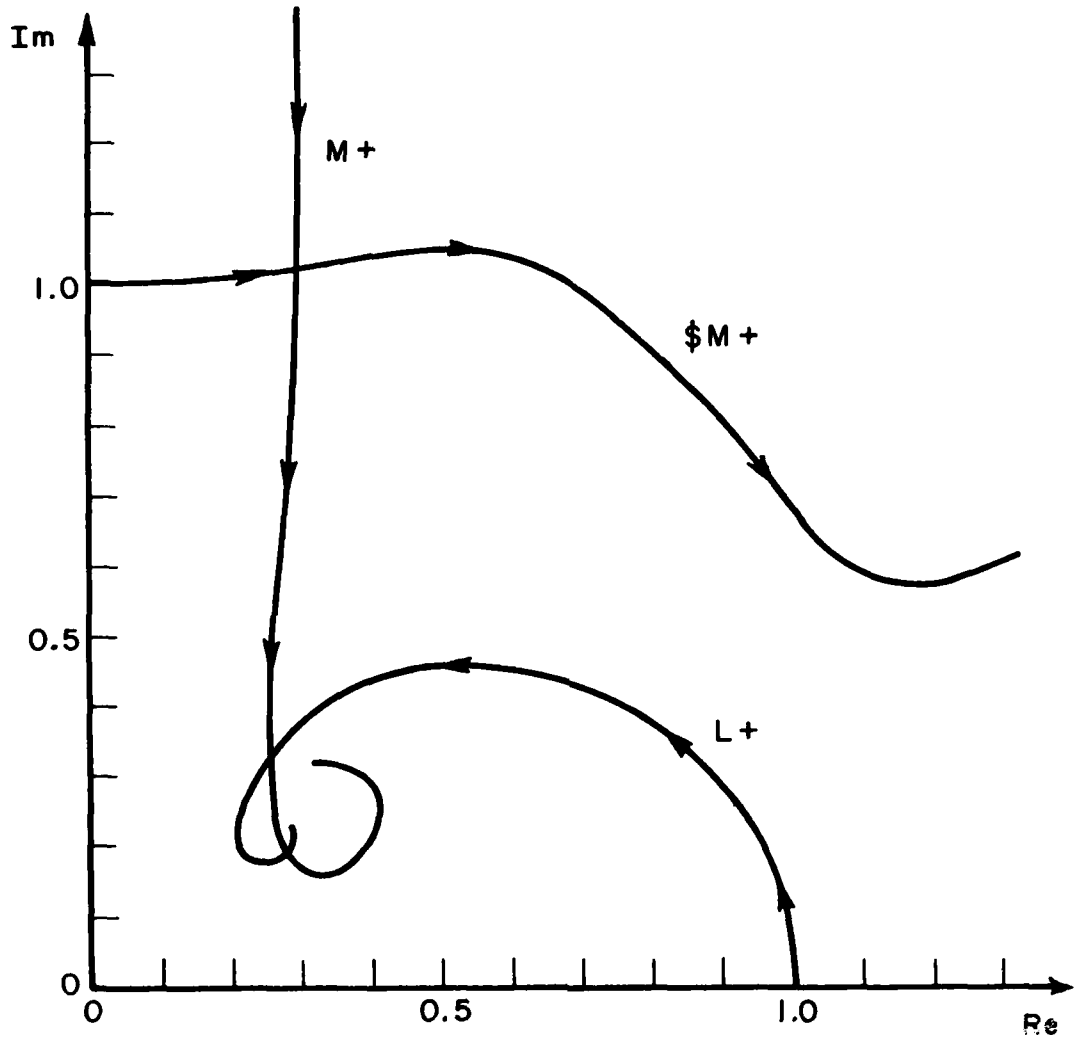

Figure A-1. Factorization functions L+, M+, $M+ for n=1, α=k. Arrows indicate increasing k.

$$L_+(\alpha)L_+(-\alpha) = \pi i J_n(\gamma a)H_n^{(1)}(\gamma a) \tag{A-21a}$$

$$= \pi i M_n(\gamma a)\cos\theta_n(\gamma a)M_n(\gamma a)e^{i\theta_n(\gamma a)} \tag{A-21b}$$

$$= \frac{\pi i}{2}(M_n(\gamma a))^2(1+e^{i2\theta_n(\gamma a)}) \tag{A-21c}$$

$$M_+(\alpha)M_+(-\alpha) = \pi i J_n'(\gamma a)H_n^{(1)'}(\gamma a) \tag{A-22a}$$

$$= \pi i N_n(\gamma a)\cos\phi_n(\gamma a)N_n(\gamma a)e^{i\phi_n(\gamma a)} \tag{A-22b}$$

$$= \frac{\pi i}{2}(N_n(\gamma a))^2(1+e^{i2\phi_n(\gamma a)}) \quad . \tag{A-22c}$$

Where, from Abramowitz, Equations (9.2.28) through (9.2.31)

$$M_n(z)^2 \sim \frac{2}{\pi z}\left[1 + \frac{4n^2-1}{8z^2}\right] \tag{A-23}$$

$$\theta_n(z) \sim z - (\frac{n}{2} + \frac{1}{4})\pi + \frac{(4n^2-1)}{8z} \tag{A-24}$$

$$N_n(z)^2 \sim \frac{2}{\pi z}\left[1 - \frac{4n^2-3}{8z^2}\right] \tag{A-25}$$

$$\phi_n(z) \sim z - (\frac{n}{2} - \frac{1}{4})\pi + \frac{4n^2+3}{8z} \quad . \tag{A-26}$$

For $L_+(\alpha)$ we observe that we can separately factor the two expressions, making $L_+(\alpha)$ the product of two factors, both of which are analytic in the upper half-plane.

$$L_+(\alpha) = L_+^I(\alpha)L_+^{II}(\alpha) \tag{A-27}$$

$$L_+^I(\alpha)L_+^I(-\alpha) = \frac{\pi i}{2} M_n(\gamma a)^2$$

$$\sim \frac{\pi i}{2} \cdot \frac{2}{\pi\gamma a}\left(1 + \frac{4n^2-1}{8(\gamma a)^2}\right)$$

$$\sim \frac{i}{\gamma a}\left(\frac{\gamma^2 a^2 + \frac{4n^2-1}{8}}{\gamma^2 a^2}\right)$$

$$\sim \frac{i}{a\sqrt{k^2-\alpha^2}}\left(\frac{a^2(k^2-\alpha^2) + \frac{4n^2-1}{8}}{a^2(k^2-\alpha^2)}\right)$$

$$\sim \frac{i}{a\sqrt{k^2-\alpha^2}}\left(\frac{k^2a^2 + \frac{4n^2-1}{8} - \alpha^2a^2}{a^2(k^2-\alpha^2)}\right) \qquad \text{(A-28)}$$

Hence, by inspection

$$L_+^I(\alpha) \sim \frac{e^{i\pi/4}}{\sqrt{a(k+\alpha)}}\left(\frac{\sqrt{k^2a^2 + \frac{4n^2-1}{8}} + \alpha a}{a(k+\alpha)}\right) \qquad \text{(A-29)}$$

Similarly

$$M_+^I(\alpha)M_+^I(-\alpha) = \frac{\pi i}{2} N_n(\gamma a)^2$$

$$\sim \frac{\pi i}{2} \cdot \frac{2}{\pi a\sqrt{k^2-\alpha^2}}\left(\frac{a^2(k^2-\alpha^2) - \frac{4n^2-3}{8}}{a^2(k^2-\alpha^2)}\right)$$

$$\sim \frac{i}{a\sqrt{k^2-\alpha^2}}\left(\frac{k^2a^2 - \frac{4n^2-3}{8} - \alpha^2a^2}{a^2(k^2-\alpha^2)}\right) \qquad \text{(A-30)}$$

$$M_+^I(\alpha) \sim \frac{e^{i\pi/4}}{\sqrt{a(k+\alpha)}} \quad \frac{\sqrt{k^2a^2 - \frac{4n^2-3}{8}} + \alpha a}{a(k+\alpha)} \tag{A-31}$$

In evaluating $L_+^{II}(\alpha)$ and $M_+^{II}(\alpha)$, we follow the derivation of Mittra et al, (1975) .

$$L_+^{II}(\alpha)L_+^{II}(-\alpha) = 1 + e^{i2\theta_n(\gamma a)} \tag{A-32a}$$

$$M_+^{II}(\alpha)M_+^{II}(-\alpha) = 1 + e^{i2\phi_n(\gamma a)} \tag{A-32b}$$

The exact expression for $L_+^{II}(\alpha)$ is given by

$$L_+^{II}(\alpha) = \exp\left\{ \frac{1}{2\pi i} \int_{-\infty}^{\infty} \frac{\ell n\left[1 + e^{i2\theta_n(\gamma a)}\right]}{z-\alpha} \, dz \right\} \tag{A-33}$$

Let

$$I = \int_{-\infty}^{\infty} \frac{\ell n\left(1 + e^{i2\theta_n(\gamma a)}\right)}{z-\alpha} \, dz \tag{A-34}$$

Then the identity

$$\ln(1 + x) = \sum_{m=1}^{\infty} \frac{(-1)^{m+1}x^m}{m} ; \qquad |x| \leq 1 \tag{A-35}$$

can be used to obtain

$$I = \sum_{m=1}^{\infty} \frac{(-1)^{m+1}}{m} \int_{-\infty}^{\infty} \frac{e^{i2m\theta_n(\gamma a)}}{z-\alpha} \, dz \tag{A-36}$$

provided $Im(\theta_n) \geq 0$.

Let

$$I_m = \int_{-\infty}^{\infty} \frac{e^{i2m\theta_n(\gamma a)}}{z-\alpha} dz \qquad \text{(A-37)}$$

where

$$\theta_n(\gamma a) \backsim \gamma a - (\frac{n}{2} + \frac{1}{4})\pi + \frac{4n^2-1}{8\gamma a} \qquad \text{(A-38)}$$

$$\gamma a = a\sqrt{k^2-z^2} \qquad \text{(A-39)}$$

Let

$$z = k \sin\tau \qquad \text{(A-40a)}$$

$$dz = k \cos\tau \, d\tau \qquad \text{(A-40b)}$$

$$\gamma a = a\sqrt{k^2-k^2\sin^2\tau} = ka \cos\tau \qquad \text{(A-40c)}$$

The contours of integration in the z and τ plane are shown in Figures A-2 and A-3, respectively. The contour in the τ plane is selected so that γa has the right sign, and the integrand vanishes at both ends of the contour. The contour in the τ plane is then deformed to the steepest descent contour. Since no poles are passed over in this deformation (for $Re(\alpha)>0$) the integral is unchanged. Hence

$$I_m = \int_C \frac{e^{i2m\theta_n(ka\cos\tau)}}{k\sin\tau-\alpha} k\cos\tau \, d\tau$$

$$= \int_{C_{SDP}} \frac{\cos\tau}{\sin\tau - \frac{\alpha}{k}} e^{i2m\theta_n(ka\cos\tau)} d\tau \qquad \text{(A-41)}$$

$$\text{With } \theta_n(ka\cos\tau) = ka\cos\tau - (\frac{n}{2} + \frac{1}{4})\pi + \frac{4n^2-1}{8ka\cos\tau} \qquad \text{(A-42)}$$

$$\text{Let } X_L = \frac{4n^2-1}{8(ka)^2} \qquad \text{(A-43)}$$

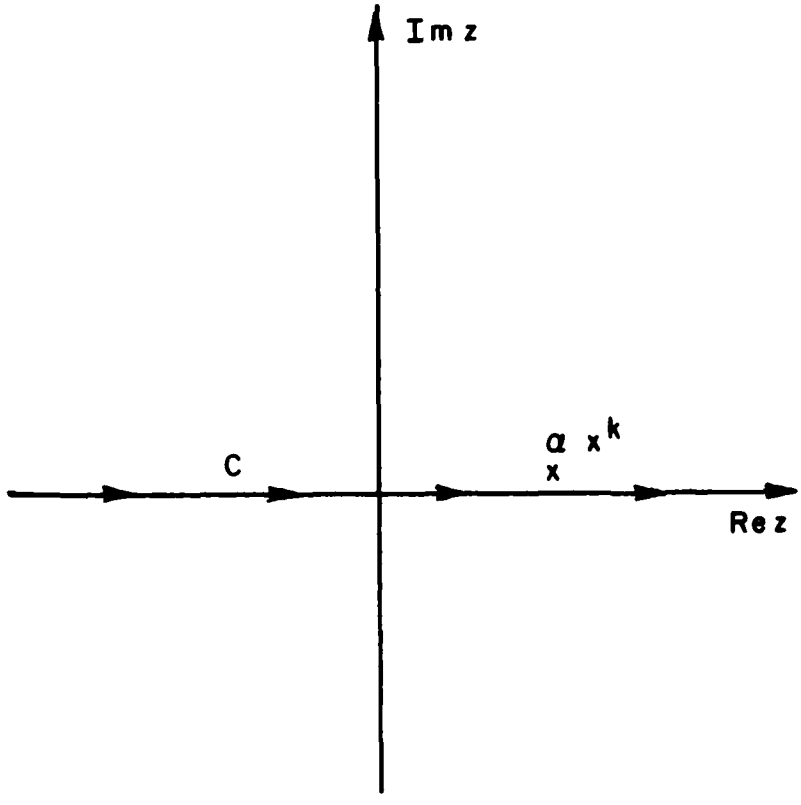

Figure A-2. Contour of integration in the complex z-plane.

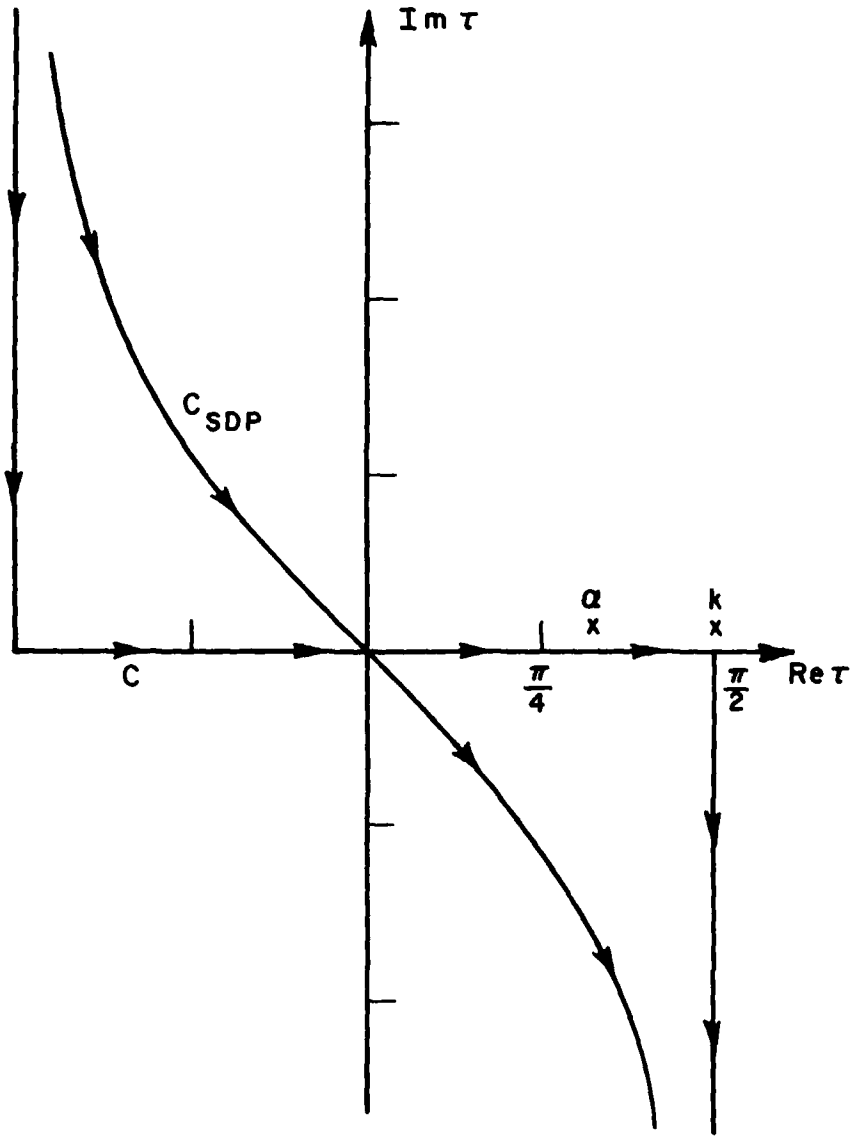

Figure A-3. Contour of integration in the complex τ-plane.

I_m is an integral in the form

$$\int_{C_{SDP}} F(\tau)\, e^{\kappa f(\tau)}\, d\tau$$

where $F(\tau) = \dfrac{\cos\tau}{\sin\tau - \frac{\alpha}{k}}$ (A-44a)

$$\kappa = ka \tag{A-44b}$$

$$f(\tau) = \frac{i2m\theta_n(ka\cos\tau)}{ka}$$

$$= i2m\left(\cos\tau - \left(\frac{n}{2} + \frac{1}{4}\right)\frac{\pi}{ka} + \frac{X_L}{\cos\tau}\right) \tag{A-44c}$$

This can be readily evaluated by asymptotic techniques. We make a first approximation by ignoring the pole near the saddle point.

$$f'(\tau_s)=0 = i2m\left(-\sin\tau + \frac{X_L \sin\tau}{\cos^2\tau}\right) \tag{A-45}$$

$$\tau_s = 0 \tag{A-46}$$

Then $f''(\tau_s) = i2m\left(-\cos\tau + \dfrac{2-\cos^2\tau}{\cos^3\tau} X_L\right)$

$$= -i2m(1-X_L) \tag{A-47}$$

The asymptotic value of the integral is then

$$I_m \sim e^{\kappa f(\tau_s)}\, e^{-\frac{i\pi}{4}} \left|\sqrt{\frac{2\pi}{\kappa f''(\tau_s)}}\right| F(\tau_s) \tag{A-48}$$

where $\frac{-\pi}{4}$ is the angle of the C_{SDP} through the saddle point.

$$f(\tau_s) = \frac{i2m\theta_n(ka)}{ka} \qquad \text{(A-49a)}$$

$$F(\tau_s) = -\frac{k}{\alpha} \qquad \text{(A-49b)}$$

$$f''(\tau_s) = -i2m(1-X_L) \qquad \text{(A-49c)}$$

Thence

$$I_m \sim e^{i2m\theta_n(ka)} e^{-i\pi/4} \left| \sqrt{\frac{2\pi}{2mka(1-X_L)}} \right| (-\frac{k}{\alpha}) \qquad \text{(A-50)}$$

$$I = \sum_{m=1}^{\infty} \frac{(-1)^m e^{i2m\theta_n(ka)} e^{-i\pi/4}}{m} (\frac{k}{\alpha}) \sqrt{\frac{\pi}{mka(1-X_L)}}$$

$$\sim \frac{k}{\alpha} e^{-i\pi/4} \sqrt{\frac{\pi}{ka(1-X_L)}} \sum_{m=1}^{\infty} \frac{(-1)^m e^{i2m\theta_n(ka)}}{m^{3/2}} \qquad \text{(A-51)}$$

The indicated sum is shown by [Chuang, Liang, and Lee (1975), p. 773] to be a modified Lerch function. They present a development of its properties and a transformation to simplify its evaluation.

$$\sum_{m=1}^{\infty} \frac{(-1)^m e^{i2m\theta_n(ka)}}{m^{3/2}} = \sum_{m=1}^{\infty} \frac{e^{i2\pi mp}}{m^{3/2}} = L(p,3/2) \qquad \text{(A-52)}$$

where $\pm im\pi + i2m\theta_n(ka) = i2\pi mp$

$$\text{or } p = \frac{\theta_n(ka)}{\pi} \pm \frac{1}{2} \qquad \text{(A-53)}$$

This function has two useful and simple properties. Since the parameter p appears only in the exponent, and

$$e^{i2\pi mp+i2\pi p} = e^{i2\pi mp}$$

$$L(p+1,3/2) = L(p,3/2) \quad . \tag{A-54}$$

Furthermore $e^{i2\pi m(1-p)} = e^{-i2\pi mp}$

$$L(1-p,3/2) = L^*(p,3/2), \text{ where } * \text{ denotes the complex conjugate.} \tag{A-55}$$

By using these relations, it is possible to transform any value of p to the range $0 \leq p \leq 0.5$. In this range, the series solution is extremely accurate

$$L(p,\nu) = \frac{\Gamma(1-\nu)e^{i(1-\nu)\pi/2}}{(2\pi p)^{1-\nu}} + \sum_{m=0}^{\infty} \frac{i^m \zeta(\nu-m)(2\pi p)^m}{m!} \quad . \tag{A-56}$$

For $\nu=3/2$, this gives

$$L(p,3/2) = -2\pi\sqrt{p}\cdot(1-i) + \sum_{n=0}^{\infty} (R_n + iI_n p)p^{2n} \tag{A-57}$$

where values of R_n and I_n are given by Table I of Chuang, Liang, and Lee (Note sign error in Equation (35) of Chuang et al (1975) corrected here).

We can similarly find an asymptotic form for $M_+(\alpha)$. The analysis is identical with $\theta_n(ka)$ replaced by $\phi_n(ka)$ and $X_L \rightarrow X_M = \frac{4n^2+3}{8(ka)^2}$. This results in $p = \frac{\phi_n(ka)}{\pi} \pm 1/2$. Otherwise the expression is unchanged.

$$\begin{Bmatrix} L_+^{II}(\alpha) \\ M_+^{II}(\alpha) \end{Bmatrix} \sim \exp \left\{ \frac{I_{L,M}}{2\pi i} \right\} \quad . \tag{A-58}$$

Where

$$I_L = \frac{k}{\alpha} e^{-i\pi/4} \sqrt{\frac{\pi}{ka(1-X_L)}} \; L(p,3/2) \qquad p = \frac{\theta_n(ka)}{\pi} \pm 1/2 \tag{A-59a}$$

$$I_M \quad \frac{k}{\alpha} e^{-i\pi/4} \sqrt{\frac{\pi}{ka(1-X_M)}} \; I(p,3/2) \qquad p = \frac{\phi_n(ka)}{\pi} \pm 1/2 \quad \text{(A-59b)}$$

A comparison of these results with those obtained by numerical integration is instructive. For $\alpha=k$, the agreement is very good down to the first zero of $J_n(ka)$ or $J_n'(ka)$ (for L_+ and M_+ respectively) if the proper form of $\theta_n(ka)$ or $\phi_n(ka)$ is chosen. This is illustrated in Figure A-4 for M+(n=1, $\alpha=k$); the exact value of M_+ is compared to that obtained by using the two term and three term approximations to $\phi_1(ka)$. It can be seen that a rather sharp minimum occurs for the exact form of M_+ for that value of ka for which $J_1'(ka)=0$. For the two-term and three-term forms of $\phi_1(ka)$, the minimum occurs at the value for which $\cos\phi_1(ka)=0$. Thus, the more accurate θ_n or ϕ_n should, in general, lead to a more accurate approximation for L_+ or M_+.

L_+ and M_+ are also functions of α/k; we must explore the accuracy of this approximation when this ratio varies. This is important since $\alpha/\kappa = \cos\theta$ for scattering, radiation, and coupling problems, and $\alpha/k = \sqrt{1 - (\frac{j_{nm}}{ka})^2}$ for coupling and radiation of waveguide modes. In Figure A-5, the value of $L_+(n=1)$ is plotted in the complex plane, where the main curve traces out the real and imaginary parts of L_+ with $\alpha=k$ and D/λ as a parameter. The dashed curves then indicate the trajectories which occur when varying α/k while holding ka (or D/λ) fixed. It is immediately evident that the preceding approximation does not, in general, capture the nature of this behavior. The reason for this can be seen from Figure A-3. As α/k varies, the pole located at $\tau_p = \sin^{-1}(\alpha/k)$ moves closer to the saddle point at $\tau_s=0$. We totally ignored this pole originally. Without belaboring the point, it will only be stated that rederiving the approximation incorporating the effect of the pole produced only a marginal improvement. It was therefore necessary to include two terms in the asymptotic expansion. This derivation follows.

With the same definitions of κ, $f(\tau)$ and $F(\tau)$, we have the asymptotic approximation

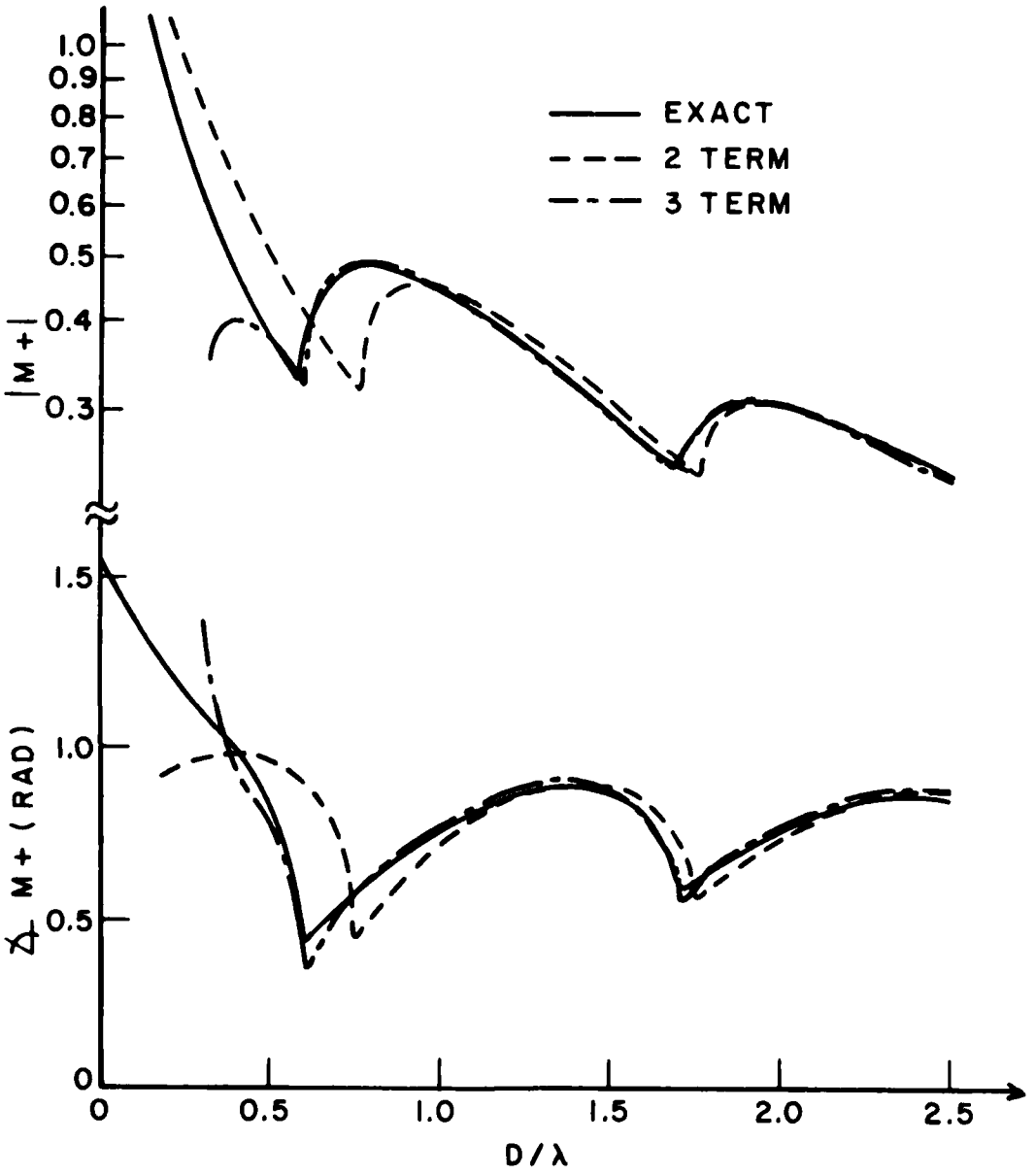

Figure A-4. Factorization function M+ for n=1, α=k, calculated by numerical integration and asymptotic approximation based on two and three term expressions for phase of Bessel function.

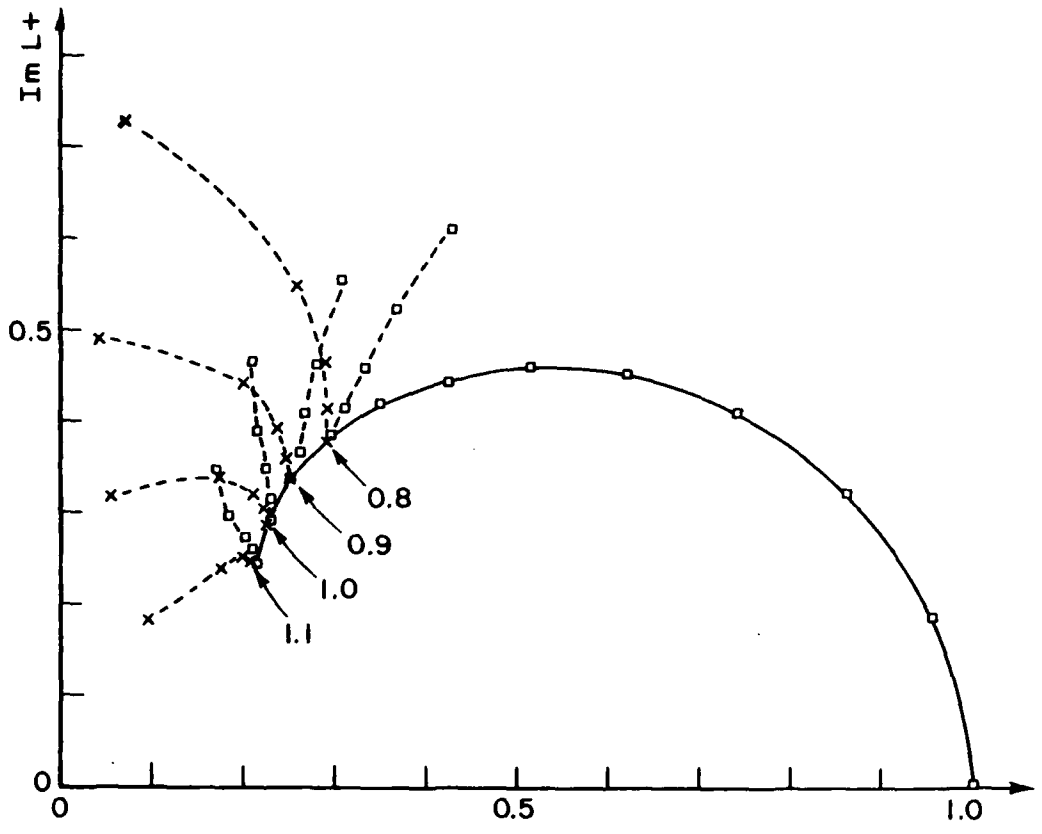

Figure A-5. Factorization function L+ for $n=1$. Solid curve gives $\alpha=k$, varying k. Dashed curves vary α/k holding D/λ fixed to the values specified by arrows.
□ = exact value (by numerical integration)
x = first asymptotic approximation.

$$I_m \sim e^{\kappa f(\tau_s)} e^{i\phi_s} \left| \sqrt{\frac{2\pi}{\kappa f''(\tau_s)}} \right| \left\{ F(\tau_s) \right.$$

$$+ i\Delta \left(1 - \mathbb{f}(\kappa\Delta)\right) \left[\frac{1}{4} F(\tau_s) \frac{3f^{(iv)}(\tau_s)f''(\tau_s) - 5f'''(\tau_s)^2}{3f''(\tau_s)^3} \right.$$

$$\left. \left. + F'(\tau_s) \frac{f'''(\tau_s)}{f''(\tau_s)^2} - \frac{F''(\tau_s)}{f''(\tau_s)} \right] \right\} \qquad \text{(A-60)}$$

where $\mathbb{f}(X)$ is the transition function defined and discussed by [Kouyoumjian and Pathak (1974), p. 1453]. Δ is a distance parameter, relating to the separation of τ_s and τ_p, defined by

$$\Delta = i(f(\tau_s) - f(\tau_p)) \qquad \text{(A-61)}$$

The saddle point is unchanged, so τ_s=0. The pole is located at

$$\tau_p = \sin^{-1} \frac{\alpha}{k} \qquad \text{(A-62)}$$

We thus derive Table A-2.

TABLE A-2

SUMMARY OF ASYMPTOTIC FUNCTIONS AT SADDLE POINT IN τ-PLANE

	Function form	Value at $\tau_s=0$
$f(\tau)$	$i2m(\cos\tau-(\frac{n}{2}+\frac{1}{4})\frac{\pi}{ka}+\frac{X_L}{\cos\tau})$	$i2m(1-(\frac{n}{2}+\frac{1}{4})\frac{\pi}{ka}+X_L)$
$f'(\tau)$	$i2m(-\sin\tau+X_L\frac{\sin\tau}{\cos^2\tau})$	0
$f''(\tau)$	$i2m(-\cos\tau+X_L\frac{2-\cos^2\tau}{\cos^3\tau})$	$i2m(-1+X_L)$
$f'''(\tau)$	$i2m(\sin\tau+X_L\frac{\sin\tau}{\cos^4\tau}(6-\cos^2\tau))$	0
$f^{(iv)}(\tau)$	$i2m(\cos\tau+X_L\frac{\cos^4\tau-20\cos^2\tau+24}{\cos^5\tau})$	$i2m(1+5X_L)$
$F(\tau)$	$\frac{\cos\tau}{\sin\tau-\alpha/k}$	$-k/\alpha$
$F'(\tau)$	$\frac{\alpha/k\ \sin\tau-1}{(\sin\tau-\alpha/k)^2}$	$-(\frac{k}{\alpha})^2$
$F''(\tau)$	$\frac{-\alpha/k\ \sin\tau\cos\tau-(\alpha/k)^2\cos\tau+2\cos\tau}{(\sin\tau-\alpha/k)^3}$	$\frac{k}{\alpha}-2(\frac{k}{\alpha})^3$

$$\Delta = i(f(\tau_s) - f(\tau_p))$$

$$= i.i2m(\cos\tau_s-(\frac{n}{2} + \frac{1}{4})\frac{\pi}{ka} + \frac{X_L}{\cos\tau_s} -(\cos\tau_p-(\frac{n}{2} + \frac{1}{4})\frac{\pi}{ka} + \frac{X_L}{\cos\tau_p}))$$

(A-63)

$$\cos\tau_s = 1$$

$$\cos\tau_p = \sqrt{1-(\alpha/k)^2}$$

$$\Delta = - 2m\left(1+X_L-\left(\sqrt{1-(\alpha/k)^2} + \frac{X_L}{\sqrt{1-(\alpha/k)^2}}\right)\right)$$

$$= - 2m\left(1-\sqrt{1-(\alpha/k)^2}+X_L\left(1- \frac{1}{\sqrt{1-(\alpha/k)^2}}\right)\right) \qquad \text{(A-64)}$$

$$I_m \sim e^{i2m\theta_n(ka)}\ e^{-i\pi/4}\left|\sqrt{\frac{2\pi}{2mka(1-X_L)}}\right| \cdot\left\{- \frac{k}{\alpha}\right.$$

$$+ i\Delta(1-\text{ff}(ka\Delta))\left[\frac{1}{4}(- \frac{k}{\alpha})\ \frac{3i2m\left[1+5X_L\right]\cdot i2m\left[-1+X_L\right]}{3\left(i2m\left[-1+X_L\right]\right)^3}\right.$$

$$\left.\left. + (- \frac{k^2}{\alpha^2}).0- \frac{\frac{k}{\alpha}(1-2(\frac{k}{\alpha})^2)}{i2m(-1+X_L)}\right]\right\} \qquad \text{(A-65a)}$$

$$\sim -\frac{k}{\alpha}\sqrt{\frac{\pi}{ka(1-X_L)}}\; e^{-i\pi/4}\; m^{-1/2}\; e^{i2m\theta_n(ka)} \cdot$$

$$\left\{1 + \frac{\Delta}{2m}(1-\text{ff}(ka\Delta))\left[\frac{1}{4}\,\frac{1+5X_L}{(-1+X_L)^2} + \frac{1-2(\frac{k}{\alpha})^2}{-1+X_L}\right]\right\} \qquad \text{(A-65b)}$$

Define

$$\Delta = m\delta$$

$$\delta = 2\left[\sqrt{1-(\alpha/k)^2} - 1 + X_L\left(\frac{1}{\sqrt{1-(\alpha/k)^2}} - 1\right)\right] \qquad \text{(A-66)}$$

$$A_o = \frac{-3+9X_L + 8(\frac{k}{\alpha})^2(1-X_L)}{8(1-X_L)^2} \qquad \text{(A-67)}$$

$$A_1 = \frac{k}{\alpha}\sqrt{\frac{\pi}{ka(1-X_L)}}\; e^{-i\pi/4} \qquad \text{(A-68)}$$

$$I_m \sim -\frac{A_1}{\sqrt{m}}\, e^{i2m\theta_n(ka)}\left\{1 + A_o\delta(1-\text{ff}(mka\delta))\right\} \qquad \text{(A-69)}$$

$$I = \sum_{m=1}^{\infty}\frac{(-1)^{m+1}}{m} I_m$$

$$\sim \sum_{m=1}^{\infty}\frac{(-1)^{m+1}}{m}\;\frac{(-A_1)}{\sqrt{m}}\, e^{i2m\theta_n(ka)}\left\{1+A_o\delta(1-\text{ff}(mka\delta))\right\}$$

$$\sim A_1\sum_{m=1}^{\infty}\frac{(-1)^m}{m^{3/2}}\, e^{i2m\theta_n(ka)}\left\{1+A_o\delta(1-\text{ff}(mka\delta))\right\}$$

$$\sim A_1\left\{L(p,3/2)+A_o\delta G(p,q)\right\} \qquad \text{(A-70)}$$

where

$$G(p,q) = \sum_{m=1}^{\infty} m^{-3/2} \pi e^{i2\pi m\rho(1-f(mq))} \qquad \text{(A-71)}$$

$$p = \frac{\theta_n(ka)}{\pi} \pm 1/2 \qquad \text{(A-72a)}$$

$$q = ka\delta \qquad \text{(A-72b)}$$

We could follow exactly the same analysis to obtain M+, except that

$$\theta_n(ka) \rightarrow \phi_n(ka)$$

$$X_L \rightarrow X_m = \frac{4n^2+3}{8(ka)^2} \qquad \text{(A-73)}$$

These formulas produce a very good agreement with the results of numerical integration, down to $\alpha/k=0.2$.

APPENDIX B
SUMMARY OF WIENER-HOPF COUPLING AND SCATTERING COEFFICIENTS

The coordinate system chosen in these equations is that described in Chapters I and II. Hence, although the results are derived from Einarsson et al (1966), they have been transformed into our coordinate system.

B-1. Direct Scattering From the Rim

These coordinates are cast in the form

$$\begin{bmatrix} E^s_\theta \\ E^s_\phi \end{bmatrix} = \begin{bmatrix} S_{\theta\theta} & S_{\theta\phi} \\ S_{\phi\theta} & S_{\phi\phi} \end{bmatrix} \begin{bmatrix} E^i_\theta \\ E^i_\phi \end{bmatrix} \tag{B-1}$$

Where both $\overline{E^s}$ and $\overline{E^i}$ are expressed by

$$\overline{E} = \frac{e^{\pm ikr}}{r} (\hat{\theta}E_\theta + \hat{\phi}E_\phi) \tag{B-2}$$

where e^{+ikr} is for E^s

e^{-ikr} is for E^i .

The expressions presented in Appendix B are all asymptotic in the sense that they are far-field and valid only far from the waveguide mouth ($kr >> 1$)

$$S_{\theta\theta} = -\frac{2i}{k} \sum_{n=o}^{\infty} \epsilon_n \cos n\phi_s \; \frac{J_n(ka\sin\theta_i)}{\sin\theta_i L_+(k\cos\theta_i)} \; \frac{J_n(ka\sin\theta_s)}{\sin\theta_s L_+(k\cos\theta_s)} \cdot$$

$$\left[\frac{(1-\cos\theta_i)(1-\cos\theta_s)}{2(\cos\theta_i+\cos\theta_s)} - \frac{f_n^2}{1-f_n^2} \right] \tag{B-3}$$

$$S_{\phi\phi} = \frac{2i}{k(1+\cos\theta_i)(1+\cos\theta_s)} \sum_{n=0}^{\infty} \varepsilon_n \cos n\phi_s \frac{J_n'(ka\sin\theta_i)}{M_+(k\cos\theta_i)} \frac{J_n'(ka\sin\theta_s)}{M_+(k\cos\theta_s)}$$

$$\left[\frac{(1+\cos\theta_i)(1+\cos\theta_s)}{2(\cos\theta_i+\cos\theta_s)} + \frac{f_n^2}{1-f_n^2}\right] \qquad \text{(B-4)}$$

$$S_{\theta\phi} = \frac{4i}{k(1+\cos\theta_i)} \sum_{n=1}^{\infty} \sin n\phi_s \frac{J_n(ka\sin\theta_s)}{\sin\theta_s L_+(k\cos\theta_s)} \frac{J_n'(ka\sin\theta_i)}{M_+(k\cos\theta_i)} \cdot \frac{f_n}{1-f_n^2} \qquad \text{(B-5)}$$

$$S_{\phi\theta} = -\frac{4i}{k(1+\cos\theta_s)} \sum_{n=1}^{\infty} \sin n\phi_s \frac{J_n'(ka\sin\theta_s)}{M_+(k\cos\theta_s)} \frac{J_n(ka\sin\theta_i)}{\sin\theta_i L_+(k\cos\theta_i)} \frac{f_n}{1-f_n^2} \qquad \text{(B-6)}$$

Where

$\phi_i = \pi$ is assumed

$$f_n = \frac{nL_+(k)}{2kaM_+(k)} \qquad \text{(B-7)}$$

$$\varepsilon_n = \begin{cases} 1 & n = 0 \\ 2 & n = 1,2,3\ldots \end{cases} \qquad \text{(B-8)}$$

It was found that Chuang et al (1975) contained several misprints. A correction letter is reproduced on the following page.

Correction to "High Frequency Scattering from an Open-Ended Semi Infinite Cylinder"

C. A. CHUANG, MEMBER, IEEE, CHARLES S. LIANG, MEMBER, IEEE, AND SHUNG-WU LEE, SENIOR MEMBER, IEEE

In the above paper[1], there were six sign misprints.

1) Time factor should have read $\exp(-i\omega t)$.
2) In (1), x should have read $(-x)$.
3) In (4), $(1 + \cos\theta)$ in numerator should have read $(1 - \cos\theta)$.
4) In (7), $(\cos\theta + \cos\theta_0)$ should have read $(-1)(\cos\theta + \cos\theta_0)$.
5) In (11), $(\alpha - \alpha')$ should have read $(\alpha' - \alpha)$.
6) In (35), $(1 + i)$ should have read $(1 - i)$.

The above sign misprints do not affect any other equations or numerical results.

The authors wish to thank T. W. Johnson and D. L. Moffatt for bringing some of these errors to their attention.

C. A. Chuang is with Aeronutronic-Ford/WDL, Palo Alto, CA. He is now at 882 Solitaire Dr., Indialantic, FL 32903.

C. S. Liang is with the Fort Worth Division, General Dynamics, Fort Worth, TX 76101.

S. W. Lee is with the Department of Electrical Engineering, University of Illinois, Urbana, IL 61801.

[1] C. A. Chuang, C. S. Liang, and S. W. Lee, *IEEE Trans. Antenna Propagat.*, vol. AP-23, pp. 770–776, Nov. 1975.

B-2. Coupling of Incident Field to Waveguide Modes

With the same definition of the incident field (as in Equation (B-2)) the axial fields within the waveguide can be represented as follows:

$$E_z = \sum_{n=0}^{\infty} \sum_{m=1}^{\infty} \begin{Bmatrix} A^{\theta}_{nm} \cos n\phi \\ A^{\phi}_{nm} \sin n\phi \end{Bmatrix} \frac{J_n(j_{nm}\rho/a)}{J'_n(j_{nm})} e^{-i\alpha_{nm}z} \qquad \text{(B-9)}$$

$$H_z = \sqrt{\frac{\varepsilon_o}{\mu_o}} \sum_{n=0}^{\infty} \sum_{m=1}^{\infty} \begin{Bmatrix} B^{\theta}_{nm} \sin n\phi \\ B^{\phi}_{nm} \cos n\phi \end{Bmatrix} \frac{J_n(j'_{nm}\rho/a)}{J_n(j'_{nm})} e^{-i\alpha'_{nm}z} \qquad \text{(B-10)}$$

$$J_n(j_{nm}) = 0$$

$$J'_n(j'_{nm}) = 0$$

$$\alpha_{nm} = \sqrt{k^2 - \frac{j_{nm}^2}{a^2}}$$

$$\alpha'_{nm} = \sqrt{k^2 - \frac{j'^2_{nm}}{a^2}}$$

The top line of Equation (B-9) indicates that E^i_{θ} produces E_z with cos $n\phi$ dependence

The bottom line of Equation (B-9) indicates that E^i_{ϕ} produces E_z with sin $n\phi$ dependence

$$A^{\theta}_{nm} = -\frac{2\varepsilon_n i^n j_{nm}}{\alpha_{nm} a} \frac{L_+(\alpha_{nm})}{L_+(k\cos\theta_i)} \frac{J_n(ka\sin\theta_i)}{ka\sin\theta_i} \left[\frac{f_n^2}{1-f_n^2} + \frac{(\alpha_{nm}+k)(1-\cos\theta_i)}{2(\alpha_{nm}-k\cos\theta_i)} \right] \qquad \text{(B-11)}$$

$$A^{\phi}_{nm} = - \frac{4i^n j_{nm}}{k\alpha_{nm}a^2(1+\cos\theta_i)} \frac{L_+(\alpha_{nm})}{M_+(k\cos\theta_i)} J'_n(ka\sin\theta_i) \frac{f_n}{1-f_n^2} \qquad (B\text{-}12)$$

$$B^{\theta}_{nm} = + \frac{4i^n(k+\alpha'_{nm})}{\alpha'_{nm}(1-\frac{n^2}{j'^2_{nm}})} \frac{M_+(\alpha'_{nm})}{L_+(k\cos\theta_i)} \frac{J_n(ka\sin\theta_i)}{ka\sin\theta_i} \frac{f_n}{1-f_n^2} \qquad (B\text{-}13)$$

$$B^{\phi}_{nm} = - \frac{2\varepsilon_n i^n(k+\alpha'_{nm})}{k\alpha'_{nm}a(1-\frac{n^2}{j'^2_{nm}})(1+\cos\theta_i)} \frac{M_+(\alpha'_{nm})}{M_+(k\cos\theta_i)} J'_n(ka\sin\theta_i) \cdot$$

$$\left[\frac{f_n^2}{1-f_n^2} + \frac{(k-\alpha'_{nm})(1+\cos\theta_i)}{2(k\cos\theta_i-\alpha'_{nm})} \right] \qquad (B\text{-}14)$$

B-3. Radiation Patterns From an Open Waveguide

The incident field is assumed to be a single waveguide mode, either TE or TM, with axial fields given by

$$E^i_z = E_{nm} \frac{J_n(j_{nm}\rho/a)}{J'_n(j_{nm})} \cos n\phi \, e^{i\alpha_{nm}z} \qquad (B\text{-}15)$$

$$H^i_z = H_{nm} \frac{J_n(j'_{nm}\rho/a)}{J_n(j'_{nm})} \cos n\phi \, e^{i\alpha'_{nm}z} \qquad (B\text{-}16)$$

The radiated field is given by

$$\begin{bmatrix} E_\theta^r \\ E_\phi^r \end{bmatrix} = \begin{bmatrix} C_{\theta E} & C_{\theta H} \\ C_{\phi E} & C_{\phi H} \end{bmatrix} \begin{bmatrix} E_{nm} \\ \sqrt{\frac{\mu_o}{\epsilon_o}}\, H_{nm} \end{bmatrix} \frac{e^{ikr}}{r} \qquad \text{(B-17)}$$

$$C_{\theta E} = \frac{(-i)^{n+1}\epsilon_n k^2 a^3 \cos n\phi_s}{2j_{nm}} \frac{L_+(\alpha_{nm})}{L_+(k\cos\theta_s)} \frac{J_n(ka\sin\theta_s)}{ka\sin\theta_s}$$

$$\left[\frac{f_n^2}{1-f_n^2} + \frac{(\alpha_{nm}+k)(1-\cos\theta_s)}{2(\alpha_{nm}-k\cos\theta_s)} \right] \qquad \text{(B-18)}$$

$$C_{\theta H} = \frac{(-i)^{n+1} k^2 a^2 \sin n\phi_s}{(k-\alpha'_{nm})} \frac{M_+(\alpha'_{nm})}{L_+(k\cos\theta_s)} \frac{J_n(ka\sin\theta_s)}{ka\sin\theta_s} \frac{f_n}{1-f_n^2}$$

$$\text{(B-19)}$$

$$C_{\phi E} \frac{(-i)^{n+1} a^2 k \sin n\phi_s}{j_{nm}(1+\cos\theta_s)} \frac{L_+(\alpha_{nm})}{M_+(k\cos\theta_s)} J'_n(ka\sin\theta_s) \frac{f_n}{1-f_n^2} \qquad \text{(B-20)}$$

$$C_{\phi H} = -\frac{(-i)^{n+1}\epsilon_n ka\cos n\phi_s}{2(1+\cos\theta_s)(\alpha'_{nm}-k)} \frac{M_+(\alpha'_{nm})}{M_+(k\cos\theta_s)} J'_n(ka\sin\theta_s) \cdot$$

$$\left[\frac{f_n^2}{1-f_n^2} + \frac{(k-\alpha'_{nm})(1+\cos\theta_s)}{2(k\cos\theta_s-\alpha'_{nm})} \right] \qquad \text{(B-21)}$$

B-4. Internal Reflection and Mode Conversion

With incident field as described in Section B-3, the scattered field is given by

$$E_z^s = \sum_{\ell} \frac{J_n(j_{n\ell}\rho/a)}{J_n'(j_{n\ell})} e^{-i\alpha_{n\ell}z} \left[R_{m\ell}^{nE}\cos n\phi \quad T_{m\ell}^{nH}\sin n\phi \right] \begin{bmatrix} E_{nm} \\ \sqrt{\frac{\mu_o}{\varepsilon_o}} H_{nm} \end{bmatrix} \tag{B-22}$$

$$\sqrt{\frac{\mu_o}{\varepsilon_o}} H_z^s = \sum_{\ell} \frac{J_n(j'_{n\ell}\rho/a}{J_n(j'_{n\ell})} e^{-i\alpha'_{n\ell}z} \left[T_{m\ell}^{nE}\sin n\phi \; R_{m\ell}^{nH}\cos n\phi \right] \begin{bmatrix} E_{nm} \\ \sqrt{\frac{\mu_o}{\varepsilon_o}} H_{nm} \end{bmatrix} \tag{B-23}$$

$$R_{m\ell}^{nE} = -\frac{j_{n\ell}k}{j_{nm}\alpha_{n\ell}} L_+(\alpha_{nm})L_+(\alpha_{n\ell}) \left[\frac{f_n^2}{1-f_n^2} + \frac{(k+\alpha_{nm})(k+\alpha_{n\ell})}{2k(\alpha_{nm}+\alpha_{n\ell})} \right] \tag{B-24}$$

$$T_{m\ell}^{nH} = \frac{j_{n\ell}kM_+(\alpha'_{nm})L_+(\alpha_{n\ell})}{\alpha_{n\ell}a(k-\alpha'_{nm})} \frac{f_n}{1-f_n^2} \tag{B-25}$$

$$T_{m\ell}^{nE} = \frac{ka(k+\alpha'_{n\ell})}{\alpha'_{n\ell}\left(1 - \frac{n^2}{j'^2_{n\ell}}\right)} L_+(\alpha_{nm})M_+(\alpha'_{n\ell}) \frac{f_n}{1-f_n^2} \tag{B-26}$$

$$R_{m\ell}^{nH} = \frac{k(k+\alpha'_{n\ell})M_+(\alpha'_{nm})M_+(\alpha'_{n\ell})}{\alpha'_{n\ell}(k-\alpha'_{nm})\left(1 - \frac{n^2}{j'^2_{n\ell}}\right)} \left[\frac{f_n^2}{1-f_n^2} - \frac{(k-\alpha'_{nm})(k-\alpha'_{n\ell})}{2k(\alpha'_{nm}+\alpha'_{n\ell})} \right] \tag{B-27}$$

APPENDIX C
ELEMENTS OF DYADIC GREEN'S FUNCTION FOR A CIRCULAR WAVEGUIDE

The dyadic electric Green's function, omitting the source-singular term, is given by Tai (1971). It is assumed, in this appendix, that the azimuthal dependence for E_ρ, E_z, J_ρ, J_z, and H_ϕ is $\cos n\phi$, and for E_ϕ, J_ϕ, H_ρ, and H_z is $\sin n\phi$. This azimuthal dependence is understood and suppressed. The summation over n is also suppressed.

$$i\omega\mu_o\bar{G}_{el}(\bar{R},\bar{R}_s) = -\sqrt{\frac{\mu_o}{\epsilon_o}}\ \frac{k\epsilon_n}{2\pi}\ \sum_{m=1}^{\infty}\left\{\frac{e^{i\alpha_{nm}'|z-z_s|}}{(j_{nm}'^2-n^2)\alpha_{nm}'J_n(j_{nm}')^2}\left[\bar{G}_{ETE}\right]\right.$$

$$\left. + \frac{e^{i\alpha_{nm}|z-z_s|}}{j_{nm}^2 J_n'(j_{nm})^2\alpha_{nm}k^2}\left[\bar{G}_{ETM}\right]\right\} \qquad \text{(C-1)}$$

$$\bar{G}_{ETE} = \hat{\rho}\hat{\rho}n^2\ \frac{J_n(j_{nm}'\rho/a)J_n(j_{nm}'\rho_s/a)}{\rho\rho_s} - \hat{\rho}\hat{\phi}\ \frac{nj_{nm}'}{a}\ \frac{J_n(j_{nm}'\rho/a)J_n'(j_{nm}'\rho_s/a)}{\rho}$$

$$-\hat{\phi}\hat{\rho}\ \frac{nj_{nm}'}{a}\ \frac{J_n'(j_{nm}'\rho/a)J_n(j_{nm}'\rho_s/a)}{\rho_s} + \hat{\phi}\hat{\phi}\ \frac{j_{nm}'^2}{a^2}\ J_n'(j_{nm}'\rho/a)J_n'(j_{nm}'\rho_s/a)$$

(C-2)

$$\bar{\bar{G}}_{TM}=\hat{\rho}\hat{\rho}\,\frac{\alpha_{nm}^2 j_{nm}^2}{a^2}\,J_n'(j_{nm}\rho/a)J_n'(j_{nm}\rho_s/a)-\hat{\rho}\hat{\phi}\,\frac{\alpha_{nm}^2 n\, j_{nm}}{a}\,J_n'(j_{nm}\rho/a)\frac{J_n(j_{nm}\rho_s/a)}{\rho_s}$$

$$+\hat{\rho}\hat{z}\;i\alpha_{nm}\,\mathrm{sgn}(z-z_s)\frac{j_{nm}^3}{a^3}\,J_n'(j_{nm}\rho/a)J_n(j_{nm}\rho_s/a)$$

$$-\hat{\phi}\hat{\rho}\,\frac{\alpha_{nm}^2 n\, j_{nm}}{a}\,\frac{J_n(j_{nm}\rho/a)}{\rho}J_n'(j_{nm}\rho_s/a)+\hat{\phi}\hat{\phi}\alpha_{nm}^2\, n^2\,\frac{J_n(j_{nm}\rho/a)J_n(j_{nm}\rho_s/a)}{\rho\rho_s}$$

$$-\hat{\phi}\hat{z}\,\frac{i\alpha_{nm}}{a^2}\,\mathrm{sgn}(z-z_s)\;n\;j_{nm}^2\,\frac{J_n(j_{nm}\rho/a)}{\rho}\,J_n(j_{nm}\rho_s/a)$$

$$-\hat{z}\hat{\rho}\,\frac{i\alpha_{nm}\mathrm{sgn}(z-z_s)j_{nm}^3}{a^3}\,J_n(j_{nm}\rho/a)J_n'(j_{nm}\rho_s/a)$$

$$+\hat{z}\hat{\phi}\,\frac{i\alpha_{nm}\mathrm{sgn}(z-z_s)\;n\;j_{nm}^2}{a^2}\,J_n(j_{nm}\rho/a)\,\frac{J_n(j_{nm}\rho_s/a)}{\rho_s}$$

$$+\hat{z}\hat{z}\,\frac{j_{nm}^4}{a^4}\,J_n(j_{nm}\rho/a)J_n(j_{nm}\rho_s/a) \qquad \text{(C-3)}$$

$$G_{m2}(R,R_s)=\frac{i\epsilon_n}{2\pi}\sum_{m=1}^{\infty}\frac{e^{i\alpha_{nm}|z-z_s|}}{j_{nm}^2\alpha_{nm}J_n'(j_{nm})^2}\left[\bar{\bar{G}}_{HTM}\right]+\frac{e^{i\alpha_{nm}'|z-z_s|}}{\alpha_{nm}'(j_{nm}'^2-n^2)J_n(j_{nm}')^2}\left[\bar{\bar{G}}_{HTE}\right]$$

(C-4)

$$\bar{\bar{G}}_{HTM}=\hat{\rho}\hat{\rho}\; i\alpha_{nm}\,\mathrm{sgn}(z-z_s)\,\frac{n\,j_{nm}}{a}\,\frac{J_n(j_{nm}\rho/a)}{\rho}\,J_n'(j_{nm}\rho_s/a)$$

$$-\hat{\rho}\hat{\phi}\; i\alpha_{nm}\,\mathrm{sgn}(z-z_s)\,n^2\,\frac{J_n(j_{nm}\rho/a)J_n(j_{nm}\rho_s/a)}{\rho\rho_s}$$

$$-\hat{\rho}\hat{z}\,\frac{nj_{nm}^2}{a^2}\,\frac{J_n(j_{nm}\rho/a)}{\rho}\,J_n(j_{nm}\rho_s/a)$$

$$+\hat{\phi}\hat{\rho}\,\frac{i\alpha_{nm}}{a^2}\,\mathrm{sgn}(z-z_s)\,j_{nm}^2\,J_n'(j_{nm}\rho/a)J_n'(j_{nm}\rho_s/a)$$

$$-\hat{\phi}\hat{\phi}\; i\alpha_{nm}\,\mathrm{sgn}(z-z_s)\,\frac{n\,j_{nm}}{a}\,J_n'(j_{nm}\rho/a)\frac{J_n(j_{nm}\rho_s/a)}{\rho_s}$$

$$-\hat{\phi}\hat{z}\,\frac{j_{nm}^3}{a^3}\,J_n'(j_{nm}\rho/a)J_n(j_{nm}\rho_s/a) \qquad \text{(C-5)}$$

$$G_{HTE}=\hat{\rho}\hat{\rho}\; i\alpha_{nm}'\,\mathrm{sgn}(z-z_s)\,\frac{n\,j_{nm}'}{a}\,J_n'(j_{nm}'\rho/a)\,\frac{J_n(j_{nm}'\rho_s/a)}{\rho_s}$$

$$-\hat{\rho}\hat{\phi}\,\frac{i\alpha_{nm}'\mathrm{sgn}(z-z_s)j_{nm}'^2}{a^2}\,J_n'(j_{nm}'\rho/a)J_n'(j_{nm}'\rho_s/a)$$

$$+\hat{\phi}\hat{\rho}\; i\alpha_{nm}'\mathrm{sgn}(z-z_s)n^2\,\frac{J_n(j_{nm}'\rho/a)J_n(j_{nm}'\rho_s/a)}{\rho\rho_s}$$

$$-\hat{\phi}\hat{\phi}\,\frac{i\alpha_{nm}'}{a}\mathrm{sgn}(z-z_s)nj_{nm}'\,\frac{J_n(j_{nm}'\rho/a)}{\rho}\,J_n'(j_{nm}'\rho_s/a)$$

$$+\hat{z}\hat{\rho}\,\frac{n\,j_{nm}'^2}{a^2}\,J_n(j_{nm}'\rho/a)\,\frac{J_n(j_{nm}'\rho_s/a)}{\rho_s}$$

$$-\hat{z}\hat{\phi}\,\frac{j_{nm}'^3}{a^3}\,J_n(j_{nm}'\rho/a)J_n'(j_{nm}'\rho_s/a) \qquad \text{(C-6)}$$

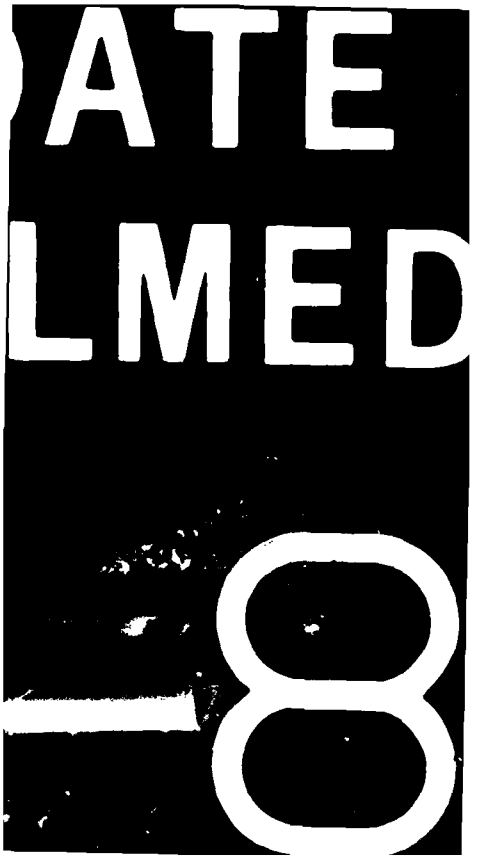
ATE
LMED
8